The energy loss of relativistic cosmic ray muons in plastic scintillator

Jones, I. S.

The Energy Loss of Relativistic Cosmic Ray Muons in Plastic Scintillator

A Thesis submitted to the
University of Durham for the
Degree of Master of Science

by

I.S. Jones

November 1969.

CONTENTS

ABSTRACT

The energy loss for a small area plastic phosphor scintillation counter as a function of particle momentum has been investigated using the Durham Mk 3 Spectrograph with the intention of clarifying the position regarding the decrease in energy loss for particles of momenta greater than 10 $\frac{\text{Gev}}{c}$ recently predicted by Tsytovitch. The results are consistent with the theory of Sternheimer and show only a slight decrease in the momentum range 10 $\frac{\text{GeV}}{c}$ to 100 $\frac{\text{GeV}}{c}$ which is much less than that predicted by Tsytovitch.

PREFACE

This thesis describes the work done by the author in the Cosmic Radiation Group of the Physics Department of Durham University under the supervision of Dr. M.G. Thompson.

The work on the small area scintillator counter with regards to the energy loss was done by the author, the running and construction of the spectrograph to obtain the particle momenta was carried out with the assistance of the other members of the group.

CHAPTER 1

1.1 Introduction

When fast charged particles namely muons pass through a medium they interact with the atoms of the medium transferring energy to the atoms by ionization or excitation processes. These are the most important sources of energy loss for muons of energy less than 10^{12} eV. Bethe and Ashkin (1952), Price (1955) and later Cousins and Nash (1962) have reviewed the studies made on the processes of energy loss.

In studying the rate of energy loss as a function of particle momentum it is necessary to have a method for measuring the energy lost by ionization accompanied by an accurate determination of the energy i.e. momentum, of the incident particle. There have been few experiments using the scintillation counter as the detector and these have suffered from either insufficient statistics or uncertainty in the energy determinations and usually the momentum range over which the energy loss has been taken has been restricted.

The study presented in this thesis describes the energy loss of muons in a small area plastic phosphor scintillation counter of thin cross-section using the Durham Mk 3 Spectrograph and covering a momentum range of 0.4 to 100 GeV/c. The energy loss processes are discussed in Chapter 2 and a qualitative expression for the most probable energy loss in the plastic phosphor as a function of momentum derived. Chapter 3 reviews the recent experiments by other workers on the energy loss of charged particles in plastic phosphor. Chapter 4 describes the Durham Mk 3 Spectrograph including all the electronic circuits, coincidence units and pulsing units for operation, with the details

of the photographic technique and gating system used to record the pulse heights. The construction and test of the scintillation counter used to record the energy loss is described in Chapter 5. The calculations required to find the momentum of the incident particles, their accuracy and the final result are presented in Chapter 6. Chapter 7 concludes the study with a critical comparison of the results with the theory. The introduction closes with a short discussion of the theoretical work investigating ionization loss.

1.2 Previous Investigations of Ionization Loss

It has already been indicated that the two most important processes by which a particle losses energy in traversing matter are ionization and excitation. Using the simple orbital model of the atom, excitation occurs when an electron is displaced to an orbit of larger radius and ionization when the electron is completely removed from the atom. Bohr (1913, 1915) presented the first theoretical treatment deriving the expression given below for the rate of energy loss $-\frac{dE}{dx}$ of a particle for energy transfers less than η

$$-\frac{dE}{dx}_{<\eta} = \frac{2\pi m_e c^2 z^2}{\beta^2}\left[\ln\left\{\frac{2m_e c^2\beta^2\eta(1.123)^2\beta^2}{(1-\beta^2)I^2Z^4\alpha^2z^2}\right\}-\beta^2\right] \qquad 1.1$$

where $\eta = 2m_e\beta^2c^2$ for non relativistic particles $m >> m_e$ which is the case for muons. βc is the velocity of the incident particle of charge ze, m_e is the mass of the electron, and m the mass of the incident particle.

$I(Z)$ is the mean ionization potential of the absorber of atomic number Z, α the fine structure constant and $C = \frac{\pi N Z}{A}\left(\frac{e^2}{m_e c^2}\right)^2$, the other symbols have their usual meanings.

Although Bragg (1912) verified the variation of $-\frac{dE}{dx}$ with $1/\beta^2$ predicted by equation 1.1 it was later shown that the theory was inadequate. Williams (1945) has shown this particularly well. Bethe (1930, 1932) using Quantum Mechanics extended the treatment to cover relativistic particles giving equation 1.2. for the rate of energy loss, $-\frac{dE}{dx}$, for energy transfer less than η

$$-\frac{dE}{dx}_{<\eta} = \frac{2\pi e^2}{\beta^2}\left[\ln\left\{\frac{2m_e c^2\beta^2\eta}{(1-\beta^2)I^2(Z)}\right\} - \beta^2\right] \qquad 1.2$$

The work of Williams (1945) shows that this expression agrees well with experiment however Swann (1938) indicated that the logarithmic increase of $-\frac{dE}{dx}_{<\eta}$ with particle energy E would be reduced by polarisation of the medium because this would directly effect the energetic particle's field.* Fermi (1940) and later experimental workers showed a plateau in the energy loss curve at higher energies due to the reduction in the logarithmic increase as a result of this polarisation; the onset of the plateau region depending on the material.

Extensions to the Fermi theory have been made by several authors, ~~Price (1955), Cousins and Nash (1962)~~ but particularly by Sternheimer (1956) who calculated the error introduced by Fermi's assumption that the electrons of the absorber have only one dispersion frequency. This he found to be a few per cent in the region of the minimum and zero at high energies.

* When a particle traverses the absorber the atoms are polarised by its field in such a way that their field opposes that of the incident particle, this reduces the interaction of the particle and hence the energy loss.

Recently Tsytovitch (1962 a,b,c) has predicted a reduction in the energy loss due to small energy transfers ($<$20 KeV) at particle energies above 10 GeV ($\gamma > 100$) which occur as the result of radiative corrections not considered in the earlier theory. His work has been supported by the experimental work of Zhdanov et al (1963) and Alekseeva et al (1963) using nuclear emulsions. However other workers have not found this decrease and the present study was undertaken to try and clarify the position.

CHAPTER 2

The Theory of Energy Loss by Ionization

2.1 Introduction

Before looking in detail at the 'theory of energy loss due to ionization' it is necessary to understand why the many other mechanisms by which fast particles lose energy in traversing an absorber are not considered. These include, direct pair production, bremsstrahlung, Cerenkov radiation and nuclear interactions.

When the energy loss of a relativistic particle is measured using a thin absorber, high energy losses which include pair production and knock-on electrons, cannot be measured because the resulting high energy knock-on electrons escape from the absorber. What are measured are the more frequent low energy collisions of the particle with the atomic electrons of the absorber which result in the 'ionization' or 'excitation' of the atom. Moreover, this means that the average or mean energy loss cannot be measured using a thin absorber because either it fails to record these high energy losses or if they are recorded the electronics associated with the counter become saturated. What is measured is the most probable energy loss or mode value which it is shown later is insensitive to these high energy losses.

Consider now the various phenomena that may take place when a charged particle passes in the neighbourhood of an atom. The impact parameter b is defined as the perpendicular distance from the trajectory of the incident particle to the atom, such that the 'collisions' can be divided into three groups:

(a) Distant collisions, where the impact parameter is large compared with the atomic dimensions. The particle passes at some distance away from the atom and the field set-up at the atom by it increases to a maximum and decreases as the particle passes. Energy is transferred to the atom which undergoes 'excitation' or 'ionization'. For these distant collisions the binding energy of the electrons to the atoms must be taken into account, while the passing particle may be considered as a point charge.

(b) Close collisions, where the impact parameter is of the order of the atomic dimensions. The interaction no longer involves the whole atom but rather the passing particle and one of the atomic electrons. The energy transfer becomes much greater, exceeding the ionization potential of the atomic electron which is ejected from the atom with considerable energy.

(c) Where the impact parameter is smaller than the atomic radius so that the deflection of the trajectory of the passing particle in the electric field of the nucleus becomes the most important effect. This results in either photon emmision (bremsstrahlung) or in the creation of an electron pair (pair production). However these effects only become predominant at muon energies in excess of 10^{12} eV and will therefore not be discussed.

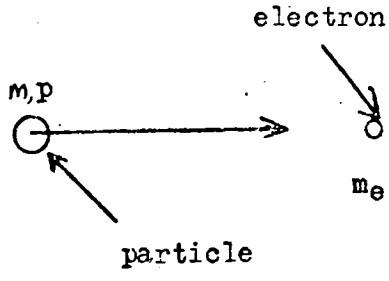

(a)

Dynamics of the collision between a charged particle and an electron, (a) Before, (b) After. (p refers to momentum and E to energy)

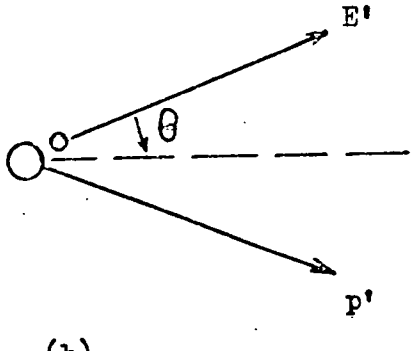

(b)

Fig 2:1

2.2 Energy Loss by Ionization

The theory of energy loss by ionization which is taken to include loss by excitation has been covered in detail by Fano (1963) and Rossi (1952). The summary presented here is taken from Rossi (1952) and also Wolfendale (1963).

When considering the problem of calculating the total rate of energy loss by ionization it is convenient to treat separately the close and distant collisions. When an atom becomes ionized an electron is ejected with a given energy. If we select a predetermined value η for the electron energy, a distant collision can be regarded as one where the electron is ejected at an energy less than η and a close collision where the electron is ejected with energy greater than η. Providing the value of η is sufficiently small and the corresponding impact parameter sufficiently large it is possible to treat all distant collisions by considering the incident particle as a point charge. Conversely close collisions can be treated by considering the atomic electrons as free particles if the value of η is sufficiently large and the corresponding impact parameter sufficiently small. A value of the limiting energy η between 10^4 and 10^5 eV simultaneously satisfies both conditions.

2.2.1 Close Collisions

As indicated previously a close collision is not unlike a collision between a charged particle and a free electron. Consider the collision shown in Figure 2.1 between a heavy particle of mass m and an electron of mass m_e. The initial momentum of the particle

is p and its momentum after collision p'. Then the energy of recoil of the electron E' which is ejected at an angle θ to the direction of the incident particle is given by:

$$E' = 2 m_e c^2 \frac{p^2 c^2 \cos^2\theta}{([m_e c^2 + (p^2c^2 + m^2c^4)^{1/2}]^2 - p^2c^2 \cos^2\theta)} \qquad 2.1$$

Thus the energy of recoil E' increases as θ decreases such that electrons knocked on at small angles have high energy. The maximum transferable energy corresponds to a 'head on' collision and putting $\theta = 0$ in equation 2.1 takes the value;

$$E'_m = 2 m_e \frac{c^2 . p^2 c^2}{[m_e^2c^4 + m^2c^4 + 2m_e c^2 (p^2c^2 + m^2c^4)^{1/2}]} \qquad 2.2$$

For relativistic particles where $p >> mc$ and for muons where $m_\mu = 207 m_e$ the term $m_e^2 c^4$ can be neglected such that equation 2.2. reduces to:-

$$E'_m = 2 m_e c^2 . \frac{p^2 c^2}{m^2c^4 + 2 m_e c^3 p} \qquad 2.3$$

For particles of very large momenta $p >> \frac{m^2 c}{2m_e}$ then the maximum transferable energy becomes:-

$$E'_m = pc = E \qquad 2.4$$

where E is the initial kinetic energy of the incident particle. Thus a particle of extremely high energy can transfer almost all its kinetic energy to an electron even if the mass of the particle is much larger than the electron mass. However this condition applies only to muons with momentum in excess of 10 $\frac{GeV}{c}$ and when considering the most probable energy loss close collisions

with high energy transfer are neglected.

Thus the conditions which do apply are $m_\mu >> m_e$ and $p << \frac{m^2 c}{2m_e}$

such that equation 2.2. becomes:-

$$E'_m \simeq 2 m_e c^2 (p/mc)^2 = 2 m_e c^2 \frac{\beta^2}{1-\beta^2} \qquad 2.5$$

where β is the velocity of the incident particle in terms of the velocity of light. Hence for heavy particles of sufficiently small momenta ($< 20 \frac{GeV}{c}$) E'_m the maximum transferable energy depends only on the velocity.

Now when a charged particle passes through an absorber it passes the atoms at a wide variety of impact parameters. The energy transfer to the electron for each impact parameter can be calculated. To find the total energy loss of the particle as it passes through the absorber it is necessary to find the probability of the particle having a collision with a given energy transfer and then sum this over the whole energy range from η to E'_m. Note that any transfer of energy $< \eta$ is regarded as a distant collision.

Let $\phi(E,E')dE'dx$ represent the probability of a charged particle of kinetic energy E traversing an absorber of thickness $dx.g.cm^{-2}$ transferring an energy between E' and E' + dE' to an atomic electron. An approximate relation for this probability is given by the Rutherford formula,

$$\phi(E,E')dE'dx = \frac{2C m_e z^2 m^2}{\beta^2} \cdot \frac{dE'dx}{(E')^2} \qquad 2.6$$

Note that it is usual to express the thickness of the absorber in units of mass/unit area, thus a length of xcm of an absorber of density ρ $gm.cm^{-3}$ has a thickness ρx $gm.cm^{-2}$; z represents the charge on the incident particle and the constant C is given by:

$$C = \frac{\pi N Z r_e^2}{A} = \frac{0.150\, Z}{A} \; gm^{-1}.cm^2 \qquad 2.7$$

where Z is the atomic number and A the atomic weight of the material, N is Avogadro's number and $r_e = e/m_0c^2$ the classical radius of the electron. C represents the total 'area' covered by the electrons contained in one gram of absorber, each considered as a sphere of radius r_e

If the dependance of the collision probability on the parameter of particle and medium is examined: the term Cdx shows the proportionality of the collision probability to the electron density: the term $1/\beta^2$ shows the effect of the time of duration of the collision i.e. a slow particle (small β) spends a long time in the vicinity of each electron giving a correspondingly higher energy transfer: the factor z^2 shows the dependance of the energy transfer on the strength of the electric field at the electron and the $1/(E')^2$ term arises from the higher probability of large impact parameters i.e. the larger the impact parameter the smaller the energy transfer.

The Rutherford formula is valid for $E' << E'_m$ the maximum transferable energy, however when the energy of the knock-on electron is high the relation breaks down and correction terms are necessary. When higher energies are being considered obviously the impact parameter is small and because of this the spin of the incident particle must be taken into account. Bhabha (1939) and Massey and Corban (1939) calculated an expression for the collision probability for particles of mass m and spin $\frac{1}{2}$ given below:-

$$\phi(E,E')dE'dx = 2C.\frac{m_e c^2 z^2}{\beta^2}.\frac{dE'}{(E')^2}\left[1-\beta^2\frac{E'}{E'_m}+\tfrac{1}{2}\left(\frac{E'}{E+mc^2}\right)^2\right]dx \qquad 2.8$$

when $E' << E'_m$ this reduces to equation 2.6

Equations have been derived for other values of the spin of the particle these are listed by Rossi (1952).

It is now possible to calculate the average loss per gm.cm^{-2} $-dE/dx > \eta$ for the close collisions. If ϕ (E, E') dE'dx represents the probability of a particle with kinetic energy E transferring an energy between E' and E' + dE' when traversing an

absorber of thickness dx gm.cm^{-2} then $E'\phi(E,E')\,dx$ will represent the energy lost by the particle. Integrating this over the energy transfer range η to E'_m for close collisions gives the average loss:-

$$-\frac{dE}{dx}(>\eta) = \int_{\eta}^{E'_m} E'\phi(E,E')\,dE'dx. \qquad 2.10$$

Thus for an absorber of thickness 1 gm.cm^{-2}

$$-\frac{dE}{dx}(>\eta) = \int_{\eta}^{E'_m} E'\phi(E,E')\,dE' \qquad 2.11$$

where E'_m may be obtained from equation 2.1. Then substituting for $\phi(E,E')dE'$ from equation 2.8 and imposing the conditions:- $m \gg m_e$, $E \ll \frac{m^2c^2}{m_e}$ and $\eta \ll E'_m$ we find:-

$$-\frac{dE}{dx}(>\eta) = 2C\frac{m_e c^2 z^2}{\beta^2}\left(\ln\frac{E'_m}{\eta} - \beta^2\right) \qquad 2.12$$

2.2.2 Distant Collisions

When considering a distant collision it is necessary to take into account the binding of the electrons to the atoms. Bethe (1930, 1932) developed a theory for the average energy loss $-\frac{dE}{dx}$ due to distant collisions by considering the system formed by an atom and by the incident particle and computing the probabilities for the various possible transitions leading to excitation or ionization of the atom. Using Born's approximation he obtained for a particle of charge z an average energy loss $-\frac{dE}{dx}(<\eta)$ given by:-

$$-\frac{dE}{dx}(<\eta) = 2C\frac{m_e c^2 z^2}{\beta^2}\left[\ln\frac{2m_e c^2\eta\beta^2}{(1-\beta^2)I^2(Z)} - \beta^2\right] \qquad 2.13$$

where I (Z) is the average ionization potential of an atom of atomic number Z. The value of I (Z) can be found theoretically or deduced from experimental data.

Bloch (1933) suggested the relation:-

$$I(Z) = I_H Z \qquad 2.14$$

where $I_H = 13.5$ the energy corresponding to the Rydberg frequency. More accurate calculations have been carried out by Wick (1941, 1943), Halpern and Hall (1948) and Caldwell (1955), these are listed in Rossi (1952). There is an uncertainty in the actual values of I (Z), however the subsequent error introduced in calculating $-\frac{dE}{dx}(<\eta)$ will be small because I (Z) is in the logarithmic term.

2.2.3 The Total Energy Loss by Collision

The total average energy loss for both close and distant collisions will be given by:-

$$\left[-\frac{dE}{dx}(\text{total})\right] = \left[-\frac{dE}{dx}(>\eta)\right] + \left[-\frac{dE}{dx}(<\eta)\right] \qquad 2.15$$

Substitution of equations 2.13 and 2.12 gives:-

$$\left[-\frac{dE}{dx}(\text{total})\right] = 2C\frac{m_e c^2 z^2}{\beta^2}\left[\ln\frac{(2m_e c^2\beta^2 E'_m)}{(1-\beta^2)I^2(Z)} - 2\beta^2\right] \qquad 2.16$$

As would be expected this expression is independant of η the limiting energy. Then substituting for E'_m from equation 2.5 gives:-

$$\left[-\frac{dE}{dx}(\text{total})\right] = 2C\frac{m_e c^2 z^2}{\beta^2}\left[\ln\frac{(4m_e^2 c^2\beta^4)}{(1-\beta^2)I^2(Z)} - 2\beta^2\right] \qquad 2.17$$

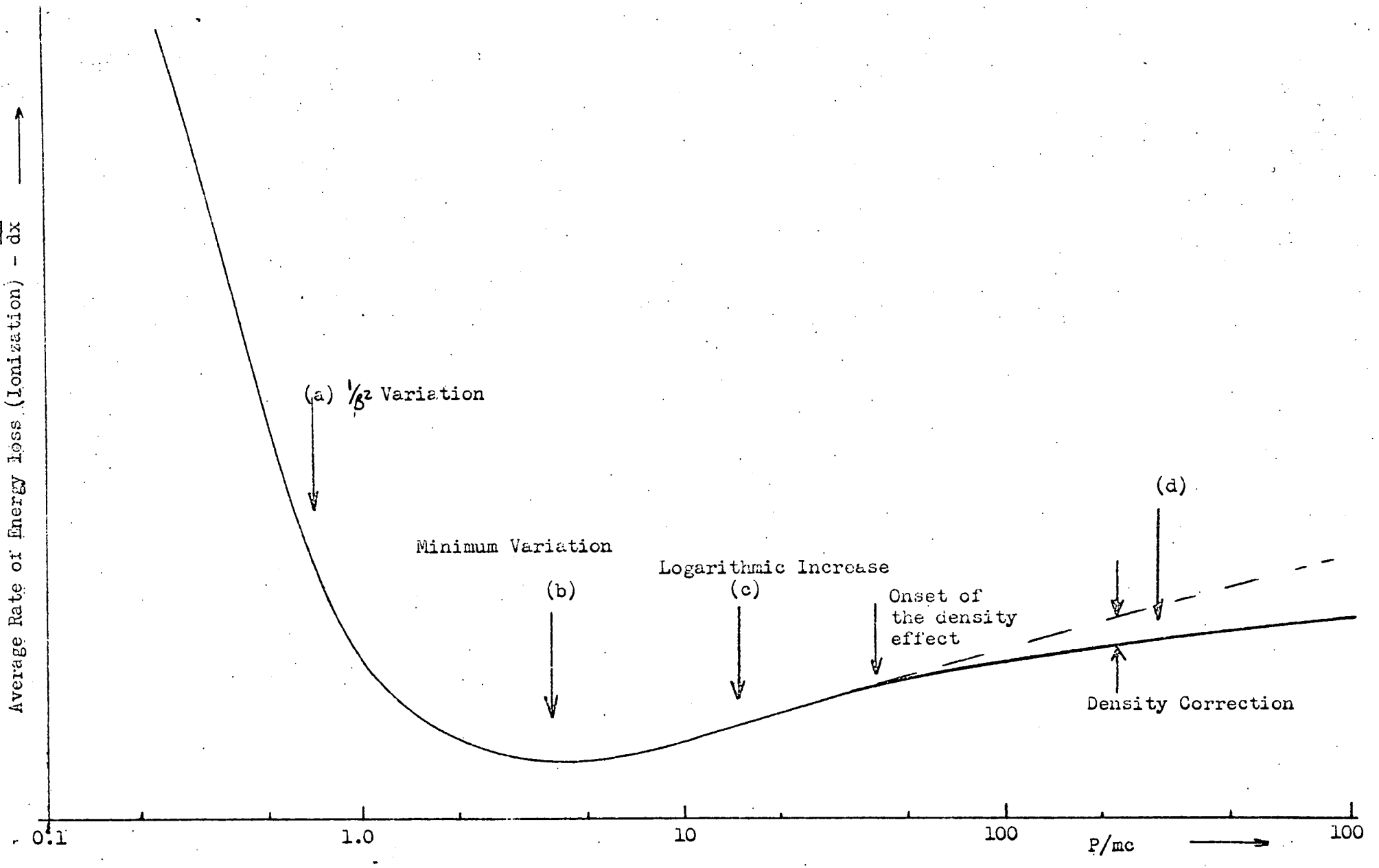

Fig. 2.2 Form of the variation of rate of energy loss with momentum

This is known as the Bethe-Bloch Formula. It will be noted that the energy loss is independant of the mass of the incident particle but a function of its velocity and charge. Further a plot of energy loss $\frac{-dE}{dx}(\text{total})$ versus $\beta (= \frac{v}{c})$ or $\frac{p}{mc} (= \frac{\beta}{1-\beta^2})$ will be a universal curve for all particles with $Z = 1$ providing the mass of the incident particle is much larger than that of the electron, which is the case for muons. Figure 2.2. shows the form of this curve; there are four distinct regions divided according to the particle velocity.

Region (a). The particle has a low velocity with β in the range $0.96 > \beta > 0.1$. This is the classical region, the rate of energy loss falls rapidly as $1/\beta^2$, as the velocity is increased, because the time of collision of the particle with the atom becomes progressively reduced.

Region (b). The particle has a velocity such that β approaches unity, the term $1/\beta^2$ becomes almost constant such that no further reduction can occur and the rate of energy loss takes on a minimum value with $\beta \simeq 0.96$.

Region (c). The logarithmic term in equation 2.16 becomes important producing a slow logarithmic rise. This is due to the increased value of the maximum transferable energy E'_m (This can best be seen by reference to equation 2.15) and to the relativistic extension of the Coulomb field of the incident particle at right angles to its path making the particles' presence felt at large distances from its path.

Region (d). As β increases the logarithmic rise is reduced by the onset of the density effect which will be discussed in the following section.

2.3 Corrections to the Basic Theory

2.3.1 The Density Effect

In studying the interactions of charged particles with atomic electrons the atoms have been considered to be isolated, thus no account has been taken of the effect that neighbouring atoms have on the collision. Any effect will of course depend on the number of atoms in the material. It is in order to neglect to a large extent this effect when considering gases and close collisions, however when the impact parameter is larger than atomic dimensions, as for distant collisions, this is not possible. For such collisions the electric field of the passing particle is screened by the intervening atoms of the media thus reducing the interaction and hence the energy loss. Since the distant collisions become more and more important as the particle velocity increases the correction applied to the energy loss expression is an increasing function of the velocity. Sternheimer (1959) showed that for lead the density effect becomes significant at $\frac{p}{mc} = 100$ i.e. $\beta = 0.99995$ with a correction of about 0.1 MeV/g.cm^{-2} on the energy loss.

Reference to Figure 2.2 shows that despite the density correction there still exists a slow rise in the energy loss. This is explained by the fact that the close collisions are not influenced by neighbouring atoms and increase the energy loss as the value of the maximum transferable energy E'm increases with increasing particle velocity (reference equations 2.12 and 2.2). Thus a density effect correction normally known as the 'Density Correction' must be inserted in equation 2.12 which then becomes:-

$$\left[-\frac{dE}{dx(total)}\right] = 2C\frac{m_e c^2 z^2}{\beta^2}\left[\ln\left(\frac{4m_e^2 c^2 \beta^4}{(1-\beta^2)^2 I^2(2)}\right) - 2\beta^2 - \delta(\beta)\right] \qquad 2.18$$

Although Swann (1938) put forward the idea of a 'Density effect' Fermi (1940) was the first to treat it theoretically. Assuming only one dispersion frequency he calculated the Poynting Vector for the radiation field of the excited macroscopic absorber and equated it to the energy loss giving the following expressions for $\delta(\beta)$ for the case of singly charged particles.

$$\text{for } \beta < \epsilon^{-1/2} \quad \delta(\beta) = 2C \frac{m_e c^2}{\beta^2} \ln \epsilon \qquad 2.19$$

$$\text{for } \beta > \epsilon^{-1/2} \quad \delta(\beta) = 2C \frac{m_e c^2}{\beta^2} \left[\ln \frac{\epsilon - 1}{1 - \beta^2} + \frac{1 - \epsilon\beta^2}{\epsilon - 1} \right] \qquad 2.20$$

where ϵ is the dielectric constant of the medium relative to vacuum.

Halpern and Hall (1940, 1948) and Wick (1941, 1943) extended Fermi's treatment by considering in detail the behaviour of atomic electrons belonging to different shells. This showed again the dependance of the collision loss on the density of the medium and that Fermi's theory over estimated the reduction in the collision loss. However agreement between the two studies was poor (see Rossi 1952). Further studies were made by A. Bohr (1948), Messel and Ritson (1950) and Schonberg (1951). They pointed out that part of the energy dissipated by high energy particles in their interactions with atomic electrons goes into Cerenkov radiation rather than into excitation or ionization of atoms. The intensity of the Cerenkov radiation increases with increasing velocity such that it appears that the relativistic increase of the energy loss by distant collisions is mainly due to the increase of this radiation. (Cerenkov radiation reabsorbed).

Finally Sternheimer (1956) evaluated the density correction for different absorbers taking into account the true dispersion frequencies of the atomic electrons. His result was identical to that of Fermi for $\beta > \epsilon^{-\frac{1}{2}}$ and differed by only a few percent in the region $\beta = \epsilon^{-\frac{1}{2}}$, Sternheimer's expression for the 'Density Correction' is used later in this chapter to evaluate a theoretical curve for the most probable energy loss in the absorber used in this experiment.

2.3.2. Radiative Corrections

Tsytovitch (1962βa,b,c) has predicted a reduction in the energy loss due to small energy transfers at high particle velocity by taking into account radiative corrections. These radiative corrections to the basic theory result from the multiple virtual emmision of photons by the incident particle and Tsytovitch has carried out a calculation of this effect ~~to the order of e^4~~. Providing the group velocity of the virtual X-ray photons is smaller than the particle velocity he stresses that the interaction of the virtual photons with the material greatly magnifies the effect, i.e. for extremely high particle energies and for high density material.

A density effect applies to these radiative corrections and occurs at energies larger than those at which the density effect in the main part of the losses arises. When these radiative corrections are taken into account Tsytovitch finds that a decrease of ionization energy loss of about 7 to 10 percent for densities of approximately 4 $g.cm.^{-3}$ and electron energies with $E > 200 mc^2$ should occur. Thus the effect if real should be detected (with muons) in the energy range 10 - 100 GeV.

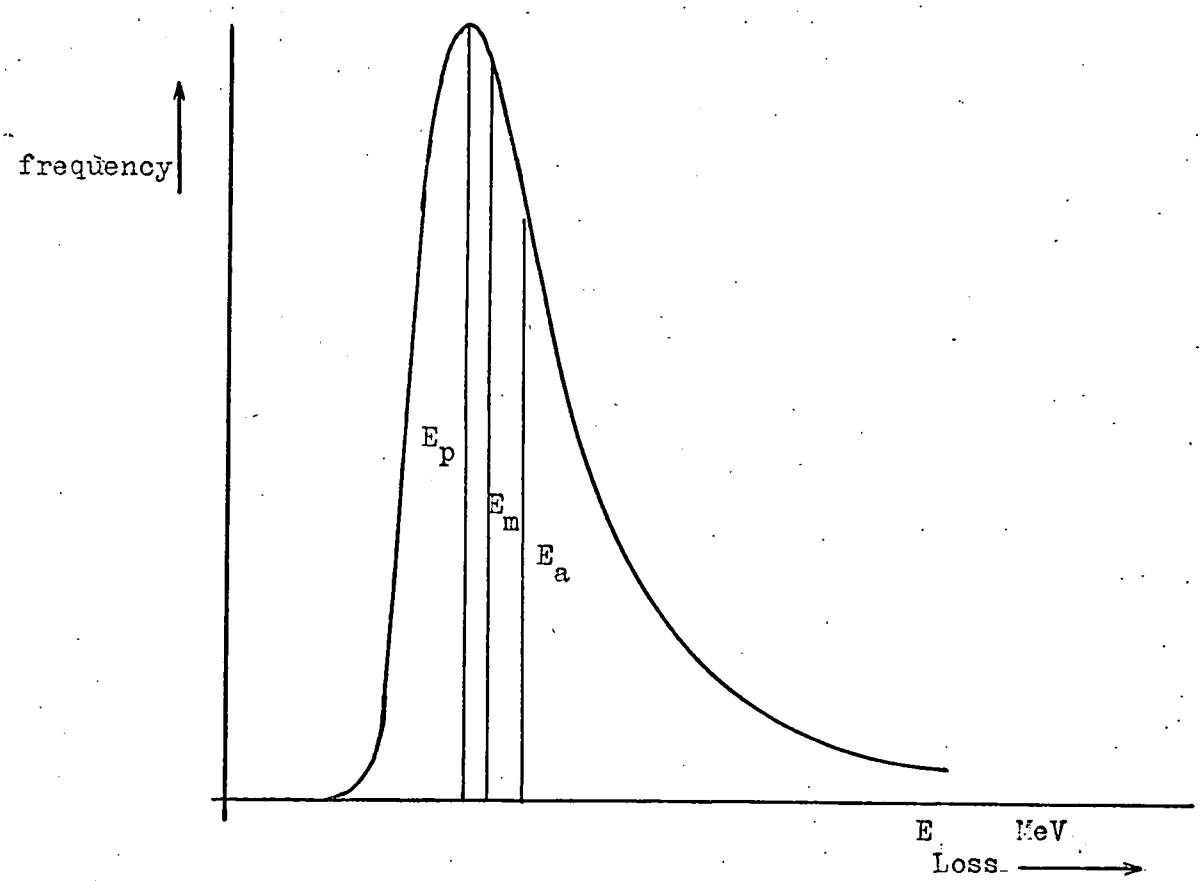

E_p = Mode Value

E_m = Median Value

E_a = Mean Value

Fig 2:3 Relative positions of the mode, median and mean

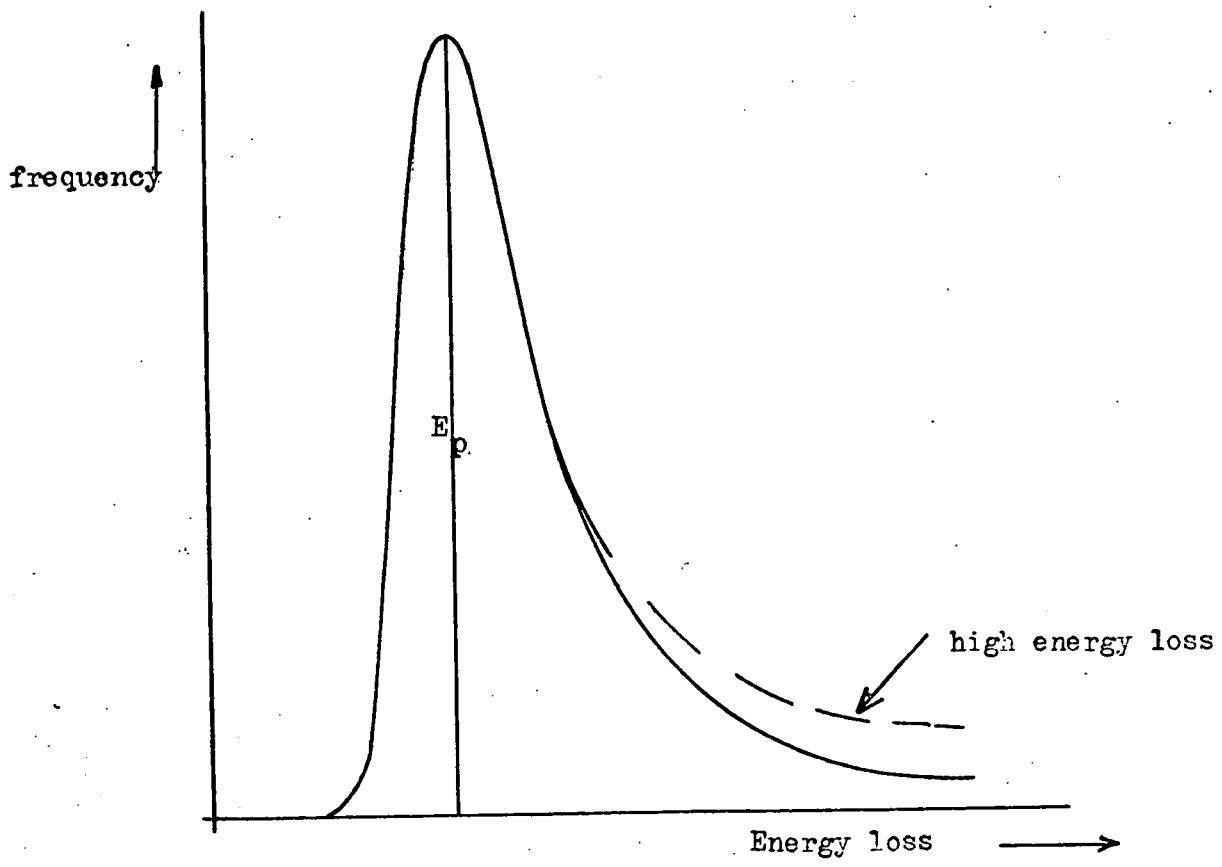

Fig 2:4 The mode value Ep is insensitive to the high energy loss

2.4 The Most Probable Energy Loss

2.4.1 Introduction

When a particle of a given incident energy passes through a given thickness of material the energy lost by it is the result of a large number of independant collisions. No unique value for the energy loss is obtained for a given energy and it must therefore follow a distribution. Landau showed the resultant distribution of energy loss to be a negatively skewed distribution Figure 2.3, the high energy tail being caused by collisions in which a large amount of energy is transferred to the target electron. It is the peak of this distribution which is measured experimentally i.e. the most probable energy loss.

It has already been indicated that experimentally it is difficult to record all the energy deposited from high energy losses using a thin absorber because the resulting high energy electrons escape from the absorber, or the associated electronics saturate although the latter problem can be overcome. Thus the mean energy loss is not recorded because these high energy losses are not present. Reference to Figure 2.4 shows that the most probable energy loss unlike the median and mean value is insensitive to these high energy losses. Thus providing the mode value or most probable energy loss is taken these high energy losses can be neglected by imposing an upper cut off. It is now necessary to give an expression for this most probable energy loss as previously we have derived an expression for the Average Energy loss.

2.4.2 An Expression for the Most Probable Energy Loss Ep.

Symon (1948) showed that the most probable energy loss of a singly charged heavy particle traversing an absorber of thickness x g.cm^{-2} is given by:-

$$E_p = 2\frac{C m_e c^2 x}{\beta^2}\left[\ln\left(\frac{4C m_e^2 c^4 x}{(1-\beta^2) I^2(Z)}\right) - \beta^2 + j - \delta(\beta)\right] \qquad 2.21$$

where j is a function of the parameter G given by

$$G = \frac{C x (1-\beta^2)}{\beta^4}$$

Note that this expression is identical to that derived by Landau for G < 0.05 where j then has the constant value of 0.38. Sternheimer (1952, 1953, 1956) also obtained the above expression and it is more convenient to use his notation. Ep the most probable energy loss is then given by:-

$$E_p = \frac{Ax}{\beta^2}\left[B + 1.06 + 2\ln\left(\frac{P}{M_\mu c}\right) + \ln\left(\frac{Ax}{\beta^2}\right) - \beta^2 - \delta(\beta)\right] \qquad 2.22$$

where m_μ = mass of the incident particle.

$$A = 2C m_e c^2 \qquad \text{and} \qquad B = \ln \frac{(m_e e^2 (10^6)\ \text{eV})}{I^2(Z)}$$

The term $\delta(\beta)$ represents the density correction and Sternheimer gave expressions for this as follows:-

$$\delta(\beta) = 4.606 . X + C_1 + a (X_1 - X)^m \quad \text{for} \quad X_0 < X < X_1 \qquad 2.23$$

$$\delta(\beta) = 4.606 . X + C_1 \quad \text{for} \quad X > X_1 \qquad 2.23a$$

where $X = \log\left(\frac{p}{m_\mu c}\right)$ and a, m, & C_1 are constants

which depend on the absorber. X_0 is the value of X which corresponds to the momentum below which $\delta(\beta) = 0$. X_1 corresponds to the momentum above which the relation between $\delta(\beta)$ and X can be considered linear.

Substituting for X in 2.23 and 2.23a.

$$\delta(\beta) = 2\ln\left(p/m_\mu c\right) + C_1 + a(X_1 - X)^m \qquad 2.24$$

$$\delta(\beta) = 2\ln\left(p/m_\mu c\right) + C_1 \qquad 2.24a$$

In the experiment to be described a plastic phospher N.E.102a was used to measure the energy loss. For this X_1 takes the value 2 i.e. $\log\left(p/m_\mu c\right) < 2$ which corresponds to a momentum $p < 10.56$ GeV/c.

Thus for particles of momentum < 10.56 GeV/c $\delta(\beta)$ is given by equation 2.24 and for particles of momentum > 10.56 GeV/c by equation 2.24a.

Substituting the expressions for $\delta(\beta)$ in the equation 2.22 for the most probable energy loss.

For particles having momentum $p < 10.56$ GeV/c

$$E_p = \frac{Ax}{\beta^2}\left[B + 1.06 + \ln\left(\frac{Ax}{\beta^2}\right) - \beta^2 - C_1 - a(X_1 - X)^m\right] \qquad 2.25$$

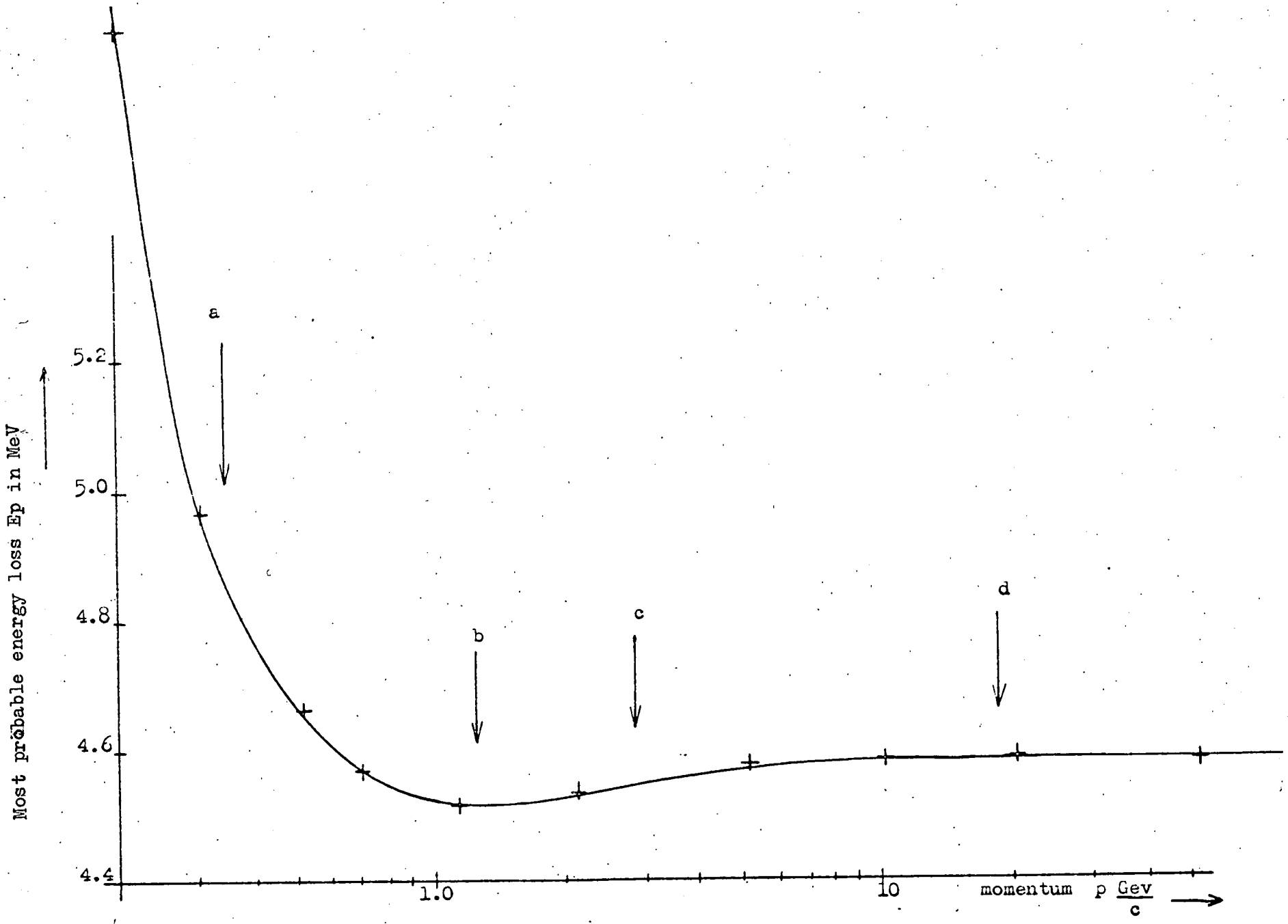

Fig. 2.5 Theoretical curve for most probable energy loss in plastic phosphor 2.5 cms thick.

For particles having momentum $p > 10.56$ GeV/c

$$E_p = \frac{A x}{\beta^2}\left[B + 1.06 + \ln\left(\frac{A x}{\beta^2}\right) - \beta^2 - C_1\right] \qquad 2.26$$

Equations 2.25 and 2.26 show that Ep depends only on the constants of the absorber and the particle velocity For particles having momentum $>$ 10.56 GeV/$_c$ β may be taken as unity such that Ep becomes invariant for incident particles with momentum higher than 10.56 GeV/c.

The constants in the Sternheimer equations 2.25, 2.26, have the following values for the N.E.102a plastic phosphor absorber.

A = 0.0833 MeV/g	B = 18.69
a = 0.514	C_1 = -3.13
m = 2.595	x_1 = 2
I(z) = 62.6eV	x_0 = 0.044

Using equations 2.25 and 2.26, the values of Ep for various momentum in the range 50 meV to 1000 GeV have been calculated for a plastic phosphor 2.5 cms. thick and are presented graphically in Figure 2.5

2.4.3. Comparison of the Most Probable Energy Loss Curve with the Average Energy Loss Curve

The regions denoted by (a), (b), (c), and (d) in Figure 2.5, the most probable energy loss curve, refer to the same regions as in the average energy loss curve given in Figure 2.2. It can be seen that there is little difference in the shape of the curve over the regions (a) and (b), however in the region (c) the logarithmic rise is less than that for the average loss curve. This

is easily understood because although the maximum transferable energy E'_m is increasing it does not influence the mode value Ep. ~~such~~ Thus the increase in Ep in this region is due solely to the relativistic extension of the Coulomb field. The fact that Ep is invariant to the increasing values of E'_m becomes more pronounced in the region (d). In the average energy loss curve, E_a increases in this region with increasing values of β because of the corresponding increase in E'_m for close collisions, this is despite the reduction in E_a caused by the density effect. Without this increase for close collisions, which is the case when considering Ep the most probable energy loss, Ep approaches a constant value and the curve takes on the form of a plateau.

CHAPTER 3

Recent Work on Energy Loss in Plastic Phosphor Scintillation Counters

Because the relativistic rise in the energy loss curve depends on the magnitude of the density correction which varies depending on the value of the atomic number Z for the absorber, (see Sternheimer 1952) it is only of interest to consider experiments which have used similar absorbers. Three experiments are described; Barnaby (1961), Crispin and Hayman (1964), and Smith and Stewart (1966).

3.1 Experiment by Barnaby 1961

This was one of the first experiments to use plastic phosphor as an absorber with which to measure ionization loss and was a fore-runner to the experiment by Crispin and Hayman. Figure 3.1 shows the experimental set up which was placed 55 m.w.e. underground where the incident radiation is more homogeneous than at sea level. A large plastic phosphor 58 cm. x 17.5 cm. x 3.8 cm. was used to measure the energy loss of the incident muons and their energies estimated by using lead absorbers in the telescope. A simple hodoscope arrangement indicated whether the muons had stopped between Geiger trays C and D or Geiger trays D and E or had passed through tray E. 12.5 cms. of lead was placed between the trays C and D and between trays D and E. Different thicknesses of lead 10, 35, 85 cm. were placed succesively between trays A and C. This enabled six different muon energy ranges to be detected because some particles were stopped between C and D and others between D and E.

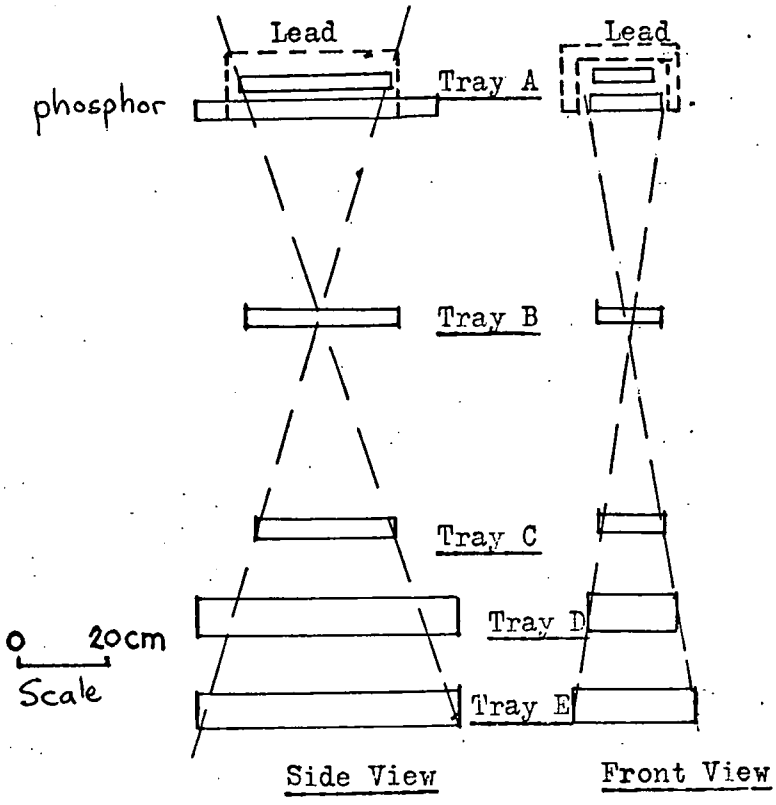

Fig 3:1 The telescope used by Barnaby

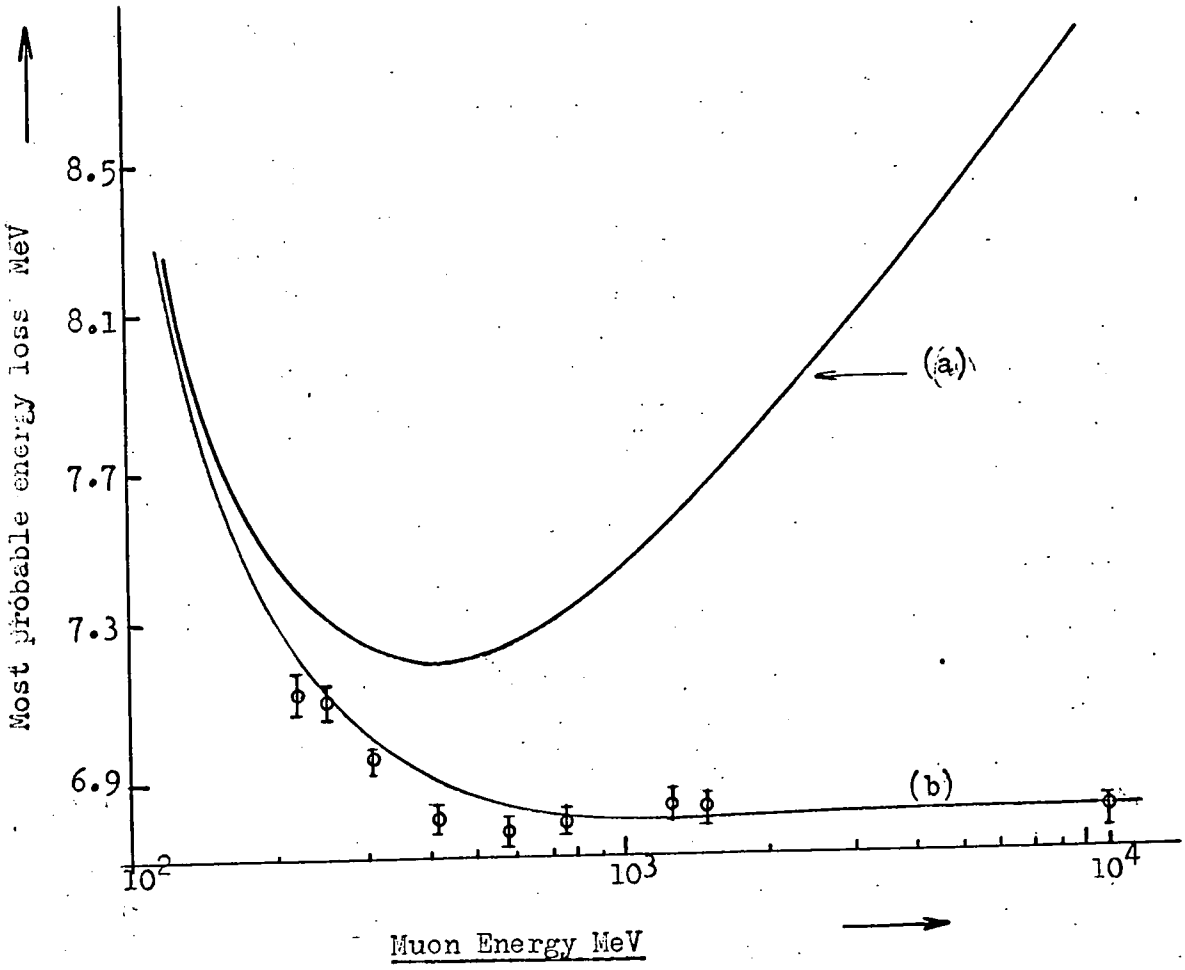

Fig 3:2 The experimental results of Barnaby

Two final points were determined by using 7.5 cm. of lead between tray C and D, 7.5 cm. between D and E and 10 cm. between A and C. With the maximum amount of lead in the telescope the minimum energy of the particles which just passed through was 1.55 GeV. Then for all particles which passed right through, a median energy of 10 GeV was calculated from the energy spectrum at 55 m.w.e. Thus the energy loss was determined for nine values of particle momentum.

The results are shown in Figure 3.2. Curve (a) shows the most probable energy loss distribution for muons in the phosphor calculated according to ~~Sternheimer~~ Bethe-Bloch without the density correction and curve (b) shows the distribution with the density correction. Barnaby concluded that the results did not show any significant rise (less than 1%) between 0.5 and 10 GeV and were in agreement with the Sternheimer prediction that the density effect in organic materials is sufficiently large to eliminate the relativistic increase of the most probable energy loss of muons.

3.2. Experiment by Crispin and Hayman 1964

This experiment was designed to extend the previous investigation by Barnaby to energies approaching 200 GeV. The scintillation counter of dimensions 55 cm. x 17.5 cm. x 3.7 cm. was similar to that used by Barnaby. This was mounted in the middle of the Durham cosmic ray spectrograph; the experimental arrangement is shown in Figure 3.3. Geiger counters were used as detectors and recorded the particle track automatically. The associated electronics and automatic recording systems have

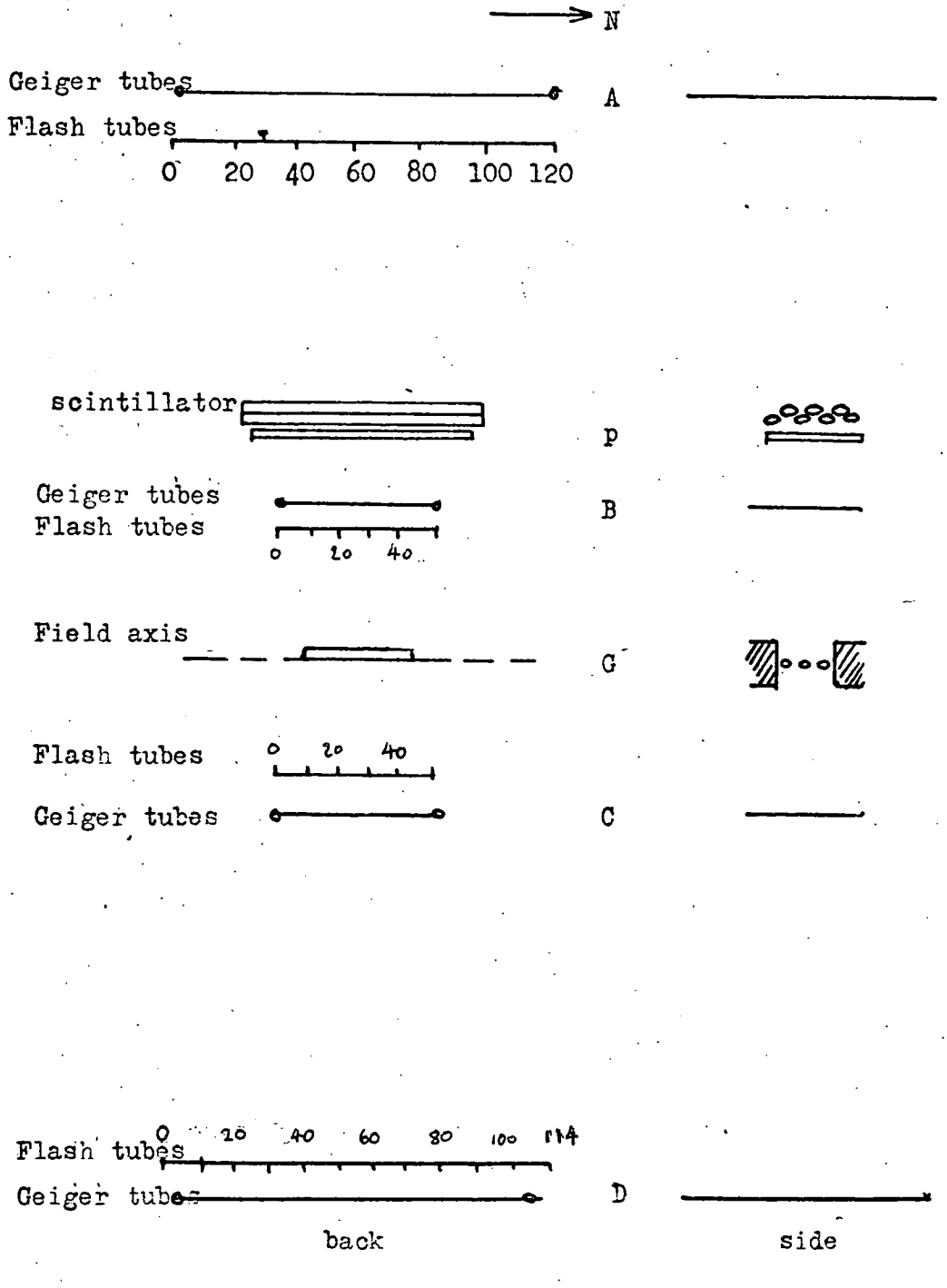

Fig 3:3 The experimental arrangement of Crispin and Hayman

been described by Brooke et al (1962) and Jones et al (1962). In order to make high energy measurements, requiring greater accuracy, layers of neon flash tubes were used. These have been described in detail by Hayman and Wolfendale (1962) and it is the results from these measurements that are discussed.

There were four measuring levels A B C and D in the spectrograph, two above and two below the large electromagnet. Each level had a tray of Geiger counters and eight layers of flash tubes. P and G are the counters associated with the scintillator and magnet gap respectively, Figure 3.3. The pulses from the scintillation counter were analysed using a logarithmic pulse height analyser, Barton and Crispin (1962).

Two series of experiments were performed, the first in the momentum range 0.4 to 10 GeV/c ran concurrently with a proton absorption experiment in which a layer of lead was placed above the level D. Particles passing through this layer were recognised as muons. In the second, particles having momenta above 3 GeV/c were selected electronically using a momentum selector described by Hayman and Wolfendale (1962).

The two sets of data were combined for the final result and are shown in Figure 3.4 together with the results obtained by Barnaby 1961 and the theoretically predicted curve using Sternheimer's density correction. Since it was possible to distinguish the charge of particles passing through the spectrograph the ratio of positive to negative muons was measured, a value of 1.009 ± 0.015 was obtained which is consistent with there being no difference in ionizing power between the two.

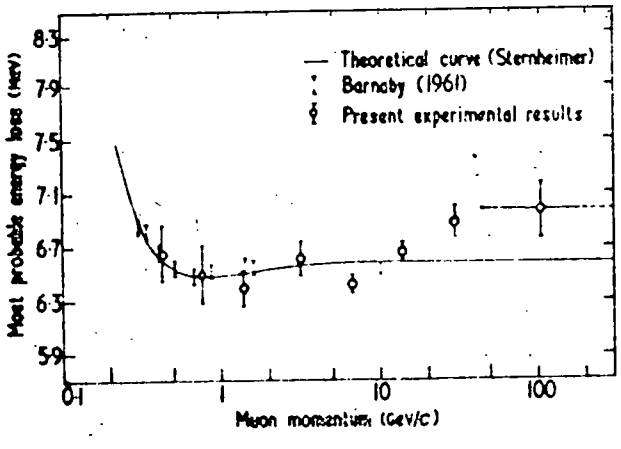

Fig 3:4 The results of Crispin and Hayman

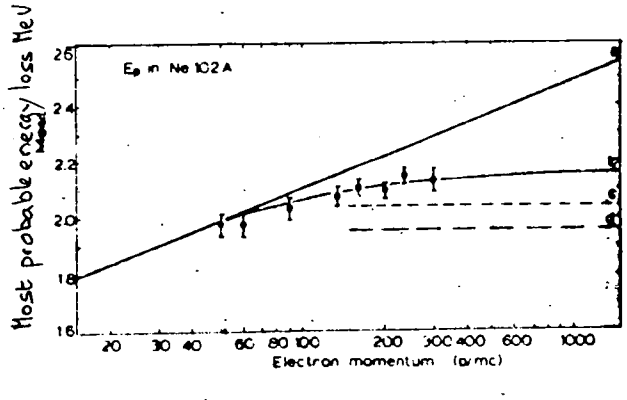

Fig 3:5 The results of Smith and Stewart

Crispin and Hayman concluded that within the experimental error their results agreed with Sternheimer's theory up to a momentum of 15 GeV/c which predicts a 1.5% rise over the range 0.2 to 10.5 GeV/c and no further rise above this momentum. There was however an indication of a slight increase of 3% $\pm$1% over the theoretical value at 100 GeV/c. The results are comparable with those of Barnaby within the experimental error and lend no support to the theory of radiative corrections by Tsytovitch.

3.3 Experiment by Smith and Stewart

The ionization loss of relativistic electrons in the energy range 20 - 150 MeV has been studied in a small area scintillator consisting of a N.E. 102a plastic phosphor disc 3.1 mm. thick and 2.5 cm. in diameter. The electron beam was obtained from a pair spectrometer placed in the bremsstrahlung beam of a 320 MeV electron synchroton. The field of the spectrometer could be varied to supply electrons up to 156 MeV energy. The beam after passing through the counter under investigation C1 was defined by two small counters C2 and C3 to within $\pm 1^{o}$, these counters were also used to gate a pulse height analyser recording the pulse height from C1.

The experimental results are given in Figure 3.5 together with the theoretical curve predicted by Sternheimer's theory for the energy loss. Curve (a) shows the loss without the density corrections and (b) with it included. The results agreed well with Sternheimers theory and did not support the decrease predicted by Tsytovitch.

3.4 Summary

All three experiments support the Sternheimer theory of energy loss and give no indication of the 7 - 10% decrease over the momentum range 10 - 100 GeV/c predicted by Tsytovitch.

Of the three experiments that by Crispin and Hayman is the most reliable. The muon energies were determined using a cosmic ray spectrograph such that errors affecting the energy loss i.e. Systematic drift in the electronics and ageing of the plastic phosphor of the scintillation counter, could be neglected. This is because a spectrograph accepts particles of all momenta in each day's run so that any drift etc. will not affect the actual energy loss values relative to each other.

The experiment by Barnaby suffered from lack of precision in determining the particle energy because the method relies on estimating a mean value of particle energy for all particles which have been stopped in a given thickness of absorber.

The results of Smith and Stewart show a rise of about 8% over the measured range $\gamma = 50$ to 300, this is inconsistent with theory, for these values of γ the energy loss curve for plastic phosphor will have reached the plateau value. The theoretical curve given by the authors does not correspond to that predicted by the Sternheimer theory for a plastic phosphor counter and it is unfortunate that the momentum range is too restricted to enable the general form of the energy loss curve to confirm the validity of the results. A systematic drift in the electronics could account for the rise in the curve because the energy loss was measured separately for each value of momentum i.e. the field of the synchroton was adjusted so that the beam contained particles

of a given momentum and the energy loss for this value of momentum was then measured. However the authors confirm that the electronics were checked against drift during the experiment.

CHAPTER 4

The Durham Mk 3 Horizontal Spectrograph

This instrument was designed to supersede the Mk II spectrograph by providing a much larger accepting power to inclined muons, with a magnetic air gap deflection to reduce errors due to elastic scattering of the muons.

4.1 A Brief Description of the Instrument

A deflection plane view and a back plane view of the spectrograph are given in Figures 4.1 and 4.2. The spectrograph consisted of four flash tube trays A.B.C. and D. which defined the trajectory of the particles in the deflection plane passing through it. S1. S2.S3.S4. and S7. were plastic phosphor coincidence scintillators. S5. and S6. were plastic phosphor anti-coincidence scintillators i.e. a pulse from S1. or S7, S2, S3 or S4, and no pulses from S5, and S6, constituted an event which triggered the flash tube trays.

The electromagnet used was of the Blackett type, constructed by Metro Vickers with an air gap of 38 cm. producing a field of 4 kilogauss at 40 amps. The field could be increased further by reducing the air gap and this would serve to increase slightly the maximum detectable momentum (M.D.M). The deflection of the muons was in the horizontal plane and thus was symmetrical for both positive and negative muons, hence the acceptance for both particles was the same. It should be noted that in the previous Mk II spectrograph the deflection was in the vertical plane which lead to possible assymetries in the results. Probably the most important advantage over this Mk II spectrograph was the air gap magnet which reduced considerably the problems of scattering. The Mk III spectrograph was positioned to select particles from a direction 27° East of geomagnetic North.

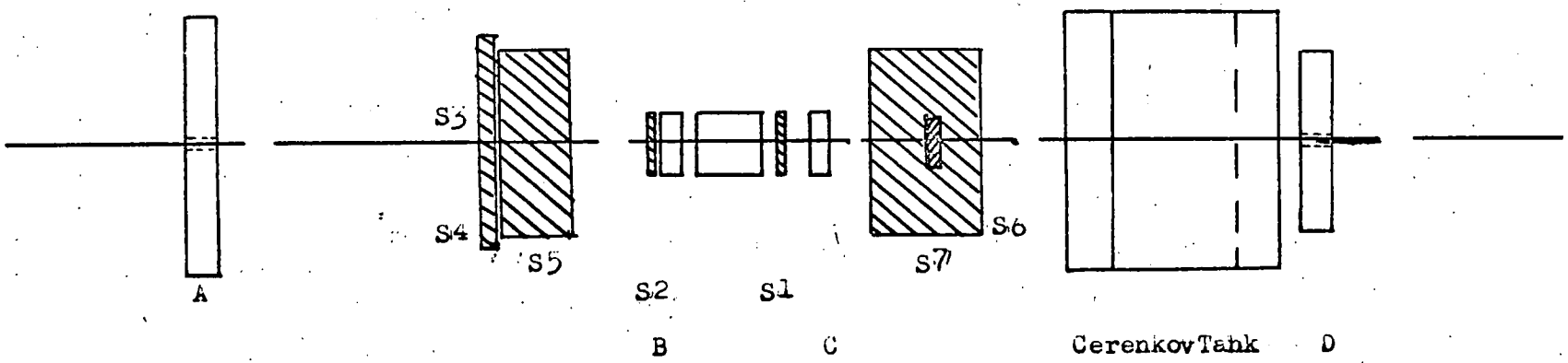

Fig. 4.1. Deflection plane view of the spectrograph

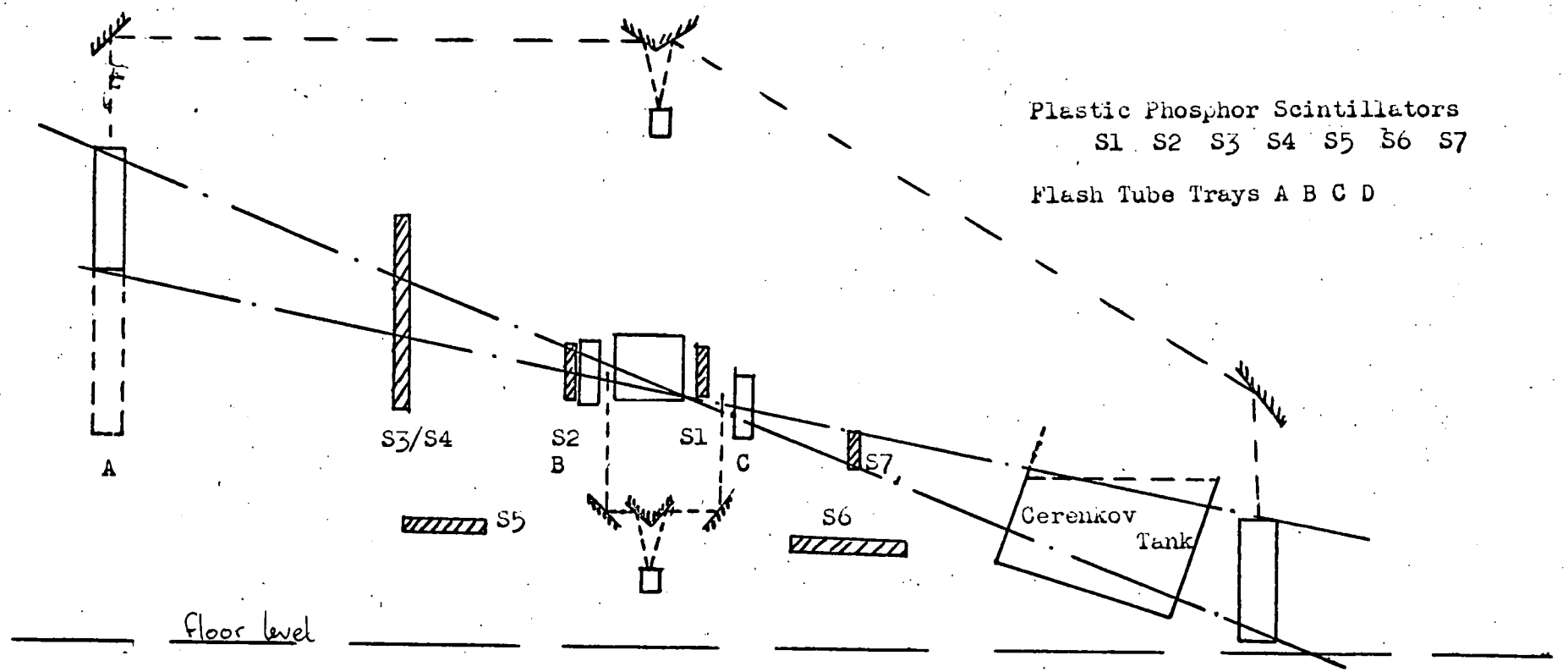

Fig. 4.2 Back plane view of the spectrograph

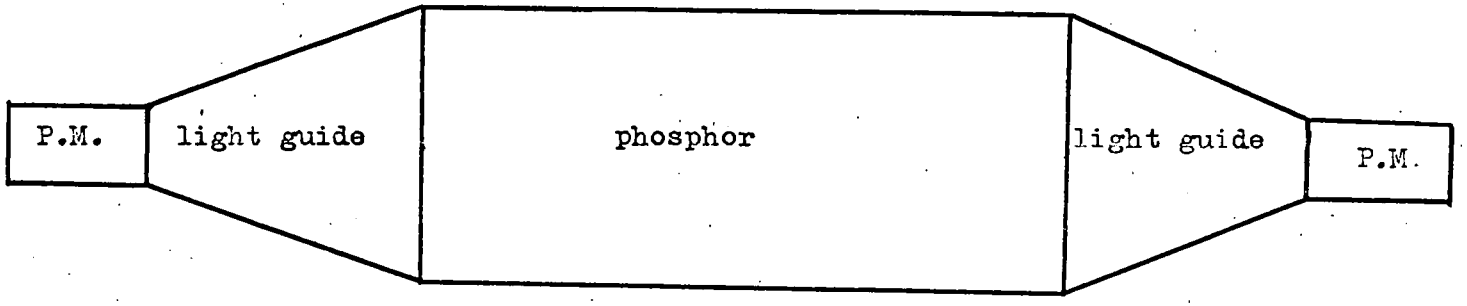

Fig 4:3 Schematic diagram of a scintillation counter

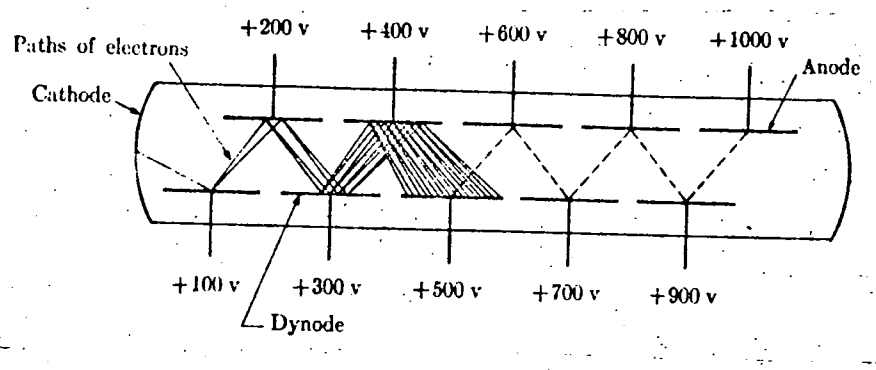

Fig 4:4 Schematic diagram of a photomultiplier tube.

4.2 The Scintillation Counters

The scintillation counters S3, S4, S5 and S6, which were identical and counter S7 are described in this section. Counters S1 and S2 which were also identical are discussed in Chapter 5. A Scintillation counter normally consists of a rectangular phosphor with ~~two~~ a light guide at each end to which are attached photomultipliers. Schematic diagram Figure 4.3. A particle passing through the counter excites or ionizes the atoms in the phosphor. Most of the excitation energy is lost in heat but about 20% (for the most efficient phosphors, Breitenberger 1955) reappears as light as the atoms return from their metastable excited state to the ground level state. This light, (say 25%) is then picked up by the photocathodes of the photomultiplier tubes cemented to the ends of the perspex light guides; a small fraction of the light will of course be lost due to reabsorption in the phosphor and by total internal reflection trapping within the phosphor and light guide assembly. The incident photons on the photocathode of the photomultiplier tube produce photoelectric emmision and the subsequent electron current is amplified by secondary emmision from the dynodes of the tube. A schematic diagram of a photomultiplier tube is given in Figure 4.4. The final pulse is produced between the anode of the tube and earth and is proportional to the energy absorbed by the phosphor.

4.2.1 Description of the Counter Assembly for Counters S3,S4,S5,S6.

A diagram of the scintillation counters S3, S4, S5 and S6, is given in Figure 4.5. ~~These~~ Each counter consisted of a rectangular piece of plastic phosphor N.E. 102a manufactured by Nuclear

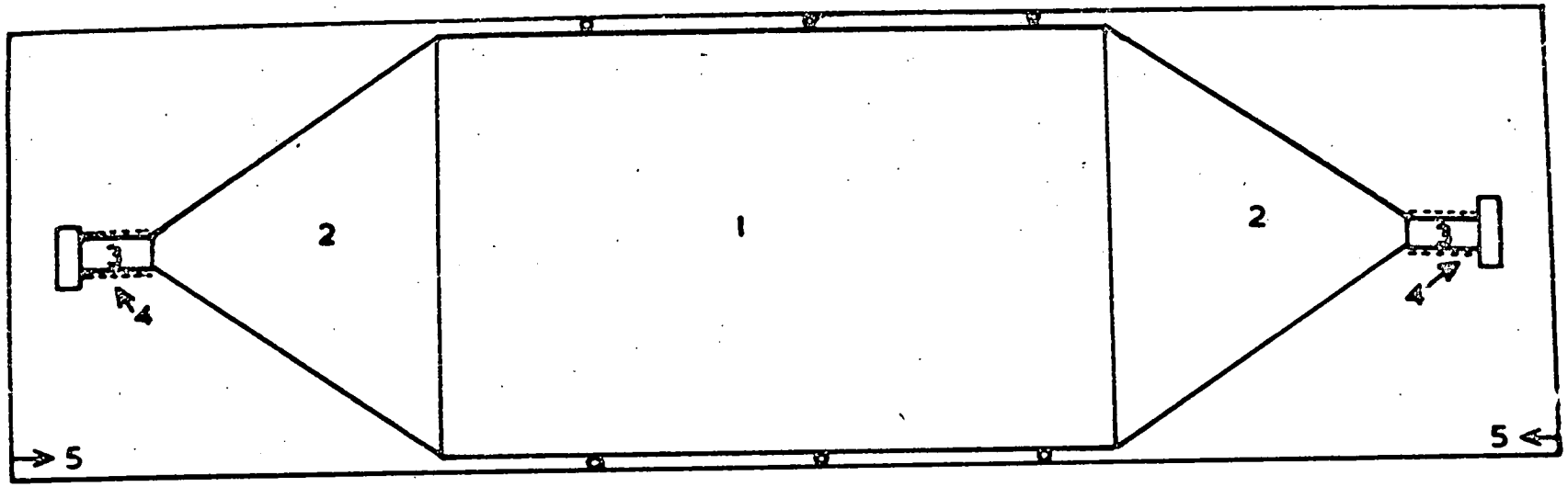

1. Phosphor
2. Perspex Light guide
3. Photomultipliers
4. Mu-metal shield
5. Aluminium Frame

Fig. 4.5 The basic design of the scintillation Counters

Enterprises. The makers quote a density of 1.032 $gm.cm.^{-3}$ and a decay time for the fluorescence of about 3 n sec.i.e. this is the average time for an atom to decay from its metastable state back to its ground state. The dimensions of each counter are given in table 4.1

TABLE 4.1

Counter	Length	Breadth	Thickness
S3	133	75	5
S4	133	75	5
S5	155	55	3.8
S6	133	75	5
S7	22.86	22.86	2.54

Dimensions given are in cms.

To this phosphor were attached two perspex light guides and to the end of each of these a Mullard 53 AVP photomultiplier. All joints were cemented with an optical cement type N.E.580 again supplied by Nuclear Enterprises. It was necessary to screen the photomultiplier tubes from any stray magnetic field which would deviate the secondary electrons passing between the dynodes of the tube and hence affect the gain of the tube. To do this a cylindrical mu-metal shield, and then an outer iron shield concentric with it, was placed over each photomultiplier tube. The iron shield served to reduce any large magnetic field to the order of a few gauss which was then eliminated by the mu-metal shield. Each counter assembly after being cleaned very carefully was placed in a frame of aluminium channel on supports which held the phosphor firmly in place. To make the whole assembly light tight the sides of the frame were covered with 20 gauge (0.022") aluminium sheet screwed in place and all joints were then covered with plastic tape supplied by the '3M' Company. On the first counters the joints were first filled

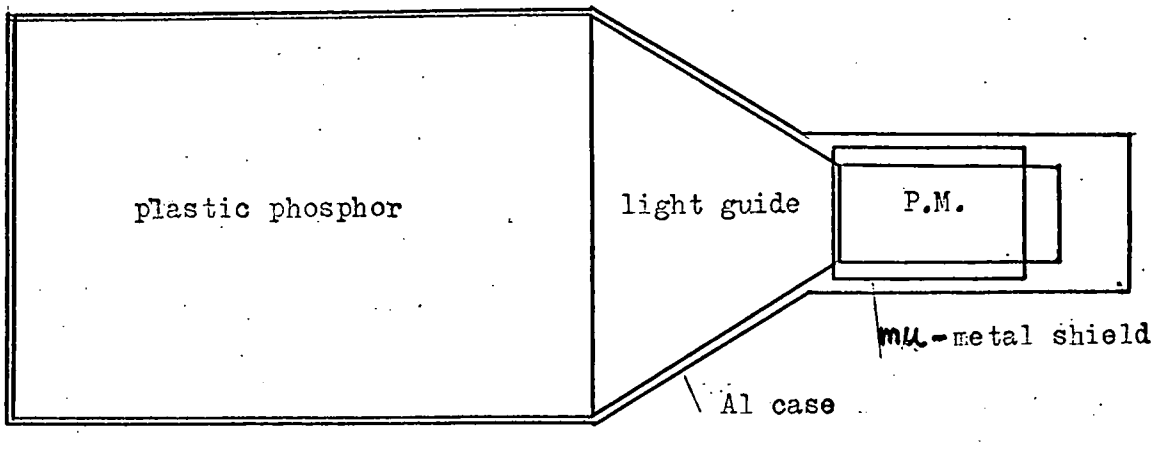

Fig 4:6 Schematic diagram of counter S7.

with plasticine however it was found later that this was an unnecessary precaution and possibly affected the adhesion of the tape. The base of each photomultiplier tube was earthed to the counter frame, and the E.H.T. and pulse output leads were taken from each base through holes drilled in the counter frame to make the necessary connections to the head amplifier units of each counter.

4.2.2 Description of the Counter Assembly for Counter S7

A diagram of counter S7 is shown in Figure 4.6. This counter had only one light guide attached to the plastic phosphor N.E.102a, the dimensions are given in Table 4.1. A Mullard 53 AVP photomultiplier was cemented to this light guide with optical cement N.E.508. Construction details were as for counters S3, S4, S5 and S6, and the assembly was mounted in an aluminium box sealed with plastic tape. This type of counter is obviously not as efficient as those fitted with two photomultiplier tubes as part of the light collection relies on reflection from the blank end of the counter.

4.2.3 The Positions of the Counters in the Spectrograph

Figures 4.1 and 4.2 show the relative positions of the counters. Counters S1, S2, S3, S4 and S7 were all mounted ~~with their broadside~~ vertically at right angles to the axis of the spectrograph. Counters S1 and S2 (described in Chapter 4) were mounted ~~vertically~~ with the axes of the photomultipliers horizontal, in an aluminium frame. This was necessary to eliminate any distortion of the mounting frame by the field from the electromagnet. Counters S3 and S4 were mounted vertically with the axes of the photomultipliers

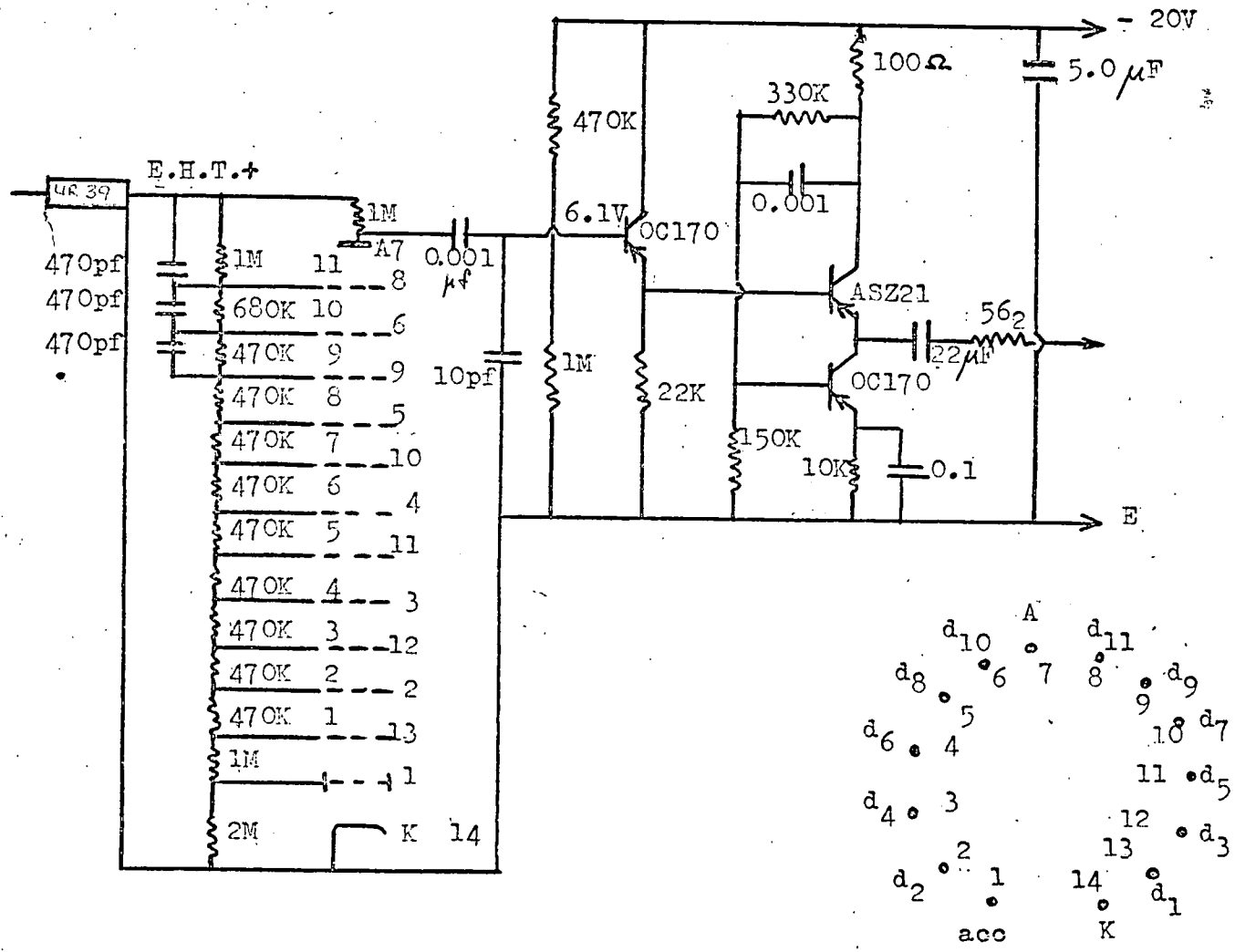

Fig 4:7 Photomultiplier chain and head unit for scintillator counters
Inset – pin connection on PM base

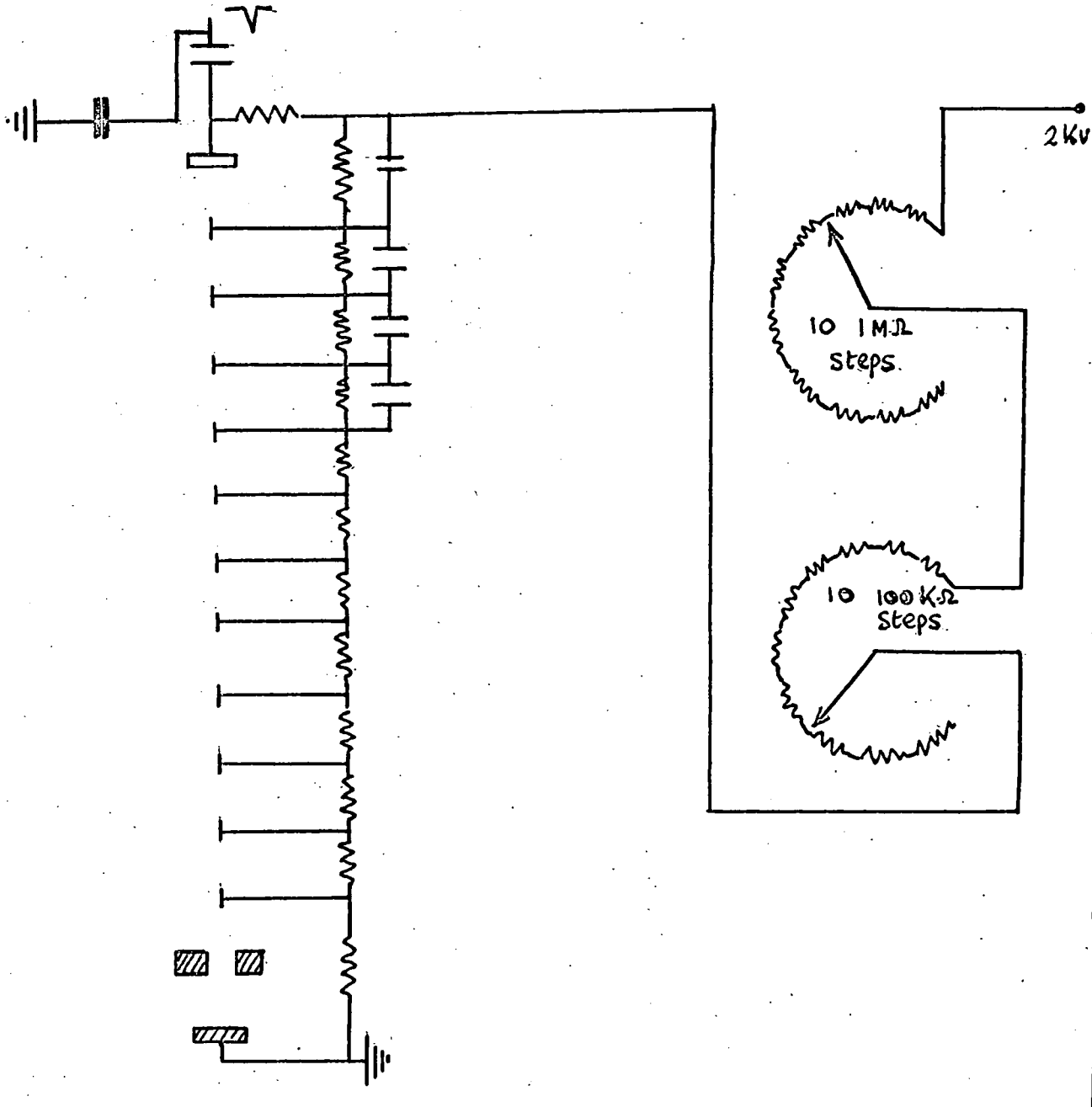

Fig 4:8 E.H.T. Supply to photomultipliers

vertical in a steel frame-work. The anti coincidence counters S5 and S6 were placed horizontally while counter S7 was supported vertically with its photomultiplier at the lower end.

4.2.4 The Counter Electronics and Balancing of the Counters

Figure 4.4 shows that each consecutive dynode of a photo-multiplier tube has an increasing potential placed on it with respect to the cathode which is earthed such that the secondary electrons are accelerated from one dynode to the next. To do this a dynode resistor chain was connected to the base of each photomultiplier tube, the resistor values which were used along with the head amplifier circuit for the Mullard 53 AVP tubes are shown in Figure 4.7. The actual pin connections to the base of the photomultiplier tube are also given.

For each scintillation counter the two photomultipliers had to have equal gain, i.e. the most probable pulse height from each tube had to be the same to within a few per cent. To do this each tube was supplied with a variable high tension voltage. The circuit for this is shown in Figure 4.8. A two kilovolt high tension supply was fed to each tube through a ten position adjustable 1M Ω potentiometer for coarse control and in series with this a ten position 100k Ω potentiometer for fine control. To adjust the gain of each photo-multiplier tube for a particular counter the following procedure was adopted.

The output from one of the tubes was fed into a Pulse Height Analyser, and the Analyser was triggered by a scintillation counter telescope selecting cosmic ray particles passing through the centre of the counter Figure 4.9. The most probable pulse height for the photomultiplier tube was thus determined. This was repeated

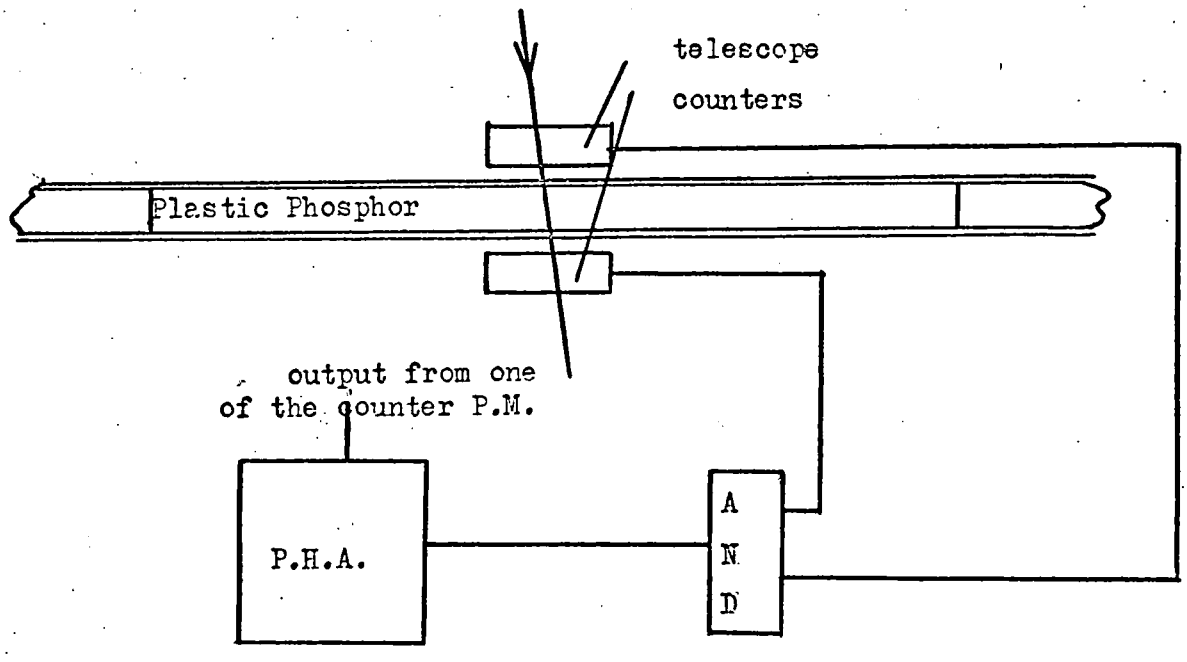

Fig 4:9 Experimental layout ~~Set up~~ used to balance the photomultipliers of each counter

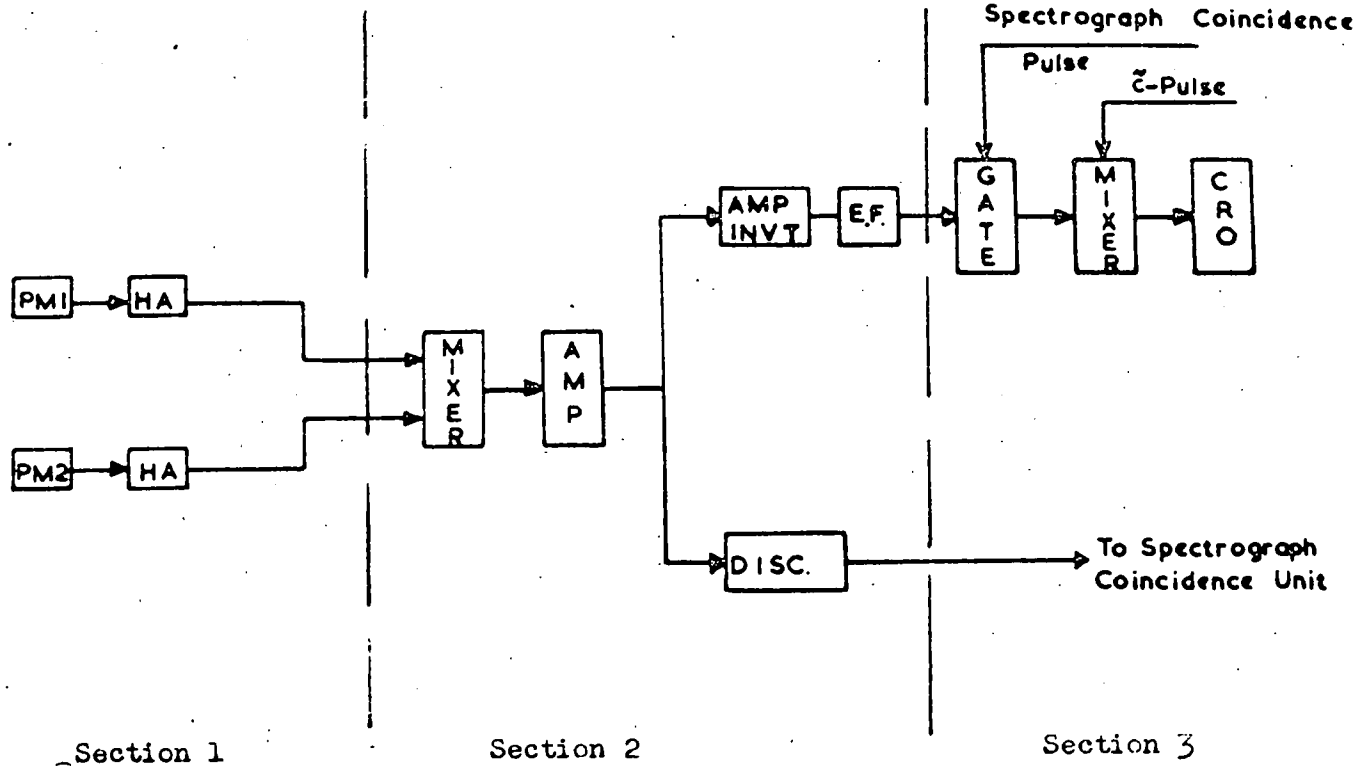

Fig. 4.10 Block diagram of electrical connections in a Scintillation Counter

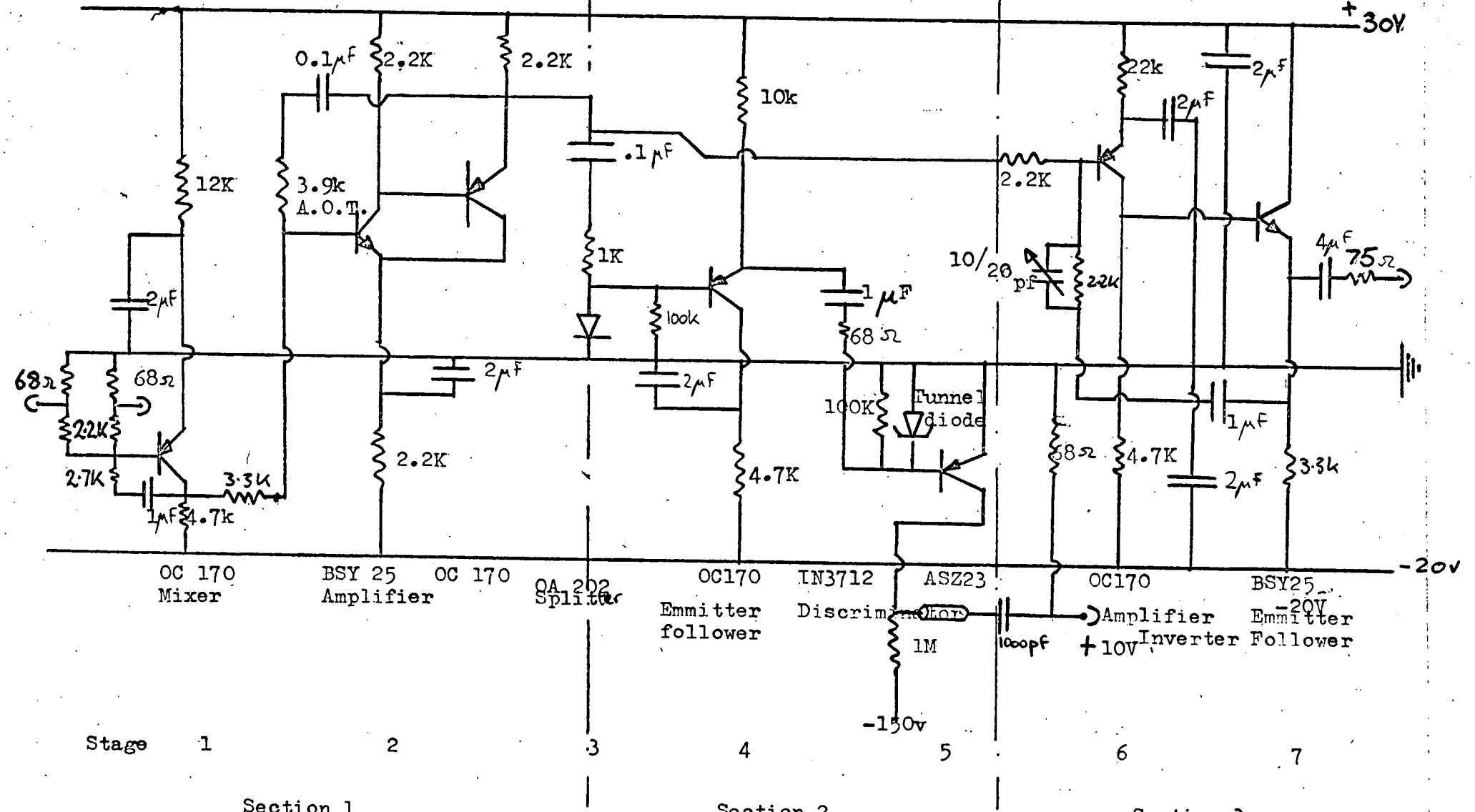

Fig 4:11 The channel adding unit

for the second tube and the gains of each tube then adjusted until their most probable pulse heights were equal to within a few per cent. Each counter was balanced in this way.

A block diagram of the electronics associated with each counter is given in Figure 4.10. The negative output pulse taken from the anode of each photomultiplier was first fed into a head amplifier. This is a three stage unit, the circuit diagram is shown in Figure 4.7, which was designed to give a gain of unity and drive the cable feeding the channel adding unit. This was necessary as the cables had to be matched and a power loss would occur.

The channel adding unit is shown in Figure 4.11 and incorporates section 2 of Figure 4.10. The two pulses from the head amplifier units of the counter were fed into this unit which has 7 stages. Stage 1 mixed the two pulses producing a single pulse which was then amplified in Stage 2. Stage 3 split this pulse which then fed the two separate sections 2 and 3. Section 2 incorporating stages 4 and 5 consisted of an Emmiter follower and Discriminator. The discriminator level was set at 250 m.V. and stopped any unwanted noise pulses of value less than this. The output pulse then had a constant height of + 10V (matched) which was used to feed the spectrograph coincidence unit.

Section 3 incorporates Stage 6 an Amplifier Inverter and Stage 7 an Emmiter follower. The positive output from this section which is still proportional to the energy loss in the counter was in the case of S2 fed through a gate and mixer and displayed on the Cathode Ray Oscillograph as shown in Section 3 Figure 4.10. Note section 3 applies only to the counter S2.

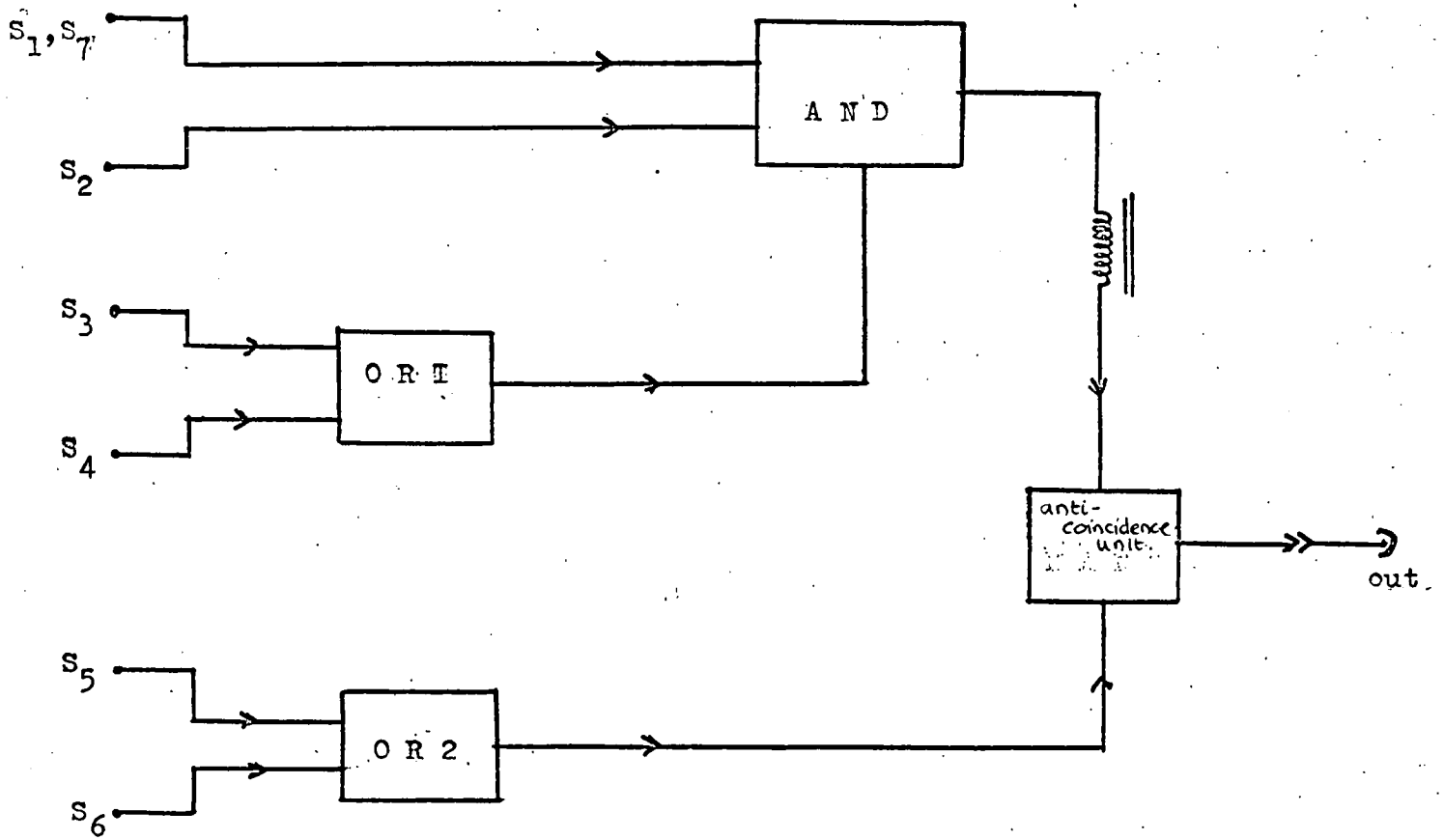

Fig. 4:12 BLOCK DIAGRAM FOR SPECTROGRAPH COINCIDENCE UNIT

Fig 4:13 Spectrograph coincidence unit

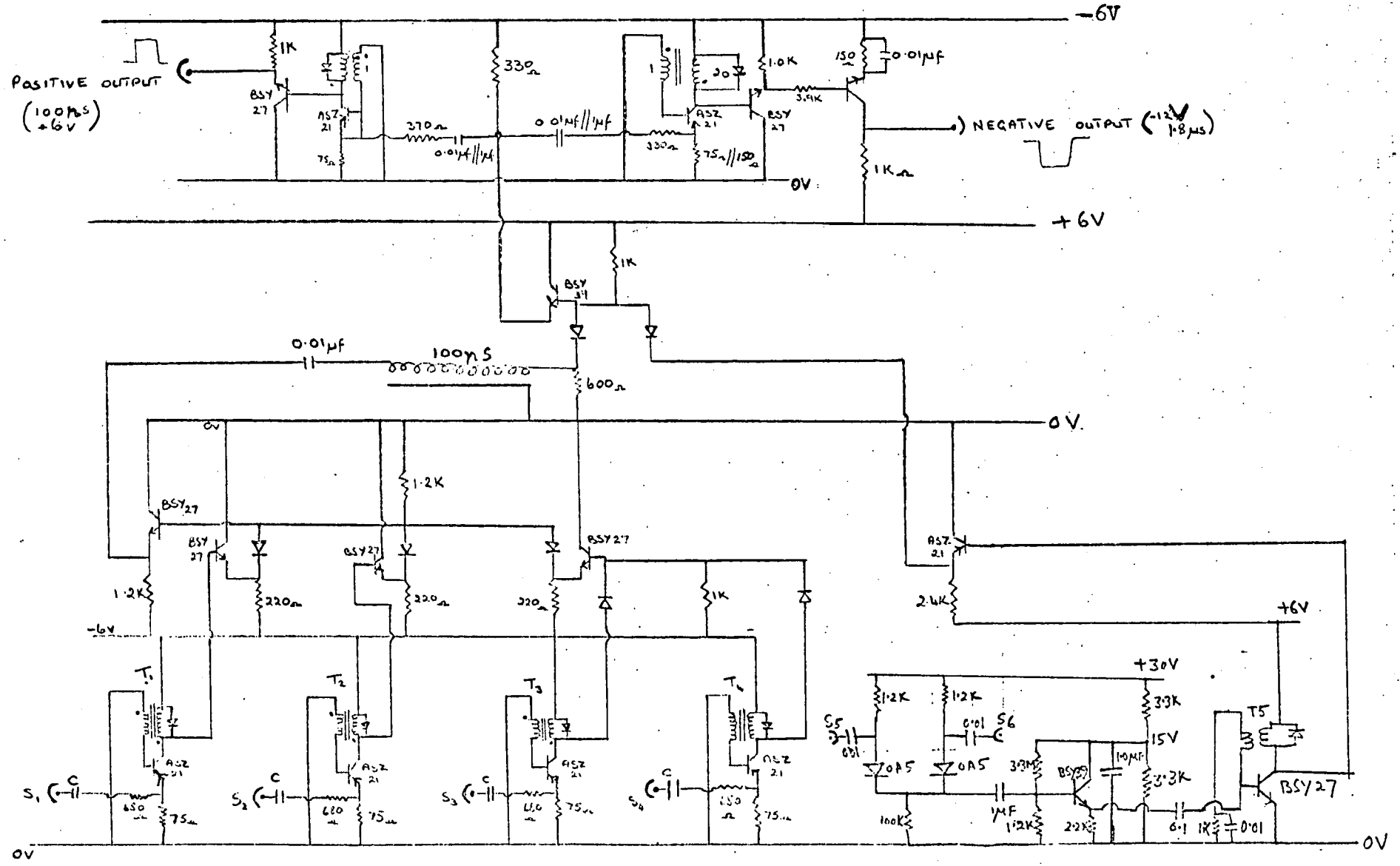

The discriminated output from each counter was fed into the Spectrograph coincidence unit. A block diagram of this is shown in Figure 4.12 and the actual circuit in Figure 4.13. Pulses from counters S3 and S4 were fed to an OR gate(1) such that a pulse from either counter would produce a pulse which was fed into the AND gate together with pulses from S1/S7 and S2. This unit gave an output pulse providing pulses were received from S1 or S7 and S2, S3 or S4. This pulse was then fed to the ~~NAND gate~~ anti-coincidence unit. Pulses from S5 and S6 were fed into an OR gate(2) and the output from this fed to the ~~NAND gate~~ anti-coincidence unit. This unit gave an output pulse providing no pulse was received from OR gate(2) when a pulse was received from the AND gate. The output pulse from this ~~NAND gate~~ anti-coincidence unit was used to trigger the Spectrograph electronics which are described later in this chapter.

4.3 The Air Gap Electromagnet

The electromagnet (Metro-Vickers) was originally used in the Durham Vertical Spectrograph, for the present experiment it had a gap of 45 cm. x 45 cm. x 38 cm. and the field was in the vertical direction. It was necessary to plot the variation of the Magnetic Induction B across this gap and to determine the fall off in field outside the gap. The field was measured using a search coil of 100 turns and area 1.1 cm^2 rotating at a constant 50 cycles per second. The output from this coil when displayed had a sine wave form with amplitude proportional to the field strength. The instrument was calibrated using a pair of Helmholtz coils specially constructed for the purpose. To determine the field distribution

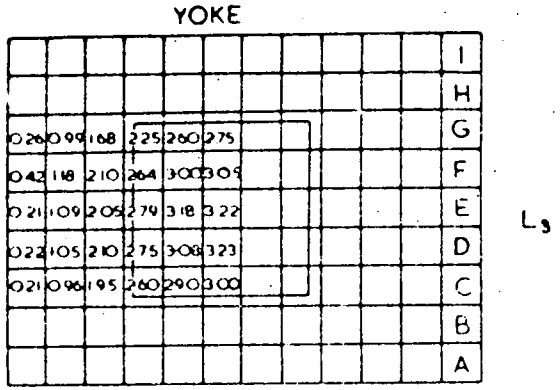

(a) Deflecting field in Kilo Gauss at levels L_2 & L_3

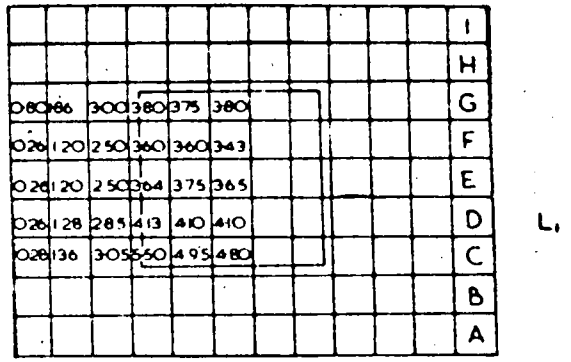

(b) Deflecting field in Kilo Gauss (horizontal section of the pole) at level L_1

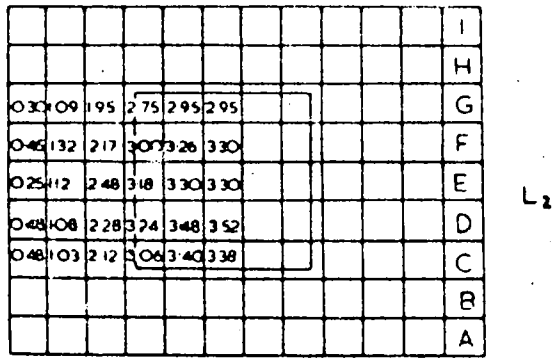

(a) Deflecting field in Kilo Gauss at levels L_2 & L_3

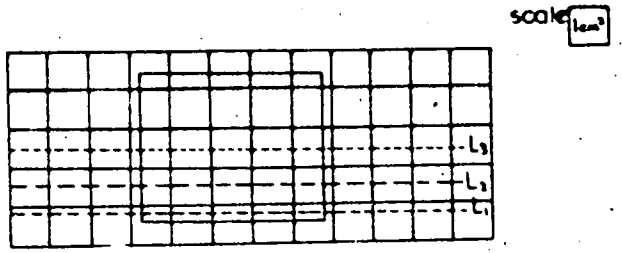

Vertical section of the pole showing levels L_1 L_2 & L_3

Fig. 4.14 The magnetic field

FIG 4:15(a) Lines of force in the central plane along the trajectories of the particle.

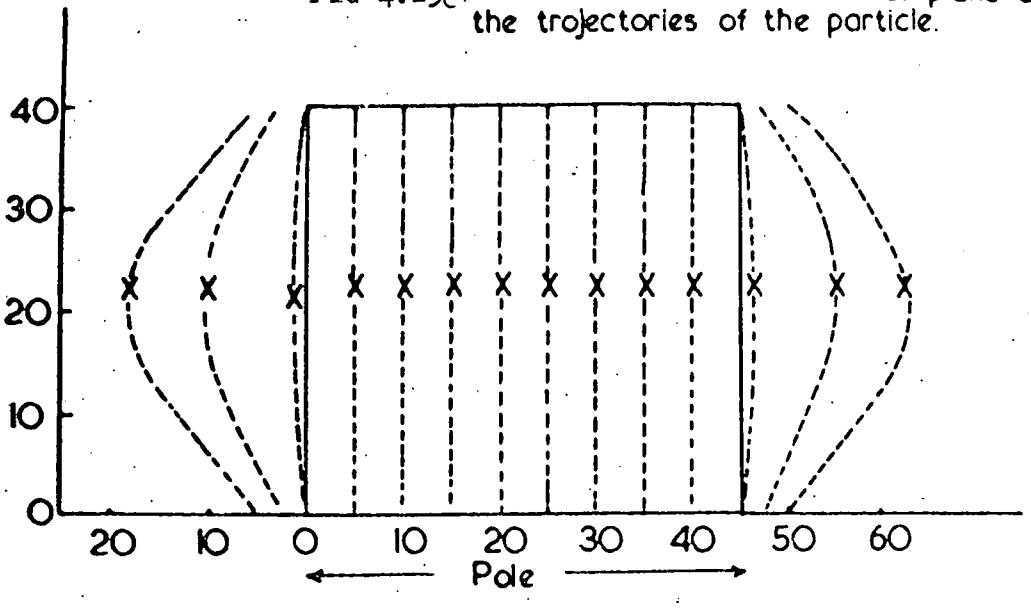

Fig 4:15(b) Lines of forces in the central deflection plane in the pole gap.

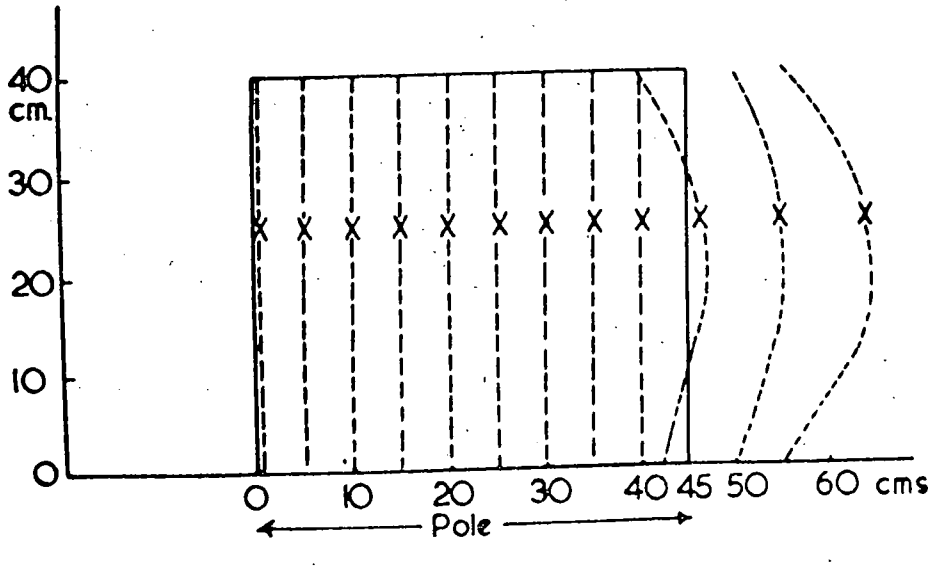

the air gap was divided into three levels L_1 L_2 and L_3 at a 10 cm. separation with level L_3 on the centre line of the gap. Each level was then given a 10 sq.cm. horizontal grid as shown in Figure 4.14 a, b. With the magnet switched on the field was measured in each of these grid squares and at each level by placing the rotating coil in it and noting the sine wave amplitude on the Cathode Ray Oscilloscope: the results are shown in Figure 4.14.

A plot of the lines of force produced by the magnet is shown in Figure 4.15. 4.15a gives the distribution of field along the particle trajectory plane and 4.15b the field perpendicular to this, i.e. the deflection plane. The field was uniform within the pole pieces and dropped off rapidly outside. Unfortunately there was still a sufficient field within the vicinity of the counters S1 and S2 to affect the gain of the photomultipliers and these had to be moved further from the magnet. The measurements indicated a maximum field strength of about 4 kilogauss in the gap at the mean working current of 43.5 amps and 210 volts.

4.4 The Particle Track Recording System

To enable the tracks of the particles to be recorded four flash tube trays were used in the positions A, B, C and D, shown in Figures 4.1 and 4.2. These trays consisted of banks of Neon Flash tubes. The neon flash tube, often called the Conversi counter because it was introduced by Conversi et al (1955), consists of a glass tube a few m.m. in diameter containing neon and is mounted between parallel electrodes. If a high voltage pulse is applied after an ionizing particle has passed through the tube

there is a high probability of an electron avalanche occurring and with it the characteristic red glow, or flash of the neon discharge. These flashes can be easily photographed through the end of the tube. Each tray was designed and constructed so that the rows of tubes were staggered relative to each other, this means that at least four tubes per tray were traversed by a particle passing through the tray and in most cases at least six tubes were observed to flash along the path of the particle. Each tray had two fiducial lights which were switched on when thespectrograph was triggered. These helped to locate the positions of the trays when the films were projected to analyse the tracks.

4.4.1 The Flash Tube Trays A and D

A different type of tube was used in trays A and D to those in trays B and C. The tubes in trays A and D described by Coxell (1961) had a mean internal diameter 1.55 cm. and a mean external diameter 1.75 cm. and were made of soda glass with a plane window at one end. The first 12 inches of each tube at the window end were coated with white paint. This reduces the collimation of the light from the flash tube so that flash tubes off axis from the camera lens become easier to record. Each tube was filled with Neon gas to a pressure of 60 cm. of mercury. When a tube flashes it is necessary that the light is contained within the tube and prevented from entering adjacent tubes, hence each tube was covered with a black polythene sleeve before being inserted in the tray.

In tray A the flash tubes were two metres long - these were used because the spectrograph was to be run later in conjunction with an Extensive Air Shower experiment. In tray D the tubes were 1 metre in length.

FIG 4:16

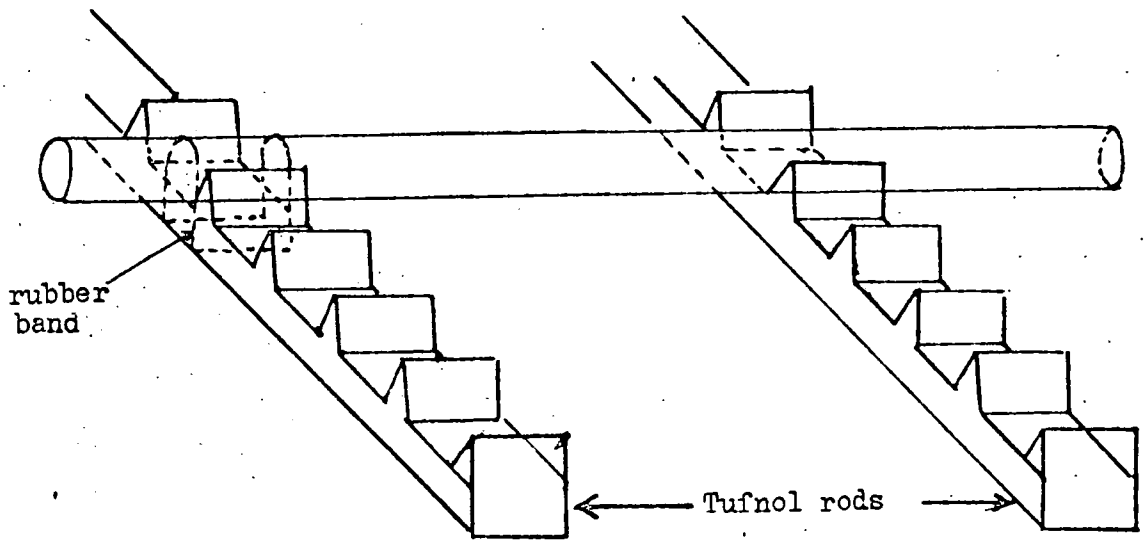

(a) Diagram showing the mounting of the flash tubes on the tufnol rods Trays A and D

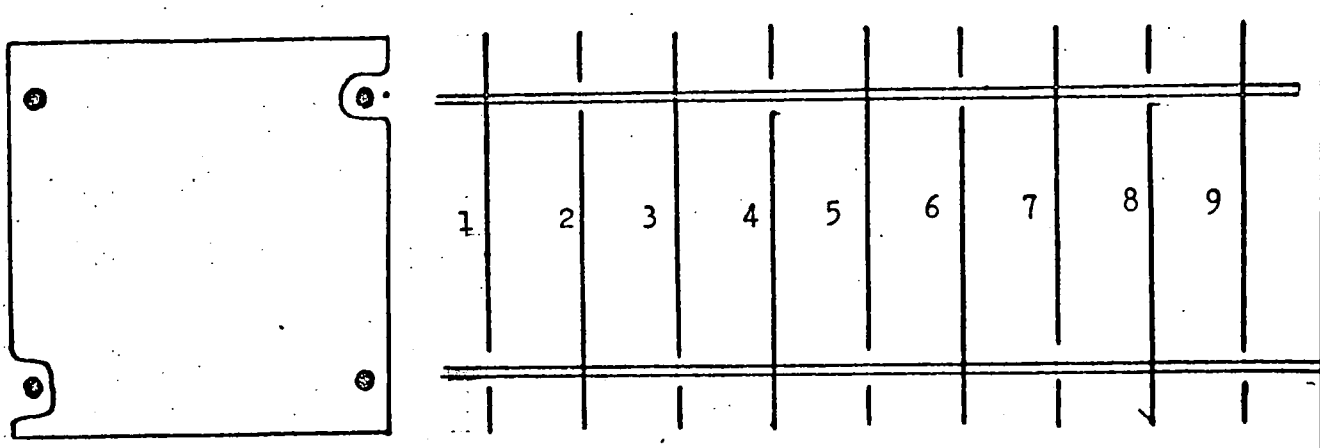

(b) Electrode System for the Trays A and D.

Both trays A and D were made up from two separate flash tube tray units (figure 4.1) since the frame work for these had already been constructed for a previous experiment. These units however had to be stiffened with a steel framework, and were then mounted vertically on adjustable screws in a steel framework constructed in position on the spectrograph. The tubes in each of the units were supported on sets of parallel Tufnol rods, Figure 4.16a accurately milled to ensure an identical spacing of each tube. Each tube was secured to the Tufnol rods using an elastic band so that it could not be displaced during the experiment. The tube separation was measured using a travelling microscope and a mean value of 1.905 ± 0.002 cm. determined. Each unit contained eight rows of tubes with a row spacing of 2.80 cm.

For tray A each unit contained 39 tubes per row giving a total of 78 tubes per row for the complete tray. For tray D each unit contained 29 tubes giving a total of 58 tubes per row for the complete tray. Before the trays were installed the electrodes for each unit were positioned between the rows. Alternate electrodes were held in position, and hence connected electrically, by two threaded brass rods set diagonally opposed at the corners of each units, Figure 4.16b Electrodes 1 3 5 7 9 were earthed so that the outer electrodes were at zero potential for safety. Finally the trays were carefully mounted in the spectrograph framework and adjusted so that the flash tubes were vertical.

4.4.2 Flash Tube Trays B and C

These two trays were identical. Because of the lack of space in the magnet area a complicated mirror system had to be designed to

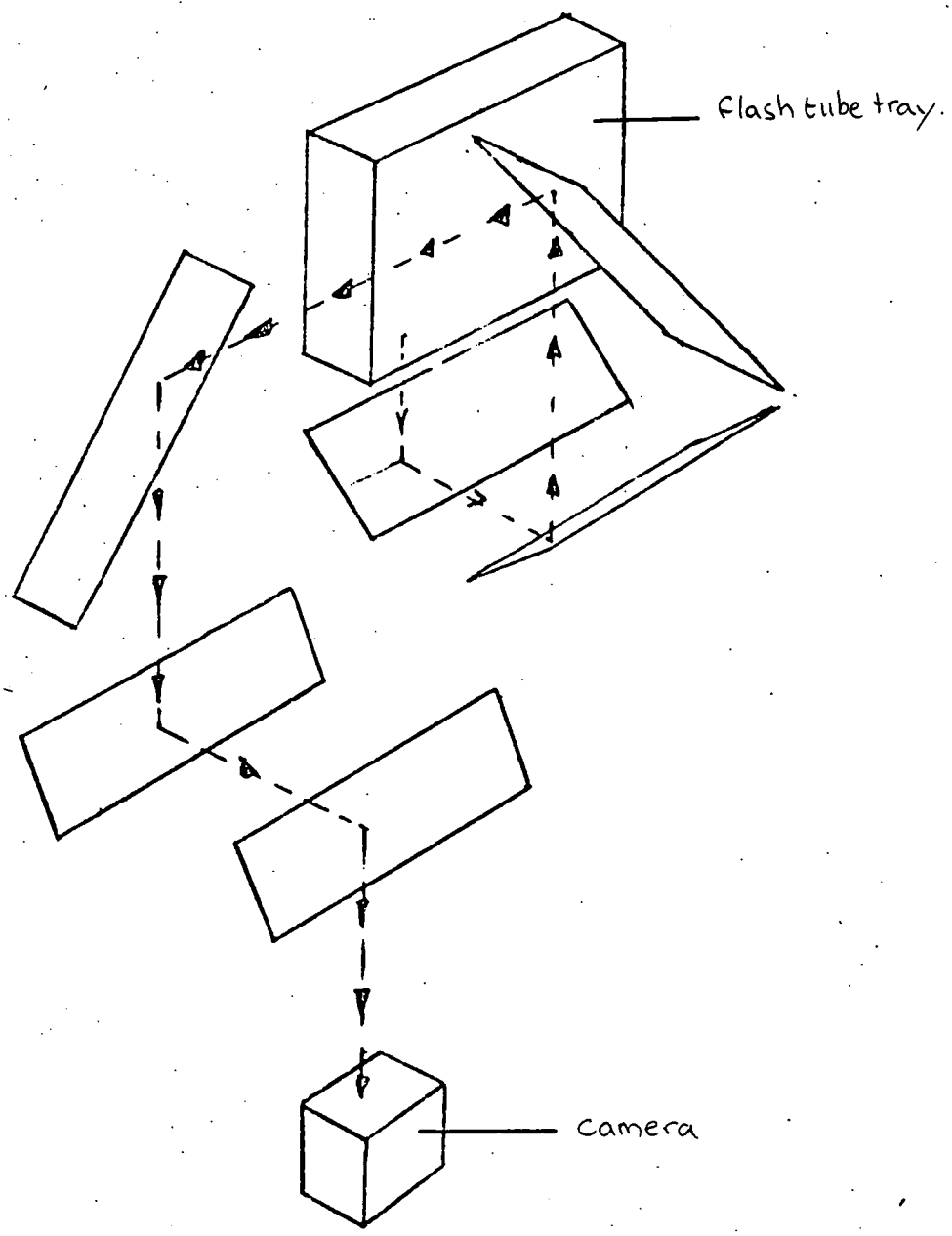

Fig 4:17 The mirror system for trays B and C

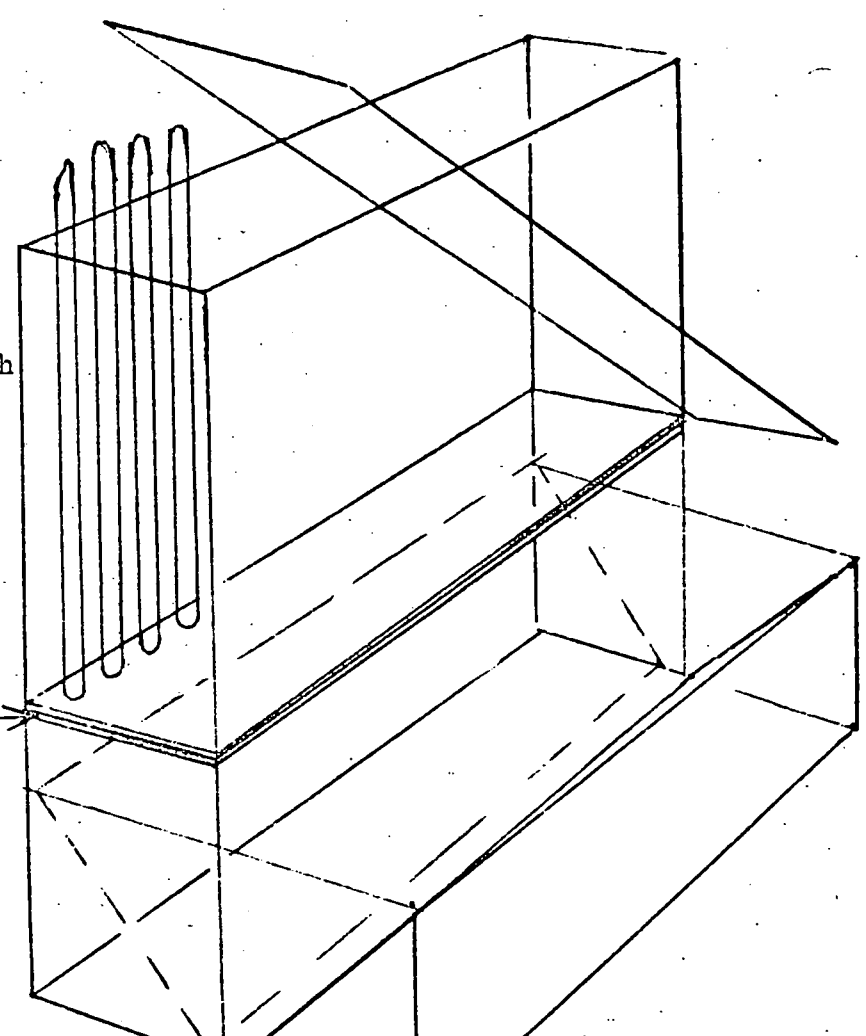

General view of flash tube tray B showing the built-in mirrors

perspex window supporting the flash tubes

Fig 4:18

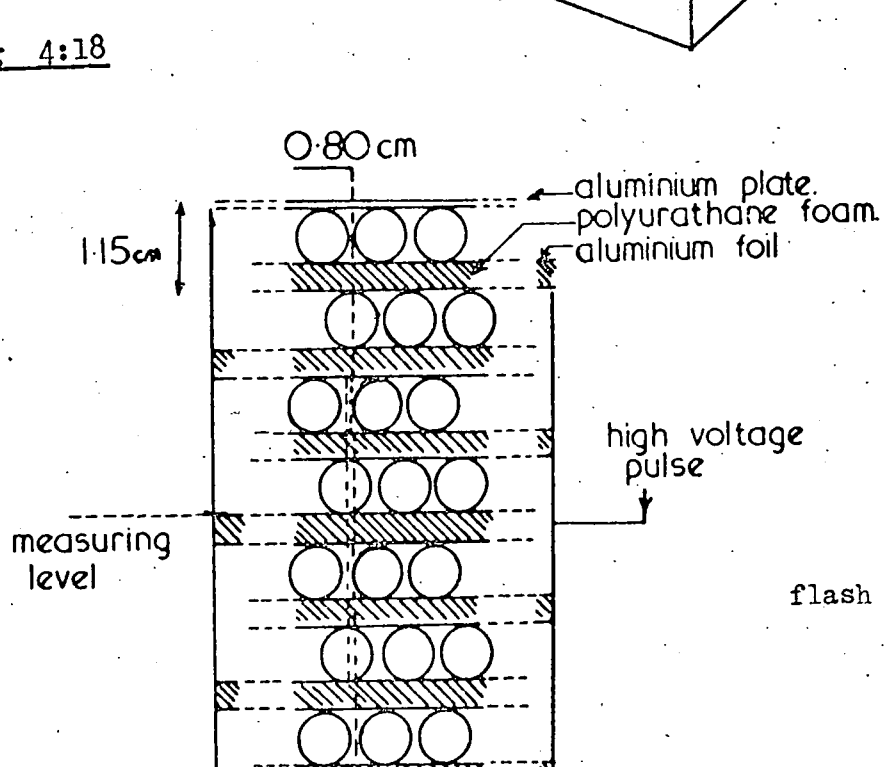

Electrode System for flash tube trays B and C.

enable the flashes to be photographed. This contained 6 mirrors and three of these were built into the framework of the tray such that the whole unit could be aligned before it was installed, Figure 4.17 shows an exploded diagram of the mirror system. All the material used in the construction of the trays had to be non-ferrous because of the proximity of the magnet. The tubes used in the trays were described by Brooke (1964) and Aurelia (1965). They were 42 cm. long with an external diameter of 0.72 cm. and internal diameter 0.59 cm. with a plane window at one end. The tubes were filled with commercial neon gas to a pressure of 2.4 atmospheres, Coxell and Wolfendale (1960), Hayman and Wolfendale (1962). As before the window end of each tube was dipped in white cellulose paint and the tubes were then painted with two coats of black cellulose to prevent any light from a tube which had flashed entering an adjacent tube. The tubes were supported on sets of parallel milled aluminium bars and held in position with strips of plastic foam acting as pressure pads glued to the adjacent bar, Figure 4.18. To prevent any vertical movement of the tubes the plane window of each tube rested on a thin sheet $^{1}/_{10}$" thick of transparent perspex fixed to the lower face of the tray - Figure 4.18.

The Electrodes for the trays were constructed from thin sheets of polyurethane foam carefully covered with Aluminium foil. These were suspended using P.V.C. tape from the aluminium bars and positioned between each row of tubes. The outer electrodes of each tray were of $^{1}/_{32}$" thick aluminium.

Using a travelling microscope the tube spacing was measured to be 0.8 cm. and the position of each row of tubes with respect to the adjacent row determined. Each tray had 8 rows of tubes

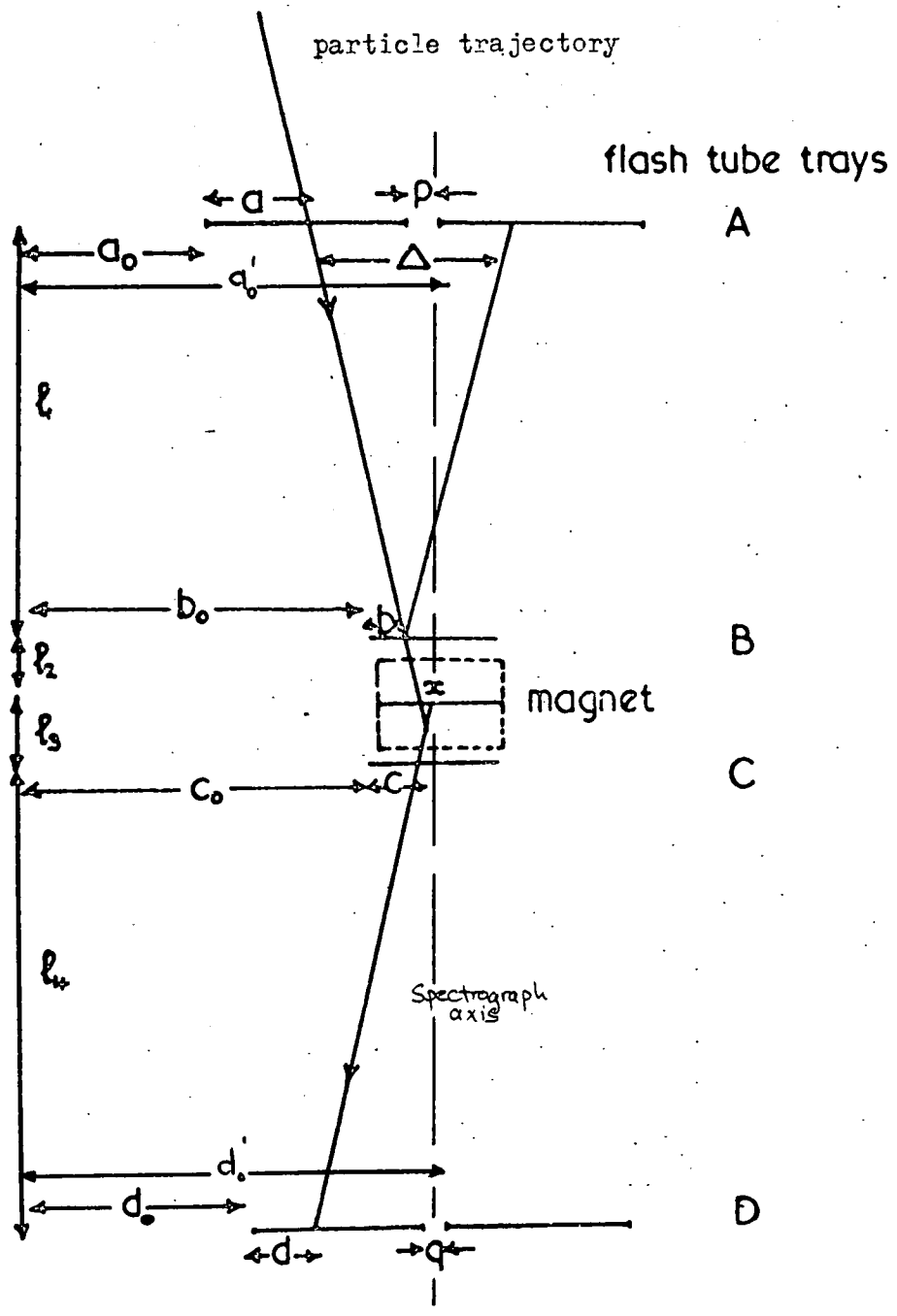

Fig 4:19 Schematic diagram of the spectrograph and a particle trajectory.

with a row separation of 1.15 cm, each row contained 46 tubes. Thus the exact position of each tube was known with respect to a predetermined reference tube.

4.4.3 The Alignement of the Flash Tube Trays

Figure 4.19 shows a schematic diagram of the flash tube trays with the measurements necessary to compute the deflection of a particle traversing the spectrograph. The fixed constants a_o, a_o', b_o, c_o, d_o, d_o' and t_1, t_2, t_3 and t_4 had to be measured. The origin of the coordinates in each tray was taken as the centre of the outer most tube on the north-west side of the spectrograph in the fourth row, counting from the centre of the magnet. Each unit of the trays A and D was given a separate origin to eliminate any error which could occur if the two units in either of the trays A or D were not exactly parallel. Before the actual measurements could be taken each tray had to be adjusted so that the flash tubes were vertical and the rows of the tray exactly perpendicular to the centre line of the spectrograph. Because each tray was at a different level it was necessary to describe a vertical plane parallel to the centre line and on the north side of the spectrograph. A single nylon fibre was suspended along the length and set parallel to the centre line of the spectrograph. From this, four plumb lines were suspended one at each of the measuring levels for the respective trays A, B, C and D, and adjusted to be in the same vertical plane as the row of tubes containing the reference tube for that tray. The distances of these plumb lines from the centre of their respective reference tube was then measured using a cathetometer to give the values of the fixed constants a_o, a_o', b_o, c_o and d_o, d_o' . The separation constants t_1, t_2, t_3, and t_4, of the trays were determined by measuring the distances between the four

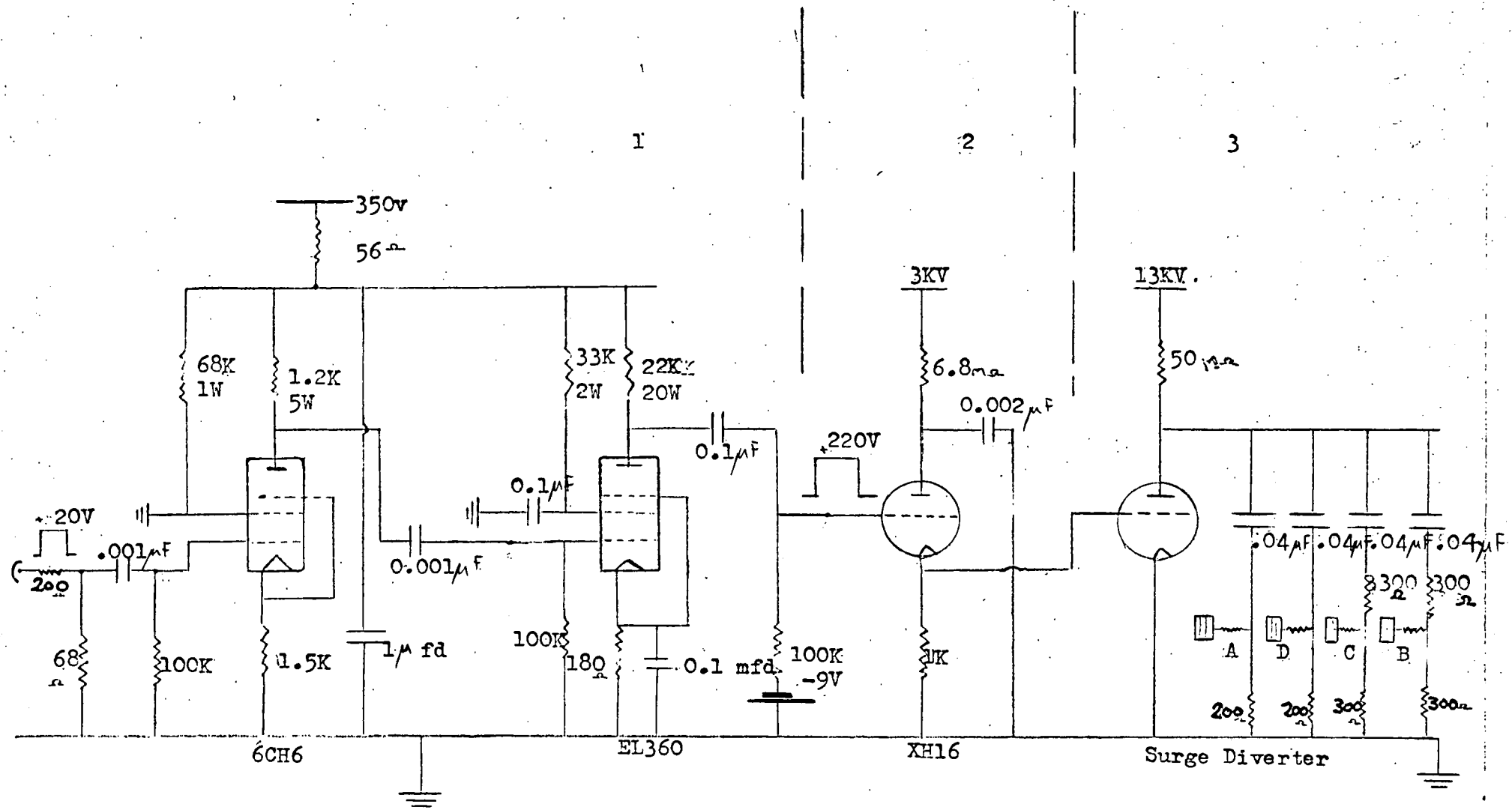

Fig 4:20 PULSING UNIT FOR THE SPECTROGRAPH FLASH TUBES

plumb lines with a steel tape. The measurements were then repeated independantly to check their accuracy. The values finally accepted for the fixed constants are given in table 4.2.

Table 4.2

Values of the Geometrical Constants

Dimension	Cm.
a_o	41.26 ± 0.002
$a_{o'} = (a_o + p)$	64.55 ± 0.004
b_o	114.52 ± 0.003
c_o	112.62 ± 0.003
d_o	68.64 ± 0.002
$d_{o'} = (d_o + q)$	87.38 ± 0.005
L_1	317.50 ± 0.05
L_2	43.75 ± 0.03
L_3	59.35 ± 0.03
L_4	368.38 ± 0.06

4.4.4. The Flash Tube Pulsing System

The pulse from the ~~NAND~~ anticoincidence gate of the spectrograph coincidence unit (6 volts positive) was amplified to about 20 volts and fed into the pulsing unit. The circuit diagram for the unit is shown in Figure 4.20. This unit consisted of three stages. Stage one further amplified the 20 volt input pulse to 220 volts positive, using two power pentodes 6 CH 6 and EL 360. Because the 350 volt supply used had a low impedance a 56 Ω resistor was placed in the supply together with a 1 μfd capacitor linked to earth; this prevented any feed-back from the EL 360 to the 6 CH6 which had caused the unit to oscillate previously. The 220 volt pulse from stage one triggered the XHI6 Thyratron of stage two. This discharged the .002 μf condenser and produced a pulse of about

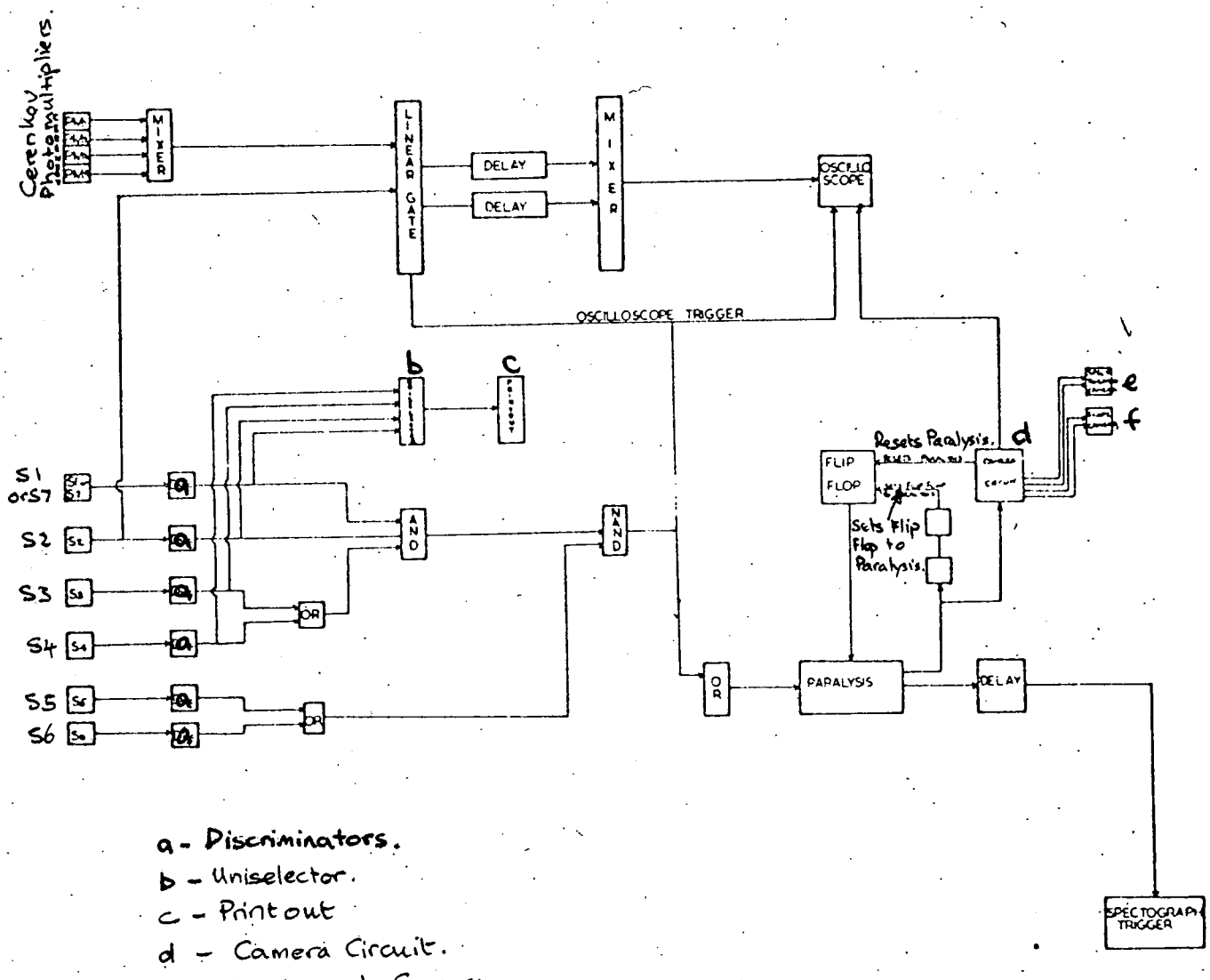

a - Discriminators.
b - Uniselector.
c - Printout
d - Camera Circuit.
e - Spectrograph Camera
f - Oscilloscope Camera.

Fig 4:21 Block diagram of the spectrograph electronics

3 Kv. This pulse triggered the surge diverter in stage three; hence discharging the four condensers connected to the flash tube trays A, B, C and D. Thus a negative pulse of about 13 Kv and 25 μ sec width was applied to each flash tube tray. The delay between a particle traversing the spectrograph and the pulse appearing on the trays was about 3 μ sec and the rise time of the pulse about 0.8 μ sec, this was well within the sensitive time of 39 μ sec for the flash tubes.

The field developed between the electrodes of trays A and D was about 4.6 Kv per cm. and about 11.3 Kv per cm. between the electrodes for trays B and C. The higher field for the two smaller trays was necessary to enable the flashes to be photographed because of the large amount of light absorption in their mirror systems.

4.5 The Spectrograph Electronics

A block diagram of the electronics associated with the spectrograph is shown in Figure 4.21. To check that the scintillators S7, S2, S3 and S4 were working correctly hourly counts were made during the running of the spectrograph. To do this the discriminated output from each counter was fed to a uniselector unit. This unit selected each input for one hour. The putput from this unit was fed to ~~an I.V.U.~~ mechanical counter which recorded the number of pulses, and when the input to the unit was changed printed out the total number of pulses counted in the previous interval. Hence a record of the counting rate for each counter was made.

The coincidence unit for the scintillator counters has already been described. The pulse from the NAND gate of this unit was split into two pulses; one was used to open the linear gate to allow the

~~the~~ pulses from the Cerenkov Counter and scintillator counter S2 to pass to the oscilloscope and also trigger externally the oscilloscope displaying these pulses: the other pulse was fed to a paralysis unit which prevented any further pulses from triggering the spectrograph. This pulse was then fed via a delay to the flash tube pulsing unit and to the camera circuit. The camera circuit consisted of a set of cams which were set in motion by the pulse. These, illuminated the clocks on the spectrograph and oscilloscope and the fiducary marks on the flash tube trays, wound the cameras on, and then via a flipflop circuit reset the paralysis unit such that it would accept the next pulse from the coincidence unit.

Thus the sequence of operations when a particle traversed the spectrograph was as follows:-

1. The coincidence unit was paralysed.

2(a) Sequence of operations on the spectrograph.

(i) High voltage pulse was applied to the flash tube trays and the flashes photographed.

(ii) The two clocks and fiducary marks were illuminated.

(iii) The cameras were wound on.

(b) Sequence of operations on the oscilloscope.

(i) The oscilloscope was triggered externally and the pulses photographed.

(ii) The clock and oscilloscope graticule were illuminated.

(iii) The camera was wound on.

3. The paralysis unit was reset ready to accept the next event.

This sequence took about 6 seconds.

4.6.1 Photographic Record of the Particle Tracks

To record the track of a particle passing through the spectrograph two Vintex 35 m.m. Cine Cameras were used. One of the cameras mounted above the magnet recorded the tracks in Trays A and D and the other mounted below the magnet recorded the tracks in Trays B and C. The cameras were used without shutters because the spectrograph was run in complete darkness. Figure 4.2. shows the positions of the mirrors on the spectrograph for each flash tube tray and Figure 4.17 shows the mirror system devised for the trays B and C. To synchronise the frames on the films of each camera two clocks, one for each camera, were illuminated together with the fiducary marks on the trays and photographed for every event.

4.6.2 Photographic Record of the Scintillator and Cerenkov Pulse Heights

The spectrograph was used to measure the energy loss in plastic phosphor and the intensity of Cerenkov Radiation as a function of muon momentum, thus for each event it was necessary to record the pulse height from the scintillator counter S2 and the pulse height from the Cerenkov counter. To do this the pulses from these counters were fed into a linear gate triggered by a pulse from the spectrograph coincidence unit. This meant that the gate was only open when the spectrograph had been triggered and thus allowed only those pulses associated with the particular event to pass through. The Cerenkov pulse was then delayed by 110 μ sec and the scintillator pulse by 660 μ sec. The two pulses were then mixed and fed into a C.R.O. (Tektronix) which was externally triggered by the spectrograph coincidence unit. Thus when the oscilloscope was triggered the Cerenkov pulse was displayed after

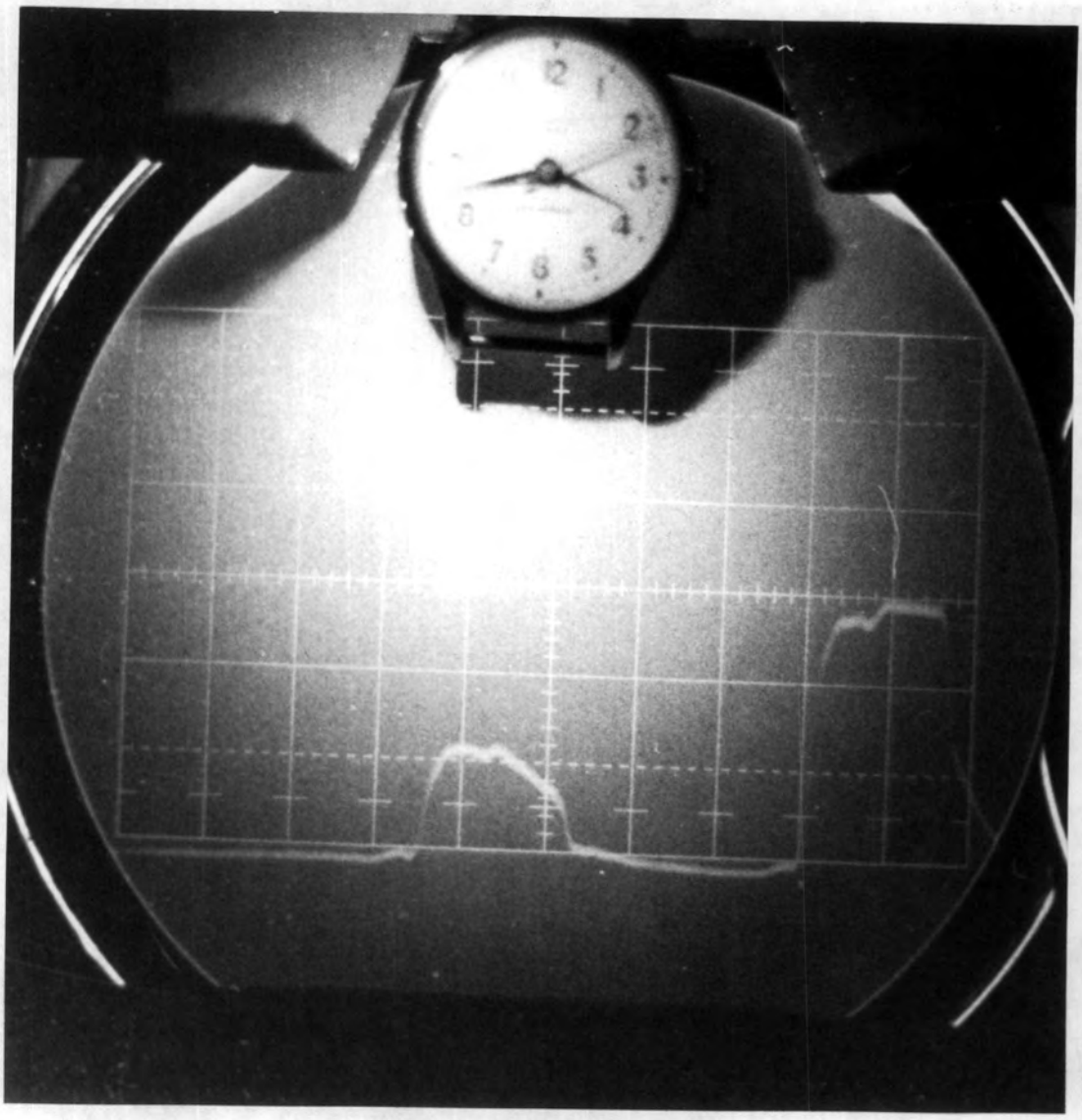

Fig 4:22 The scintillator and Cerenkov pulses displayed on the C.R.O.

a delay of 110 ∩ sec and the scintillator pulse after 660 ∩ sec. Following this the scope graticule and a clock showing the time of the event were illuminated and photographed to enable the pulses to be correlated with the particle tracks on projection of the film. A typical record of the pulses is shown in Figure 4.22. The time base setting for the oscilloscope was 200 ∩ sec per cm, this gave a full scale time of 2000∩ sec which was sufficient to accommodate both pulses. The X plate deflection of the oscilloscope was set at 0.1 volts per cm, however to accommodate both the Cerenkov and scintillator pulses the scintillator pulse had to be attenuated.

Ilford HPS film was used for all photographic recording.

4.7 The Operation of the Spectrograph

The magnet took about two hours toreach its normal working current of 43.5 ± 0.5 amps after being switched on and thus had to be switched on well before the start of each run. To minimize the possibility of any accumulative error due to magnetic effects the direction of the current through the magnet was reversed nightly. The spectrograph was run overnight and before each run the following checks were made.

(1) The counting rate of each scintillator was checked.

(2) The shape of the Cerenkov and scintillator pulses were checked.

(3) The fiducary marks and lights illuminating the clocks were checked.

(4) The pulsing unit was checked to make sure that no breakdown was occurring on it or the flash tube trays.

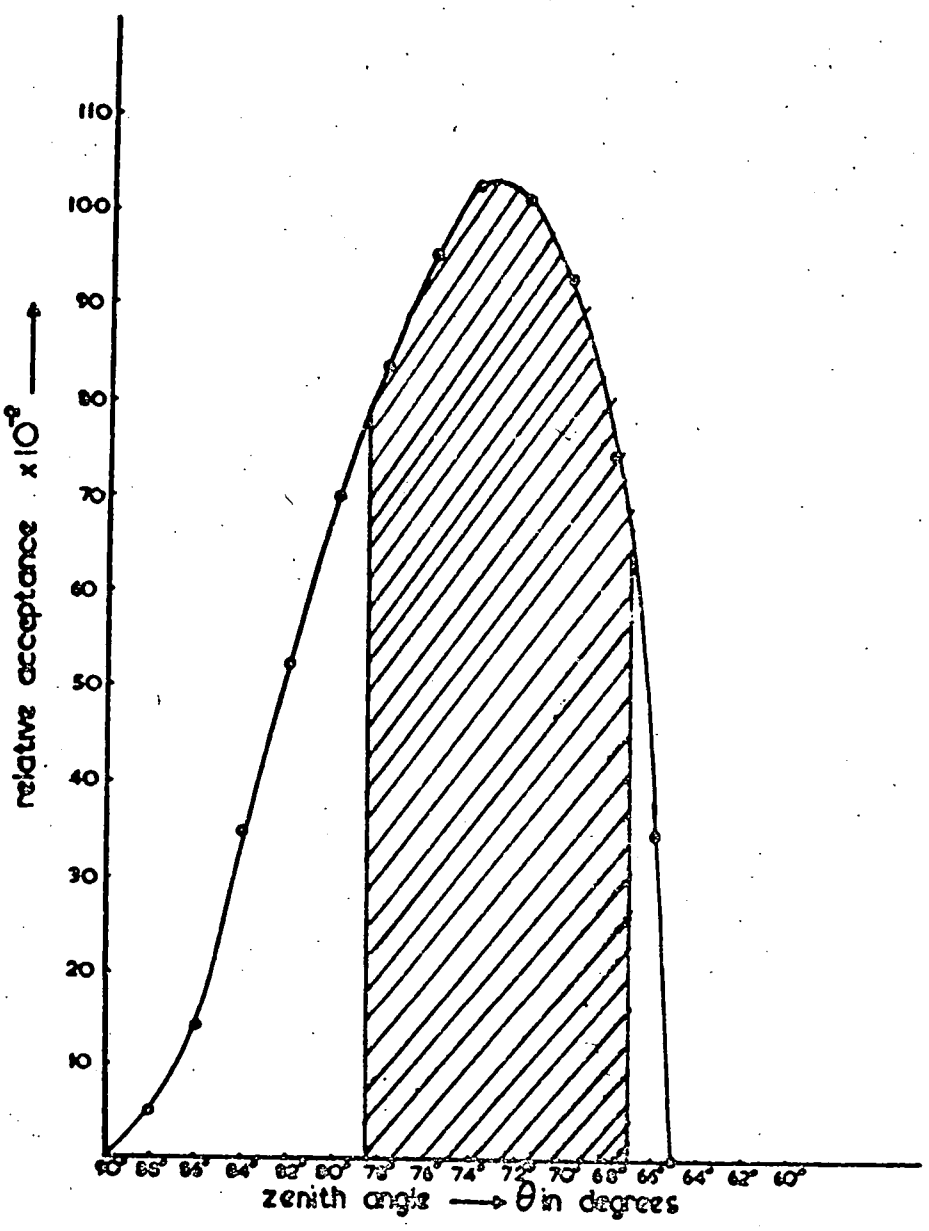

Fig 4:23 The relative acceptance of numbers of muons by the spectrograph w.r.t. the zenith angle

4.8 The Particle Rate

Using the scintillators S_1, S_2 and S_3 or S_4 to select particles the spectrograph coincidence rate was 150 ± 2.5 per hour for zero magnetic field, with the anti-coincidence counters S_5 and S_6 in this was reduced to 133 ± 2 per hour. With a coincidence rate as high as this the data analysis would have been difficult such that Counter S_1 was replaced by a smaller counter S_7. This was positioned such that the spectrograph only accepted particles which traversed all four flash tube trays. This cut the coincidence rate to 40 ± 2 per hour without a magnetic field and to 36 ± 2 per hour with the magnetic field. When the results were analysed and unsuitable events rejected the final rate was reduced to 6 ± 1 per hour. A large number of the events had to be rejected because of faint tracks in the trays B and C, and because some of the trajectories passed through the gaps in the trays A and D. The number of events in this experiment with tracks recorded in all four trays was 2037.

4.9 The Acceptance of the Spectrograph

The acceptance of the spectrograph was governed by the flash tube tray A. Figure 4.23 shows the relative acceptance plotted as a function of the Zenith Angle for the Spectrograph calculated by Pathak (1967). The shaded area depicts the working range of $67^\circ - 78.5^\circ$ for the present experiment. A detailed discussion of the acceptance function is given by Pathak (1967) and only a summary is given here.

The acceptance for an ideal spectrograph may be defined as:-

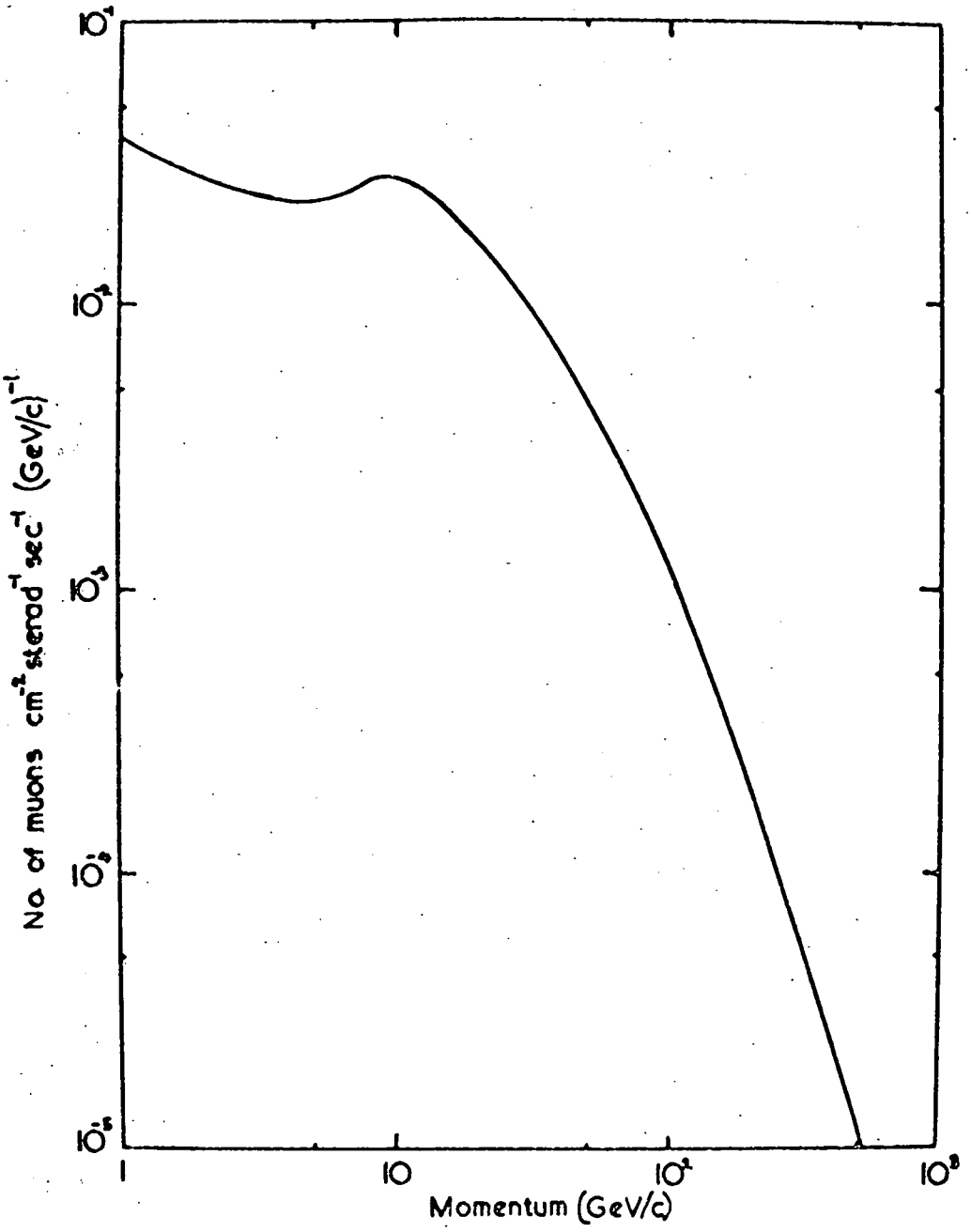

Fig 4:24 Differential acceptance rate of muons by the spectrograph

$$N(\theta, P)\, d\Omega dp = N_o(\theta, P)\ F(\theta, P) d\Omega . dp$$

where $N_o(\theta, P)\, d\Omega . dp$ is the number of particles incident on the spectrograph and $N(\theta, P)\, d\Omega\, dp$ the actual number detected by the spectrograph, in an element of solid angle $d\Omega$ at an angle θ to the horizontal in the momentum range p to p + dp. The function $F(\theta, P)$ may be replaced by:-

$$F(\theta, P) = A(\theta, P) . S(\theta, P)$$

where $A(\theta, P)$ is the geometrical differential aperture and $S(\theta, P)$ the scintillator efficiency function.

Having calculated the Relative Acceptance as a function of momentum, Pathak (1967) estimated the number of particles accepted by the Mk 3 Spectrograph as a function of their momentum, using the momentum spectrum of cosmic ray muons at large zenith angles given by Allen and Apostolakis (1961) See Figure 4:24.

Further Pathak (1967) compared the 'collecting power' of the present spectrograph with those of earlier ones. The collecting power is defined as $\iint dA . d\Omega$ where $d\Omega$ is the allowed solid angle of collection for an area dA . The integral is taken over the effective area at the scintillator level S3, S4 and at the central plane of the magnet. For the Mk 3 Spectrograph the collecting power was calculated to be 19.41 Sterad.cm^2

4.10 Scattering in the Spectrograph

Although the problem of scattering is much less when using an air gap magnet, particles traversing the spectrograph will still be scattered by the scintillation counters and the flash tube trays. Brooke (1964) has treated the problem in detail and shows that the ratio of the r.m.s. scattering displacement $\delta\Delta$ to the magnetic

displacement Δ is proportional to $1/\beta$ such that in the momentum range 2 to 100 GeV/c of the present experiment, where β approaches unity, this ratio is almost constant. Thus this scattering causes the mean momentum of each cell to be lowered by a constant amount and the overall effect is to shift the whole energy loss curve. Since the experimental curve is finally normalised to the theoretical curve the effect of scattering can be neglected.

CHAPTER 5

Construction of the Scintillation Counter used to Record the Energy Loss

5.1 Description of the Counter Assembly

The scintillation counters S1 and S2 were identical in construction apart from the thickness of the plastic phosphor; the dimensions of the phosphor are given for each counter in Table 5.1

TABLE 5.1

Counter	Length	Breadth	Thickness
S1	43.7	37.6	5.00
S2	43.7	37.6	2.54
	cm.	cm.	cm.

The specification of the phosphor N.E.102a has already been given in Chapter 4. A diagram of one of the counters is given in Figure 5.1. Two perspex light guides B were attached to the plastic phosphor and to the ends of each of these, cylindrical perspex light guides 2 inches in diameter and 2 feet in length. Each cylindrical light guide had a Mullard 53 AVP photomultiplier cemented to its end. All the joints in the counters were made with N.E. 580 optical cement. These cylindrical light guides were necessary so that the photomultipliers were positioned well outside the magnetic field of the spectrograph magnet. The counters had previously been constructed without the extension light guides and the photomultipliers had suffered a very large drop in gain when the magnet current was switched on. To further protect them from stray magnetic fields each photomultiplier was enclosed in a mu-metal shield and concentric with this an iron

Fig 5:1 Schematic Diagram of Plastic Scintillator S2

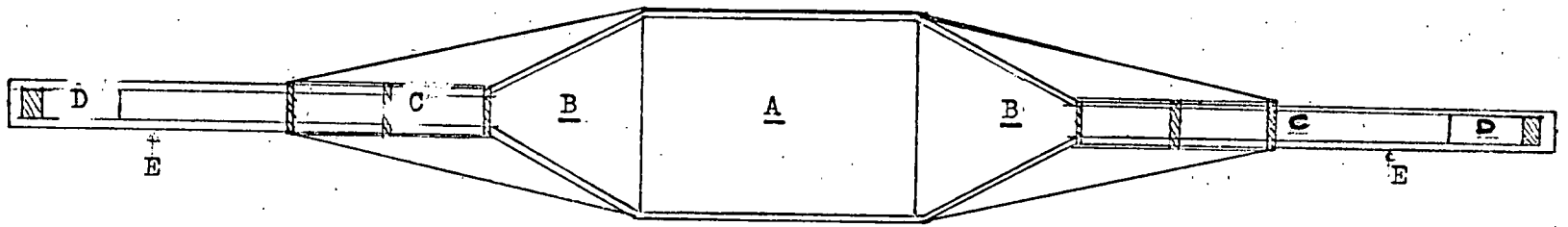

1'

A Phosphor

B Perspex light guides

C Cylindrical light guides.

D 53 AVP Photomultipliers

E Iron cylinders enclosing the light guides

cylinder which also enclosed the cylindrical light guide. The phosphor A and light guides B were housed in an aluminium box and the iron cylinders enclosing the cylindrical light guide extensions were attached and held rigidly to it using aluminium cantilever supports N. (Figure 5.1)

As has previously been described each counter was carefully cleaned before being placed in its housing and then all the joints were carefully sealed using plastic tape to make each counter light tight.

The electrical connections for the photomultipliers and the electronics associated with each counter are the same as for the counters S3 to S6 and have already been described in section 4.2.4. Similarly each counter was balanced so that their respective photomultipliers had an equal gain to within a few per cent. Since the counter was very near the magnet the counting rates of the 2 photomultipliers were checked for zero field and both polarites of magnetic field throughout the running of the spectrograph. There was no difference between the counting rates for positive or negative field although the zero field rate was slightly higher.

5.2 Measurement of the Response Curve for Counter S2

When a particle traversed the spectrograph the output pulse expressed in millivolts from the counter S2 was taken to be proportional to the energy lost by that particle when it traversed the counter. Ideally for a particle of given energy the pulse height from the counter would not vary, irrespective of where the particle traversed the phosphor. However because of absorption effects in the phosphor the counter will be least sensitive at its centre, the sensivity increasing towards the light guides. This non-uniformity

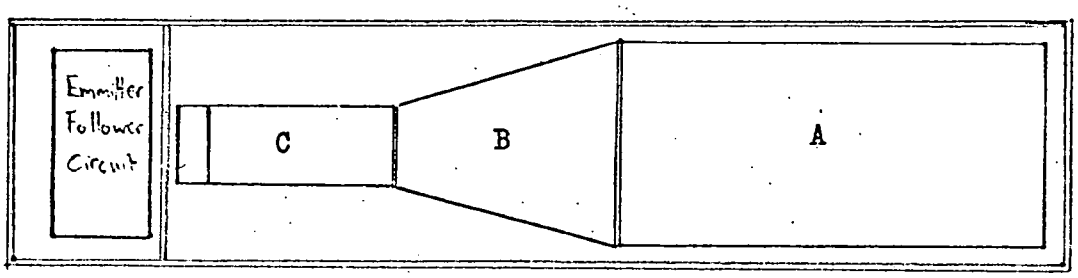

A Plastic Phosphor

B Perspex light guide

C E.M.I. photo multiplier

Fig 5:2 Diagram of telescope counter

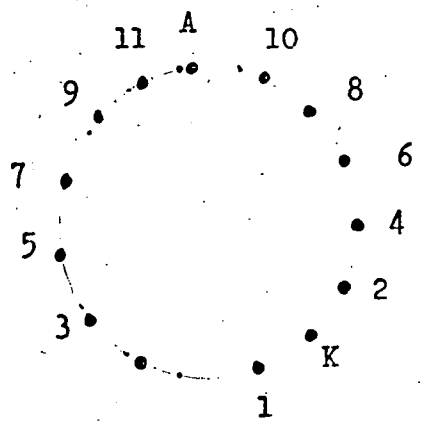

Fig. 5.3a - Base pin connections for the photomultiplier

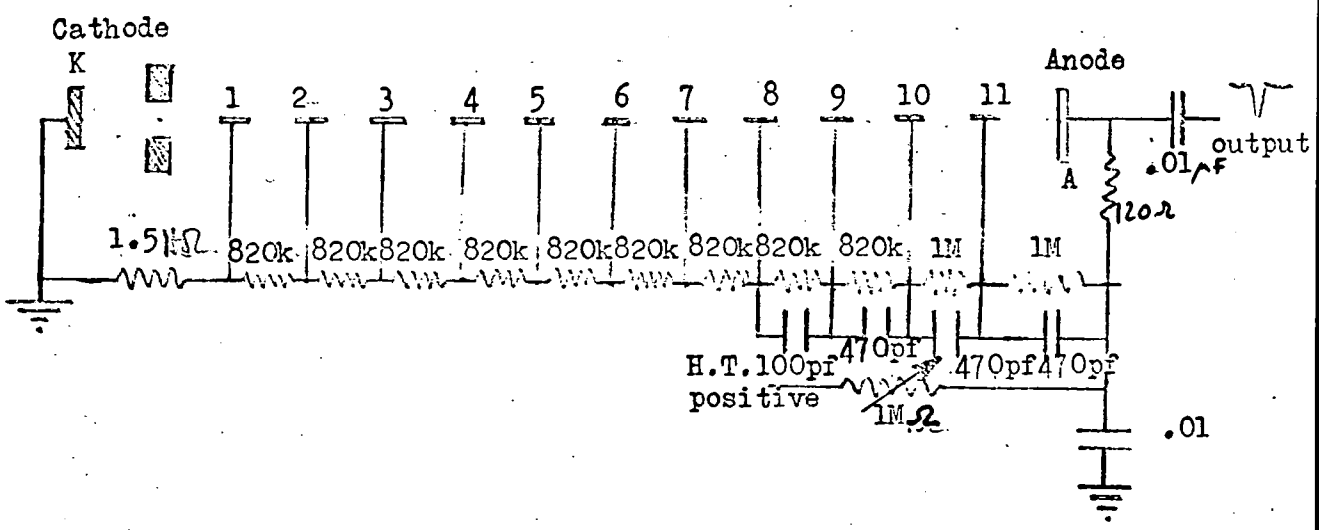

Fig. 5.3b Dynode resistor chain for the photo multiplier

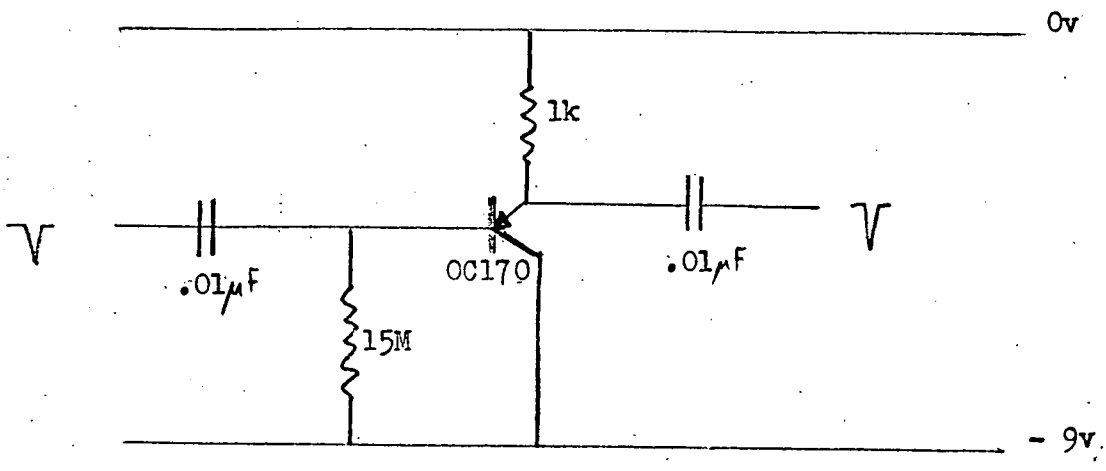

Fig 5:4 Emmitter follower circuit

is not a serious defect providing it is small. For this reason it was necessary to obtain a response curve for the counter and to do this a small telescope was used to gate the counter output such that the particles traversing a small area of the phosphor could be recorded.

5.2.1 The Telescope Counters

The telescope consisted of two small identical scintillation counters T1 and T2. A diagram of one of these counters is given in Figure 5.2. The counter consisted of a piece of plastic phosphor N.E.102a 14 cm. x 6 cm. x 2.5 cm. (A) cemented to a shaped perspex light guide (B) and a 1 inch diameter photomultiplier (C) cemented to the other end of this. The whole assembly was put in an aluminium box and then sealed with plastic tape to make it light tight.

Figure 5.3(a) shows the base pin connections for the photomultiplier and the resistor values for the dynode resistor chain Figure 5.3(b). The output from the photomultiplier was fed to an emmitter follower circuit shown in Figure 5.4. which was housed in the end section of the counter. This provided sufficient power to drive the cables to the coincidence unit.

5.2.2 The Telescope Control Unit

To make the telescope self contained all the necessary power supplies were fed to one control box and each counter was supplied from it. Each counter required an H.T. supply to run the photomultiplier and a negative 9 volt supply to power the emmitter follower circuit. Because the counters were used as a telescope it was not necessary to balance them to give an equal gain. Consequently the counters were run at the common potential of 2.3 Kv; the counting rates for each counter at this potential were 34.4

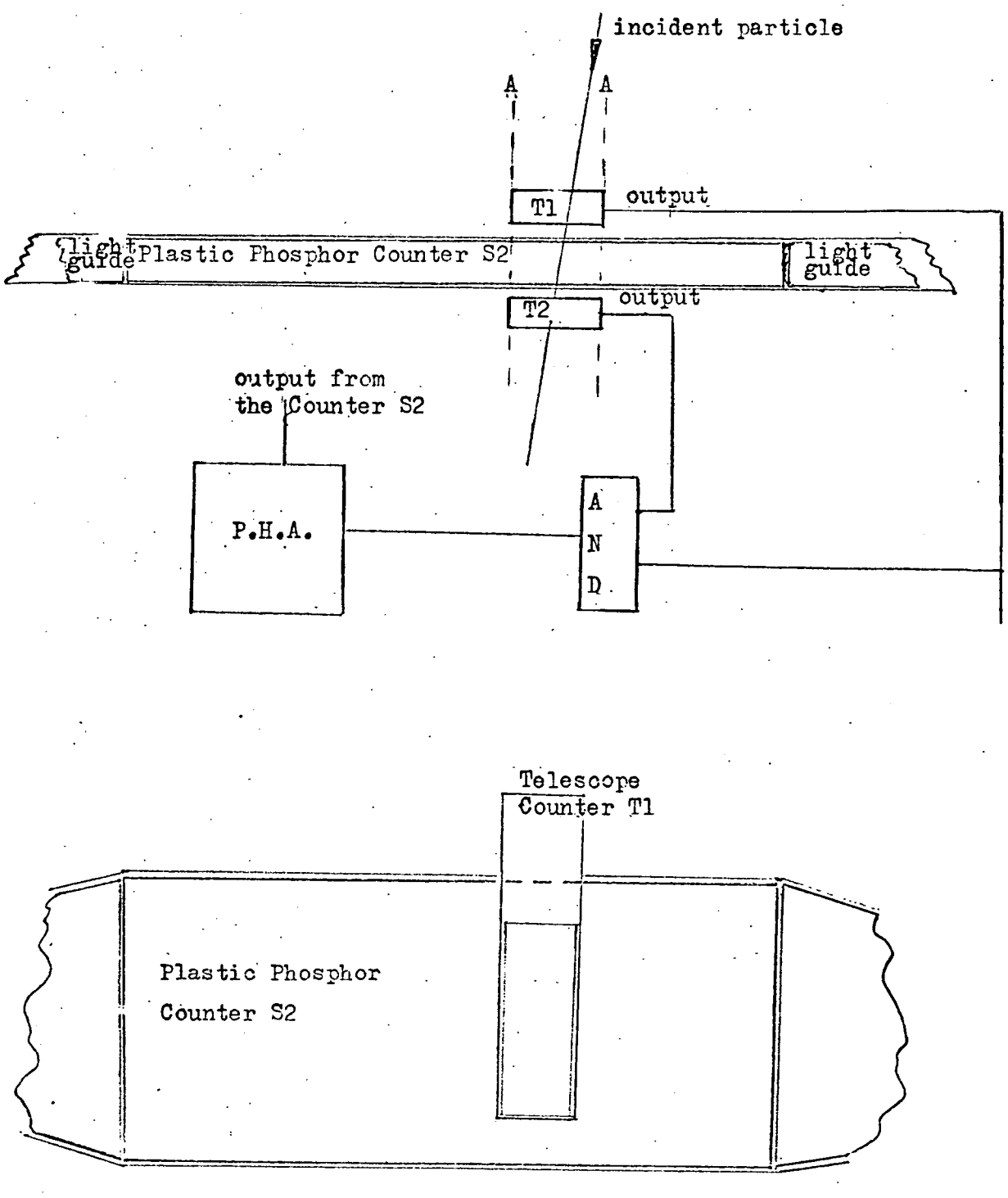

Fig 5:5 Set up for Measuring the Response Curve of Counter S2

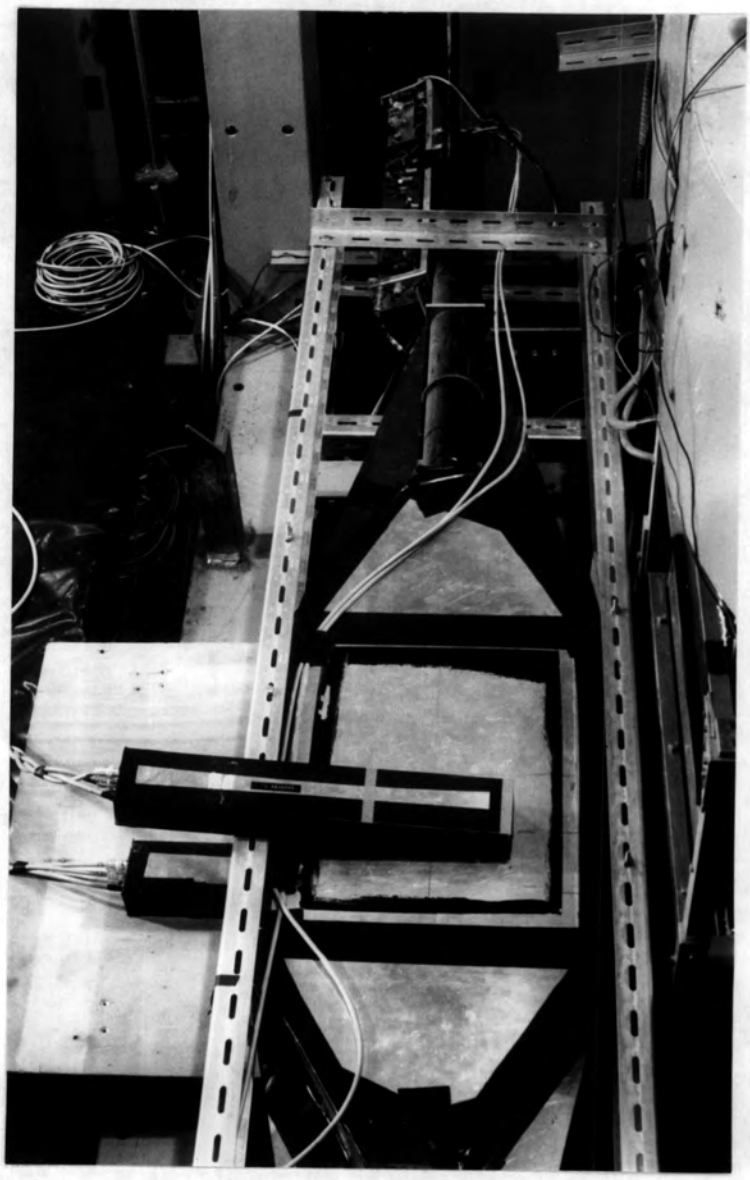

Plate 5.1

counts per sec. for counter T1 and 18.9 counts per sec. for counter T2.

The control box also contained the coincidence unit for the telescope. The output from each of the counters was fed into this unit which consisted of an AND gate such that it produced an output pulse only if pulses arrived at the gate from each counter simultaneously.

5.2.3 The Measurement of the Response Curve

The counter S2 was placed horizontally to measure the response as this gave a higher incident particle rate than the vertical position. To measure the 'response' of the counter at a particular position AA(Figure 5.5) the telescope counters T1 and T2 were placed laterally across the counter one above and the other below in the position AA. The counter positions are also shown in plate 5.1. The output from the telescope coincidence unit was fed to the gate of a Pulse Height Analyser. The output from the counter S2 was fed to the input of the P.H.A. When a particle traversed the telescope counters T1 and T2 the corresponding output pulse from the coincidence unit opened the gate on the P.H.A. so that it could accept the corresponding output pulse from the counter S2. If a particle traversed another part of the counter i.e. did not traverse the counters T1 and T2, the gate of the P.H.A. remained closed such that the corresponding pulse from the counter S2 was rejected. Thus only pulses which corresponded to particles which traversed the section AA of the counter were accepted by the P.H.A. and in this way the pulse height distribution for this section was obtained. From this pulse height distribution the most probable pulse height for the position was determined. Values for the most probable pulse height were determined at approximately 3 cm. intervals along the axis of the counter; the exact positions are given in Figure 5.6 which shows the final response curve.

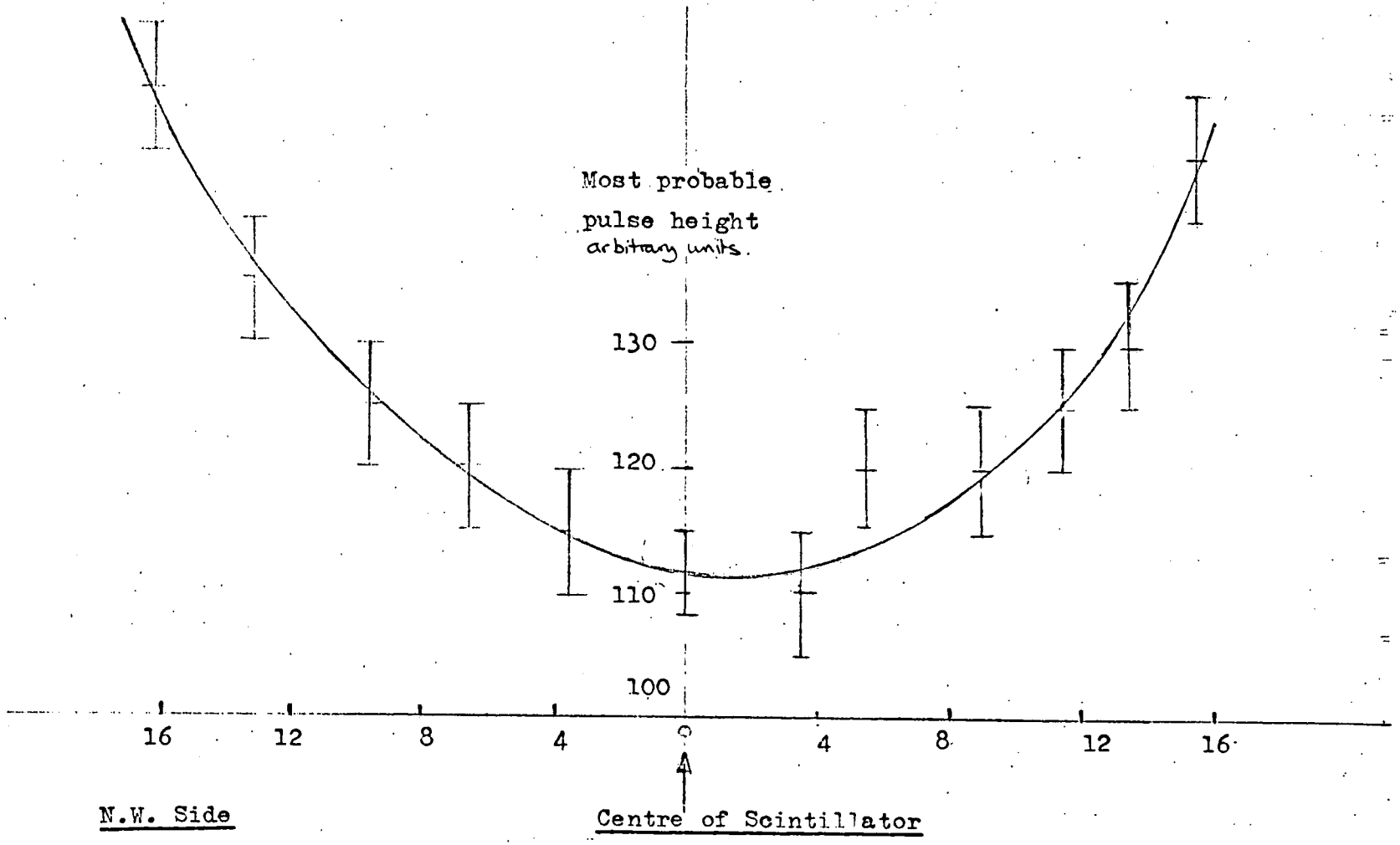

Fig 5:6 Response Curve for Scintillator Counter S2.

5.2.4 The Effect of the Non-Linear Response Curve

It can be seen that the response curve was almost symmetrical about the centre line of the counter and that the sensitivity increased outward towards the light guides. For particles of a particular energy traversing a thin section of plastic phosphor there is no unique value for the energy loss; it has already been shown in Chapter 2 that the energy loss takes the form of a negatively skewed distribution (Figure 2.3 - Chapter 2).

For particles traversing the counter in the centre, the pulse height will be less than the expected value ~~and~~ whilst for those particles traversing the ~~counter towards the edge of the phosphor~~ phosphor near to ~~the ends nearest~~ the photocathodes the pulse height will be higher than expected. Thus the overall effect is for the distribution pulse height for particles of a particular energy to be broadened about the most probable pulse height. It is estimated from the response curve that this non-uniformity will account for an 8 per cent broadening of the distribution. The non-uniformity is also evident when considering the distribution of pulse heights from the scintillation counter for particles of all momenta however this will be discussed with the results.

CHAPTER 6

Analysis of the Data and Presentation of the Results

6.1 The Reconstruction of the Particle Trajectory

Because the particle trajectories were recorded by two cameras, one photographing the inner trays B and C and the other the outer trays A and D it was necessary for correlation to project the two films simultaneously. A system of two projectors was used, with path lengths of about 8 feet to get images of acceptable size. Two moveable white boards on the projection table were used as screens, this allowed the images of the flash tube trays to be positioned by adjustment of the boards which was much easier than adjusting the film carriage of the projectors.

To obtain the projected positions of all the tubes in each tray the spectrograph cameras were loaded with film and a Gamma radiation source was placed in front of the flash tube tray A. A series of high voltage pulses were then applied to this tray and the fiduciary bulbs illuminated, the cameras were then wound on. The position of the Gamma source was altered and the procedure repeated several times to ensure that all the tubes in the tray had flashed. This was repeated for the trays B, C and D. These films were then projected, the positions of the fiduciary bulbs and the clocks were marked on the projection boards for each tray and circles corresponding to the positions of the flash tubes drawn in. The tube positions were numbered consecutively for each row starting from the North West side of the spectrograph and the rows numbered from the direction of the incident particles for each tray. By noting the tube numbers and corresponding row numbers of the tubes which had flashed in each tray a particle track could be recorded.

For each 'run' of the spectrograph three films were obtained, one recording the oscilloscope traces, the other two recording the flash tube trays A and D, and B and C, respectively. To analyse a 'run' the latter two films were projected and their respective frames synchronised using the clocks on each film. The projected images of the flashes in the trays were positioned on the boards by means of the fiducial marks.

Events were accepted if there were single tracks in all four trays, a track consisting of at least three flashes in line across the tray. Events were rejected if:-

(i) Two or more tracks were present in tray D.

(ii) If in any tray there were two adjacent flashes in two or more layers of flash tubes indicating the presence of knock-on electrons.

(iii) If any tray contained two particle tracks neither of which could be distinguished as corresponding to the tracks produced by the particle in the other trays.

When an acceptable event had been found the positions of the tubes which had flashed in each tray were recorded on a data sheet together with the time of the event given by the clock in the frame of trays A and D. When the complete film had been scanned the corresponding oscilloscope trace film was projected onto a drawing of the oscilloscope graticule. By reference to the clock recorded on the film the appropriate traces for the accepted events were found and the heights of the scintillator and Cerenkov pulses measured.

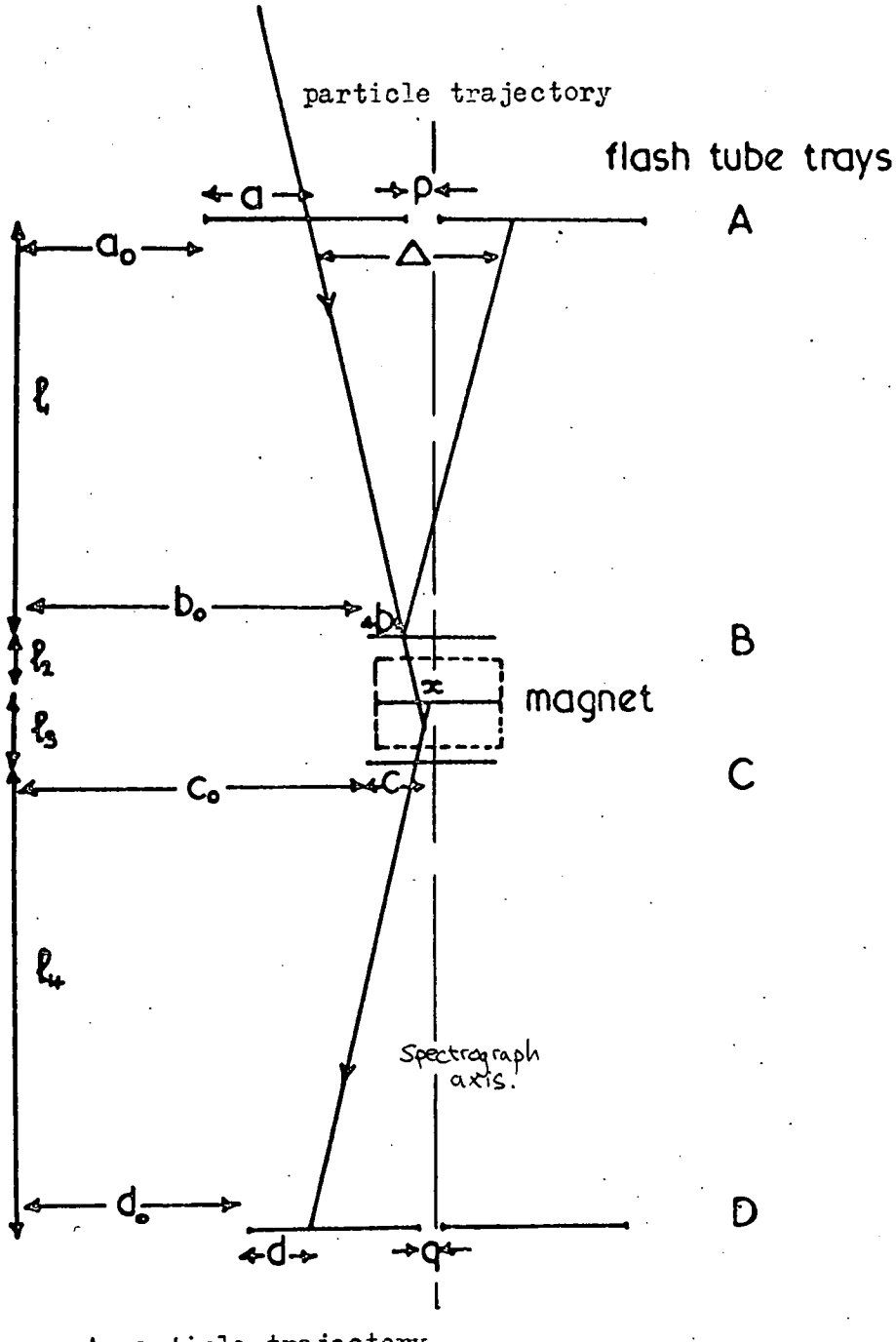

Fig 6:1 A particle trajectory

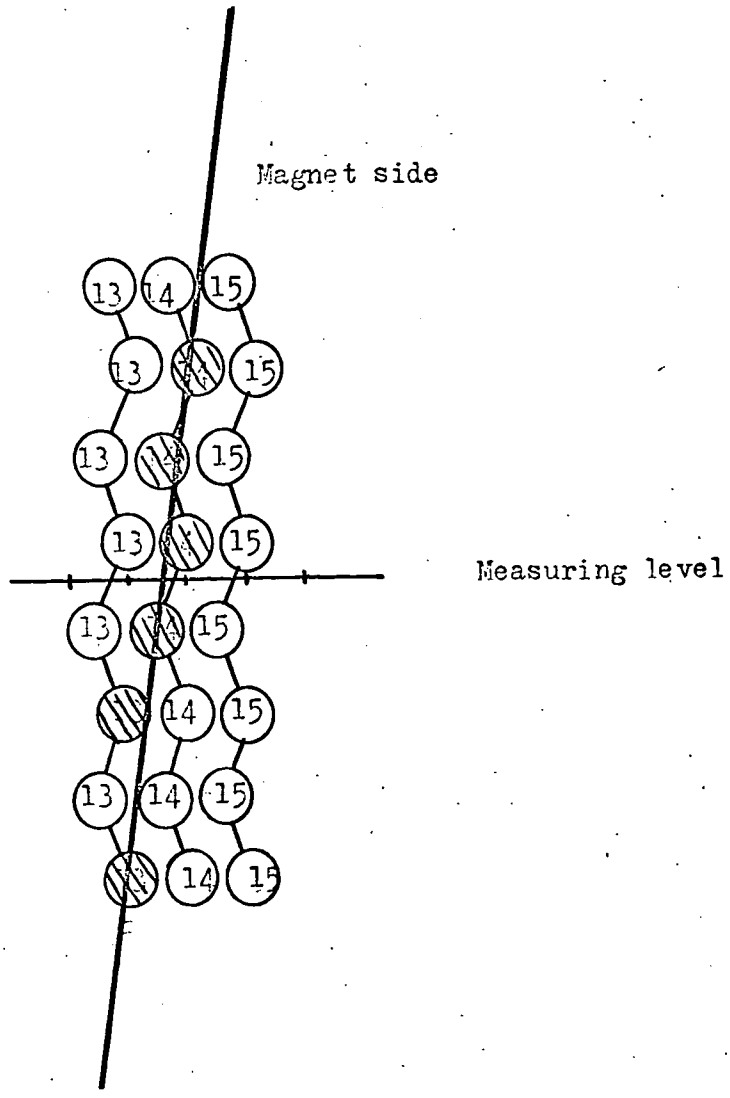

Fig 6:2 Simulator sheet for the tray C.

Thus for each accepted event the track in each tray and the pulse heights were recorded. To find the momentum of each particle it was necessary to find its coordinates with respect to the origin of coordinates in each tray. Figure 6:1 shows a particle trajectory, the required measurements are a, b, c, and d. In order to determine these, exact scale diagrams of a section of each tray A, B, C and D were drawn, the diagrams for trays B and C were enlarged by a factor of four to make the reconstruction more accurate. A scale, marked in units of one tube separation, was drawn on each diagram along the base of the fourth layer of flash tubes counting from the centre of the magnet. Figure 6:2 shows such a diagram for the tray C.

To reconstruct a particle track through a tray the tubes which had flashed were marked on the appropriate diagram from the data sheet. A cursor, consisting of a piece of perspex with a fine line scribed across it, was adjusted so that the line passed through all the tubes that had flashed and either missed or passed as near to the edge as possible those tubes which had not flashed. The point of intersection of the cursor with the scale on the diagram was recorded as the coordinate of the particle in that tray. Hence the coordinates of the particle in each tray could be determined.

To check the errors in the coordinate measurements a sample of events was analysed by three independant scanners. In most cases the agreement was to within $\pm$ 0.05 tube spaces giving an accuracy of track location of 1 m.m at levels A and D and 0.5 m.m at levels B and C.

6.2 Calculation of the Particle Momentum

A particle of charge $-e$ and momentum p moving for a distance dl through a magnetic field H will suffer a deflection $d\phi$ which is perpendicular to its own direction and that of the field by a right hand rule. The deflection $d\phi$ is given by:-

$$eHdl = p\,d\phi \qquad 6.1$$

Integrating this equation over the width l of the magnetic field gives:-

$$\phi p = e\int Hdl$$

so that

$$p\phi = 300\int Hdl \qquad 6.2$$

where p is expressed in $eV/_c$

ϕ " " " radians

Hdl " " " gauss cm.

This integral of the magnetic field was measured to be (2.0 ± 0.1) x 10^5 gauss cm. so that equation 6:2 may be rewritten:

$$p = \frac{(6.0 \pm 0.3) \times 10^7}{\phi} \qquad 6.3$$

Since the deflection ϕ is small it can be expressed as $\phi = \frac{\Delta}{l}$ radians where Δ is the lateral displacement of the trajectory over an arm of length l of the spectrograph. This is shown in Figure 6:1. Equation 6:3 may then be written:

$$p\Delta = l(6 \pm 0.3) \times 10^7 \ \frac{eV}{c}\ .\ cm \qquad 6.4$$

This lateral displacement Δ can be measured from the coordinates of the trajectory in all four trays A, B, C and D or alternatively by using only the first three trays A, B and C, which is necessary when the Coulomb scattering in the Cerenkov tank becomes too large.

For the four tray measurement

$$p\,\Delta_4 = 19.05 \quad \text{GeV}/_c \text{ cm.} \qquad 6.5$$

where Δ_4 is measured over the arm $l_1 = 317.5$ cm.

For the three tray measurement

$$p\,\Delta_3 = 21.68 \quad \text{GeV}/_c \text{ cm.} \qquad 6.6$$

where Δ_3 is measured over the arm $l_1 + l_2 = 361.25$ cm

A low momentum particle suffers large Coulomb scattering when traversing the Cerenkov tank. (4 feet deep). This produces a large location error in tray D. Thus a 3 tray calculation was used for all particles having a displacement $\Delta_4 > 2.0$ cm. The error in measuring Δ_3 was about 17% such that for particles having momentum above 10 GeV/$_c$ where this error becomes equal to that due to scattering, the four tray measurements were used.

Using the measured coordinates of the trajectory in all four trays the displacement of the trajectory Δ_4 measured over the arm l_1 is given by:-

$$\Delta_4 = (a+a_o) - (b+b_o) - \frac{l_1}{l_4}\left\{(c+c_o) - (d+d_o)\right\} \qquad 6.7$$

The measurement of the geometrical constants a_o b_o c_o and d_o has already been discussed in Chapter 5, they remain constant for all events hence equation 6.7 may be written:-

$$\Delta_4 = (a - b) - 0.868\ (c - d) + \Delta_o \qquad 6.8$$

where $\Delta_o = a_o - b_o - 0.868.(c_o - d_o)$ and $l_1/l_2 = 0.868$.

Using the measured coordinates of the trajectory in the first three trays the displacement Δ_3 measured over the arm $(l_1 + l_2)$ is given by:-

$$\Delta_3 = \frac{l_1 + l_2}{l_3}\left[(a + a_o)\ \frac{(l_2+l_3)}{l_1} - (b+b_o)\frac{(l_1+l_2+l_3)}{l_1} + (c+c_o)\right] \qquad 6.9$$

or eliminating the geometrical constants a_o, b_o, c_o.

$$\Delta_3 = \frac{l_1+l_2}{l_3}\left[a\left(\frac{l_2+l_3}{l_1}\right) - b\left(\frac{l_1+l_2+l_3}{l_1}\right) + c\right] + \Delta_o \qquad 6.10$$

where

$$\Delta_o = \frac{l_1+l_2}{l_3}\left[a_o\left(\frac{l_2+l_3}{l_1}\right) - b_o\left(\frac{l_1+l_2+l_3}{l_1}\right) + c_o\right]$$

The measurement of a, b, c and d the coordinates of a particle trajectory with respect to the origin of coordinates in each tray has already been described. These are expressed in units of tube space. Rewriting equations 6:8 and 6:10 with the coordinates a, b, c and d expressed in units of tube space:-

Equation 6:8, the four tray displacement, becomes:-

$$\Delta_4 = 1.905a - 0.86 - 0.695c + 1.655d + (\Delta_{o_1}, \Delta_{o_2}, \Delta_{o_3}, \Delta_{o_4}) \qquad 6.11$$

The value of Δ_o can take one of four values depending on the particle track position in trays A and D because these trays were each made up from two separate units, then:-

$\Delta_{o1} = -87.55$ cm. for a $\geq$ 39 t.s. d $\leq$ 30 t.s.

$\Delta_{o2} = -95.43$ cm. for a $\leq$ 38 t.s. d $\geq$ 30 t.s.

$\Delta_{o3} = -110.84$ cm. for a $\leq$ 38 t.s. d $\leq$ 29 t.s.

$\Delta_{o4} = -72.14$ cm. for a $\geq$ 39 t.s. d $\geq$ 30 t.s.

Equation 6.10, the 3 tray displacement, becomes:-

$$\Delta_3 = 3.77a - 6.45b + 4.87c + (\Delta_o', \Delta_o'') \qquad 6.12$$

again Δ_o can take one of two values depending on the position of the track in tray A.

$\Delta_o' = -156.5$ cm. for a $\leq$ 38 t.s.

$\Delta_o'' = -110.42$ cm. for a $\geq$ 39 t.s.

The relation between the two displacements Δ_3 and Δ_4 is given by:-

$$\Delta_3 = \frac{l_1 + l_2}{l_1} \Delta_4$$

$$\Delta_3 = 1.138 \cdot \Delta_4 \qquad 6.13$$

6.3 The Accuracy of the Momentum Measurements

The accuracy to which the momentum of a particle can be determined depends on the accuracy of measurement of its displacement Δ. The error in measuring the displacement depends on, the accuracy to which the coordinates of the trajectory a, b, c and d can be determined and the accuracy of the geometrical constants a_o, b_o, c_o and d_o obtained by direct measurement. In order to check the accuracy of these geometrical constants the spectrograph was run without the magnetic field.

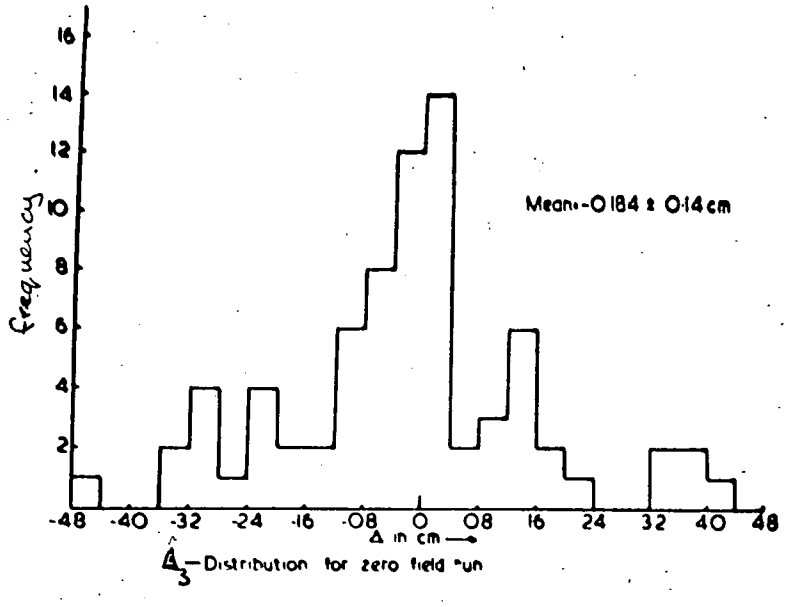

Fig 6:3a

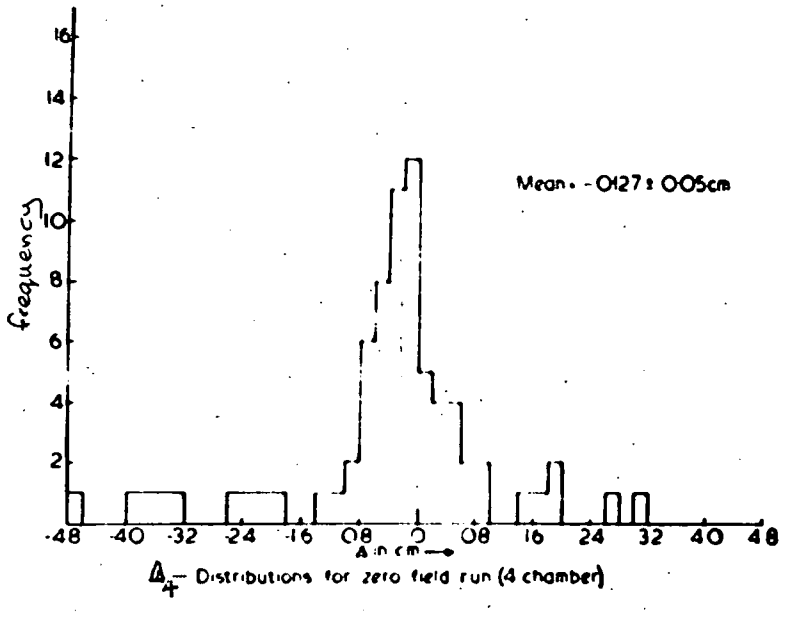

Fig 6:3b

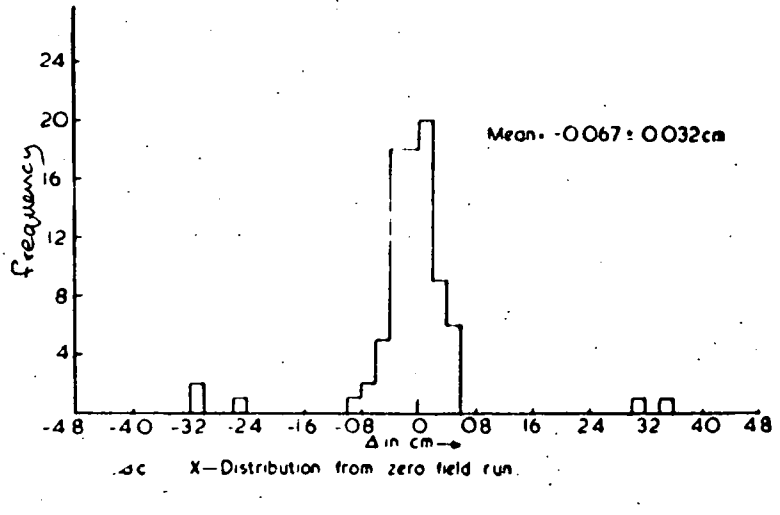

Fig 6:3c

The displacements Δ_3 and Δ_4 were calculated for all the 'events' and their frequency distributions are shown in Figures 6.3a and 6.3b.

The mean value of $\Delta_3 = (0.184 \pm 0.14)$ cm.

The mean value of $\Delta_4 = (-0.127 \pm 0.05)$ cm.

Theoretically without the magnetic field, particles traversing the spectrograph should suffer no deflection however these mean values are zero within the limit of accuracy of the track location. This indicates that the measured values for the geometrical constants are acceptable. Had the mean values been outside the limit of accuracy of track location this would have indicated that a mistake had been made whilst measuring the geometrical constants.

Obviously this zero field could not be used to check the accuracy of track location during the actual spectrograph runs. To check these coordinates, the discrepancy X at the centre of the field was calculated. This represents the difference between, the lateral coordinate of the particle trajectory at the centre of the field calculated using the particle track located by its coordinates in trays A and B and the lateral coordinate calculated using the particle track located by its coordinates in the trays C and D.

The main reasons for this discrepancy X are:-

1. Errors in location at the measuring levels i.e. the coordinates a, b, c and d.
2. Inaccuracies due to uncertainties in the positions of the flash tubes in the trays.
3. Inaccuracies in the measurement of the geometrical constants.
4. Multiple coulomb scattering in the Cerenkov tank causing location errors in tray D.

It can be shown that the discrepancy X is given by the relation:-

Fig. 6:4 Frequency distribution of pulse heights for particles of all momenta

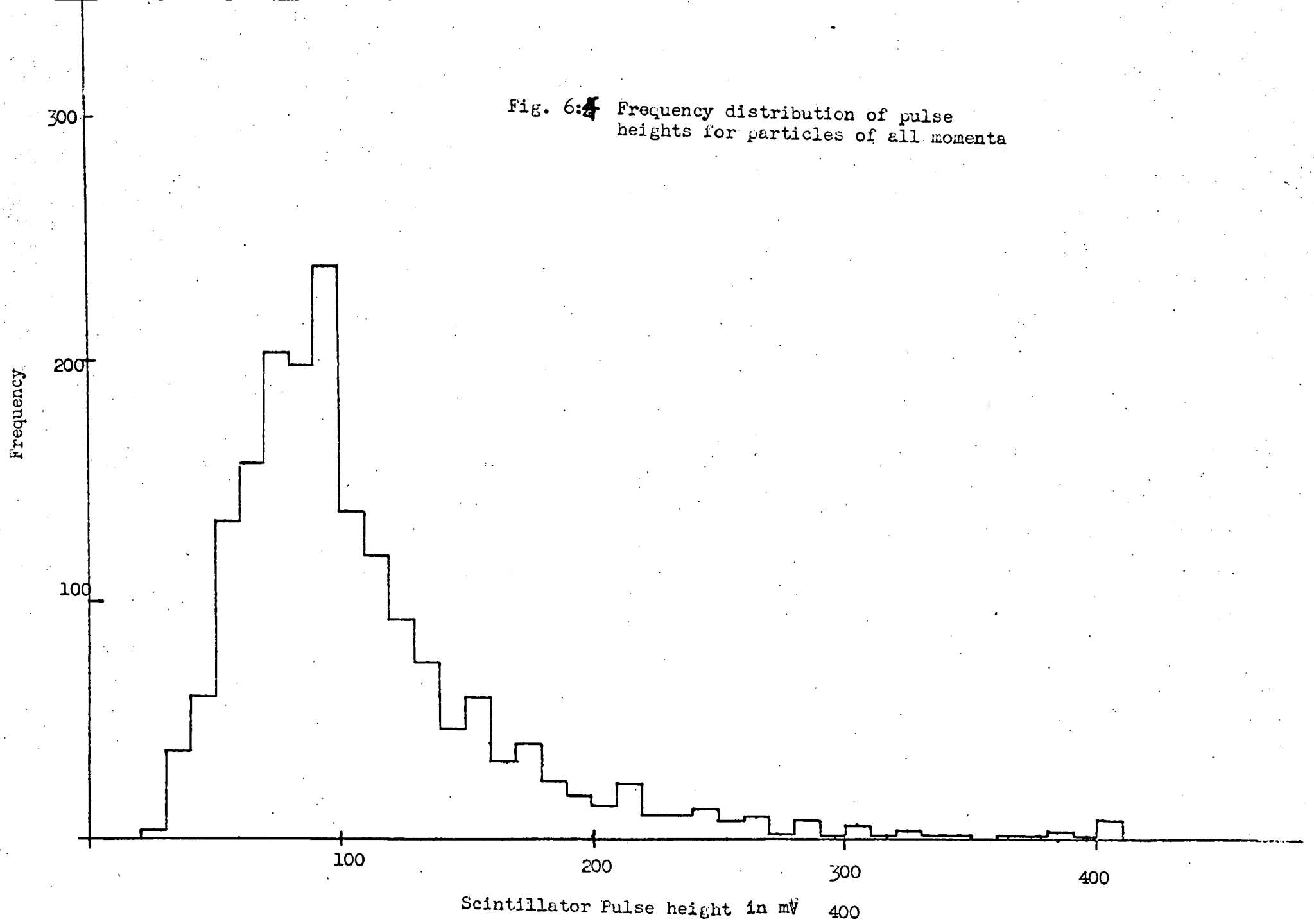

$$X = (b+b_o)-(c+c_o)-\frac{l_2}{l_1}\left\{(a+a_o)-(b+b_o)\right\}+\frac{l_3}{l_4}\left\{(d+d_o)-(c+c_o)\right\} \qquad 6.14$$

or

$$X = b - c - \frac{l_2}{l_1}(a-b)+\frac{l_3}{l_4}(d-c) + X_o \qquad 6.15$$

where $X_o = (1+\frac{l_2}{l_1})\, b_o - \frac{l_2}{l_1} a_o - (1+\frac{l_3}{l_4})\, c_o + \frac{l_3}{l_4} d_o$

Then expressing coordinates a, b, c and d in units of tube space and substituting for the numerical values of l_1, l_2, l_3 and l_4.

$$X = 0.91b - 0.263a - 0.929c + 0.307d + (X_{o_1}, X_{o_2}, X_{o_3}, X_{o_4}) \qquad 6.16$$

Again because both the trays A and D consisted of two units X_o can take one of four values depending on the particular position of the track in them.

Then, $X_{o1} = 4.93$ cm. for $a \leq 38$ $d \leq 29$

$X_{o2} = 7.95$ cm. for $a \leq 38$ $d \geq 30$

$X_{o3} = 4.73$ cm. for $a \geq 39$ $d \geq 30$

$X_{o4} = 1.71$ cm. for $a \geq 39$ $d \leq 29$

The frequency distribution of the discrepancy X has been calculated for the zero field run and is shown in Figure 6.3c.

The mean value of this distribution $= -0.067 \pm 0.032$ cm. This is close to zero and again indicates that the values for the geometrical constants are correct. Similarly the frequency distribution of the discrepancy X for all the accepted events with the magnetic field on has been compiled and is shown in Figure 6.5.

The mean value of this distribution = (0.0075 ± 0.0068) cm. This is also close to zero and indicates that track location errors are acceptable. Events which had values of $|X|$ greater than unity were rejected, these were probably due to two unassociated particles traversing the spectrograph at the same time.

6.4 The Maximum Detectable Momentum of the Spectrograph

When a particle traverses the spectrograph the scattering is a second order effect compared to the magnetic deflection thus the accuracy of track location must define the maximum detectable momentum (m.d.m.) The m.d.m. is then the momentum of a particle whose displacement Δ is equal to the probable error σ_Δ in measuring this displacement. This probable error σ_Δ can be obtained from the distribution of the discrepancy X for all accepted particles and is defined such that the area of the distribution between $-\sigma_\Delta$ and $+\sigma_\Delta$ is half the total area. The estimated value of σ_Δ was 0.187 such that the m.d.m. is given by:-

$$P \text{ m.d.m.} = \frac{21.68}{\sigma_\Delta} = 116 \text{ GeV}/_c$$

6.5 Presentation of the Results

Twenty-five overnight runs of the spectrograph were made with the magnetic field switched on, thirteen positive field runs and twelve negative field runs. A total of 2037 accepted events were recorded from the spectrograph films and of these 1822 events were finally selected as being single particles traversing the spectrograph. Those rejected either had no corresponding scintillation pulses recorded for them or their X discrepancy was too large.

The stability of the scintillation counter electronics was checked as a fuction of time by dividing the data into four successive time intervals with approximately equal numbers of events in each.

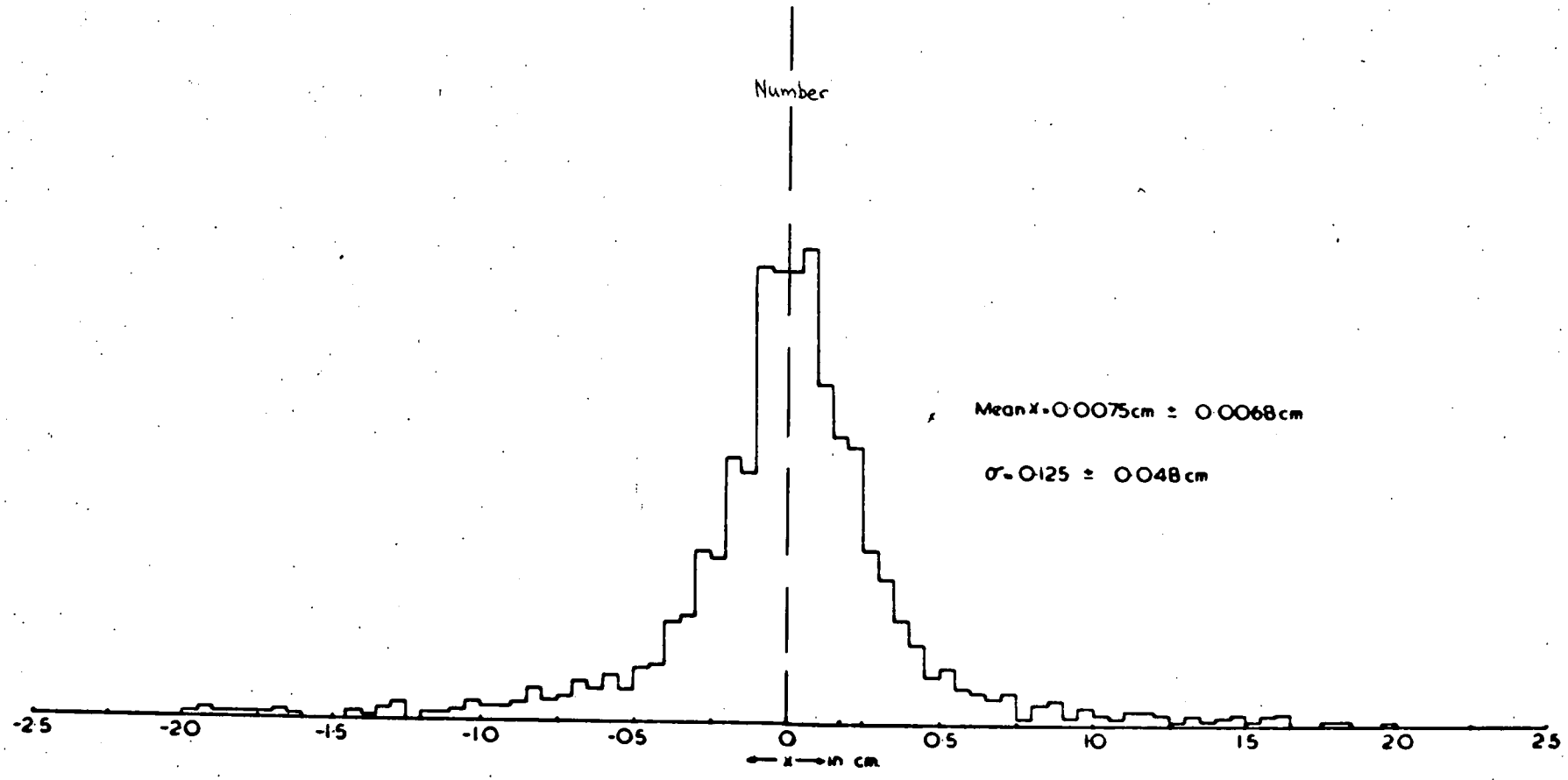

Fig. 6:5 The x distribution for all accepted particles

The frequency distribution of the scintillator pulse heights was drawn and the median pulse height calculated for each interval. These agreed to within ± 3% which indicates that the counter response was stable over the twenty-five runs of the spectrograph.

Figure 6.4 shows the frequency distribution of pulse heights for all accepted events. The peak of this distribution has a width at half height of 35 ± 3% which is close to the expected value of 29%. The width of the distribution at half the maximum height has been expressed as a percentage of the pulse height at this peak and this is sometimes referred to as the resolution of the distribution. This 'resolution' is made up from the following factors.

(i) Laudau fluctuations in the ionization loss (Laudau 1944) which are caused by the statistical variations in the energy absorbed from the radiation by the phosphor. These account for 19% broadening which includes 2% broadening to take account of the variation in muon energies.

(ii) The statistical variation in the number of electrons emmitted by the photocathodes of the photomultipliers, 20% broadening.

(iii) The non-uniformity of the counter. The maximum variation of the counter response was found to be ± 15%, but its contribution to the width of the distribution depends on the way in which the sensitivity varies throughout the phosphor. ~~Because~~ The response of the counter rises sharply as the outer edges of the phosphor are approached, the effect on the distribution was reduced to estimated to be 8%. because the size of the counter S7 reduces the effective apeture of the counter S2.

The total contribution of 29% is obtained by adding quadratically the above independant contributions.

TABLE 6:1

The momentum cells for grouping the scintillator pulses

Mean Momentum in the cell $\left(\frac{GeV}{c}\right)$	Cell Units cm.	Number of Particles
0.355	$42 < \Delta \leq 80$	59
0.723	$18 < \Delta \leq 42$	168
1.50	$12 < \Delta \leq 18$	133
2.32	$8 < \Delta \leq 12$	166
3.18	$6 < \Delta \leq 8$	163
4.56	$4 < \Delta \leq 6$	214
8.04	$2 < \Delta \leq 4$	361
15.19	$1 < \Delta \leq 2$	301
30.48	$0.5 < \Delta \leq 1$	144
98.6	$\Delta \leq 0.5$	113

TABLE 6:2

The distribution of the scintillator pulse heights in the momentum cells

	Mid Value of Scintillator Pulse Height, in mV.													
Cell	25	35	45	55	65	75	86	95	105	115	125	135	145	155
80 - 42	0	1	4	5	2	11	2	6	7	2	1	5	0	3
42 - 18	0	3	3	10	18	18	18	15	17	7	8	12	7	6
18 - 12	0	3	3	7	10	17	9	17	11	14	15	4	5	3
12 - 8	1	5	2	17	18	15	18	28	8	10	11	6	5	5
8 - 6	0	2	3	6	5	19	17	22	16	8	11	10	5	6
6 - 4	0	2	8	15	16	21	29	33	8	20	9	8	5	7
4 - 2	0	9	18	27	36	45	42	39	26	27	15	12	9	11
2 - 1	0	7	9	21	31	31	38	42	22	12	12	7	8	9
1 - 0.5	2	3	4	11	10	10	14	20	15	13	7	5	1	4
0.5	0	2	6	14	11	16	12	17	7	6	3	5	2	5

TABLE 6:2 (continued)

Mid Value of Scintillator Pulse Height, in mV.

Cell	165	175	185	195	205	215	225	235	245	255	265	275	285	295
80 - 42	1	3	2	0	0	1	0	2	0	0	0	0	0	0
42 - 18	2	4	3	2	3	3	1	1	1	1	1	1	0	2
18 - 12	1	0	2	1	0	1	1	1	2	1	1	1	0	0
12 - 8	1	1	1	1	1	2	1	2	2	0	1	0	0	2
8 - 6	3	2	1	3	2	1	3	1	1	0	1	1	1	2
6 - 4	10	2	4	2	3	3	1	0	2	1	0	0	0	1
4 - 2	5	6	6	4	2	5	2	1	0	4	2	2	0	0
2 - 1	7	15	5	2	1	4	2	1	2	4	0	3	1	1
1 - 0.5	1	5	2	2	1	3	0	1	1	2	2	1	0	0
0.5	2	2	0	1	1	0	0	1	0	0	0	0	0	0

TABLE 6:2 (continued)

Cell	Mid Value of Scintillator Pulse Height, in mV.										
	305	315	325	335	345	355	365	375	385	395	400
80 - 42	0	1	0	0	0	0	0	0	0	0	0
42 - 18	0	0	0	0	0	0	0	0	0	0	1
18 - 12	1	2	0	0	0	0	0	0	0	0	0
12 - 8	0	0	0	1	0	0	0	0	0	0	1
8 - 6	0	0	0	0	0	1	0	1	0	0	2
6 - 4	0	1	0	2	1	0	0	0	0	0	0
4 - 2	0	1	1	0	1	1	0	0	1	0	1
2 - 1	0	1	0	0	0	0	0	0	1	1	1
1 - 0.5	0	0	0	0	0	0	0	0	1	0	3
0.5	0	0	0	0	0	0	0	0	0	0	0

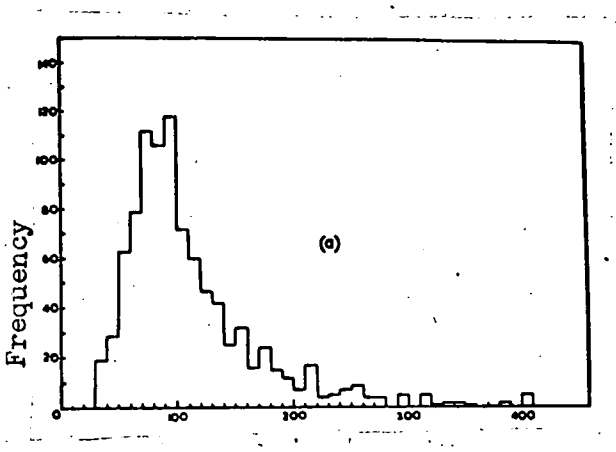

pulse heigh in mV.

(a) positive muons

Fig. 6.6 Pulse height distributions for positive and negative muons.

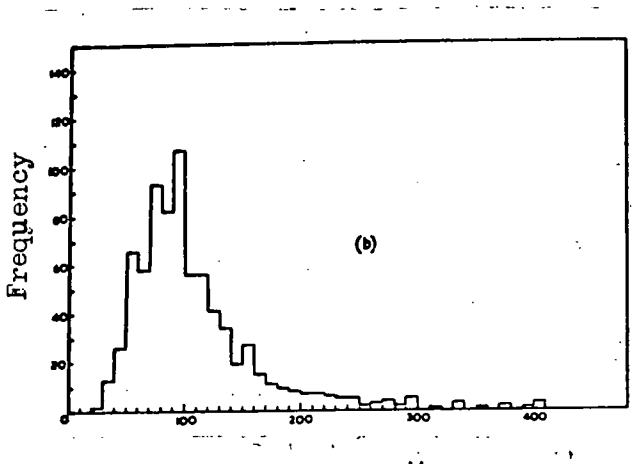

Pulse height in mV

(b) negative muons

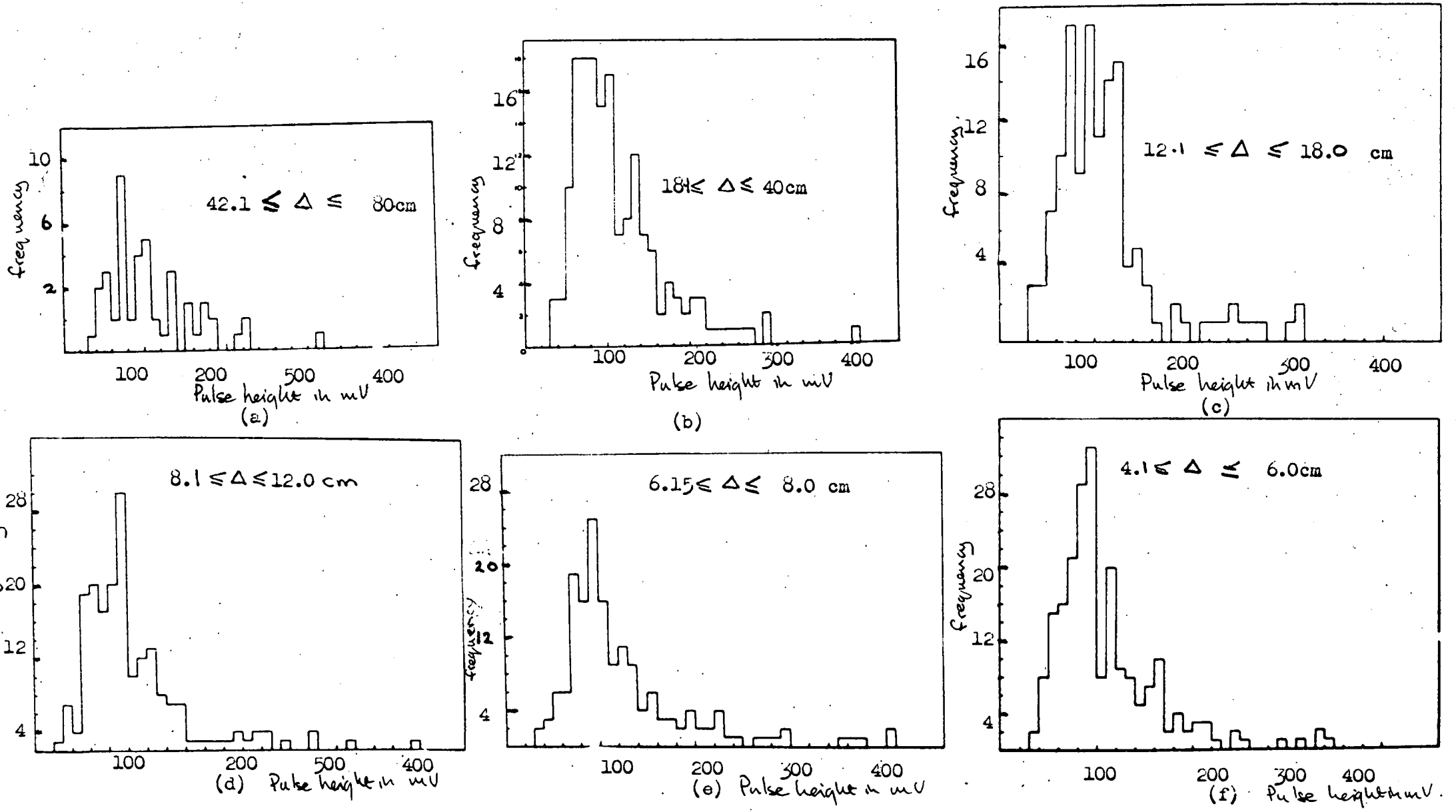

Fig. 6.7 Scintillation Pulse height distribution for different momentum cells

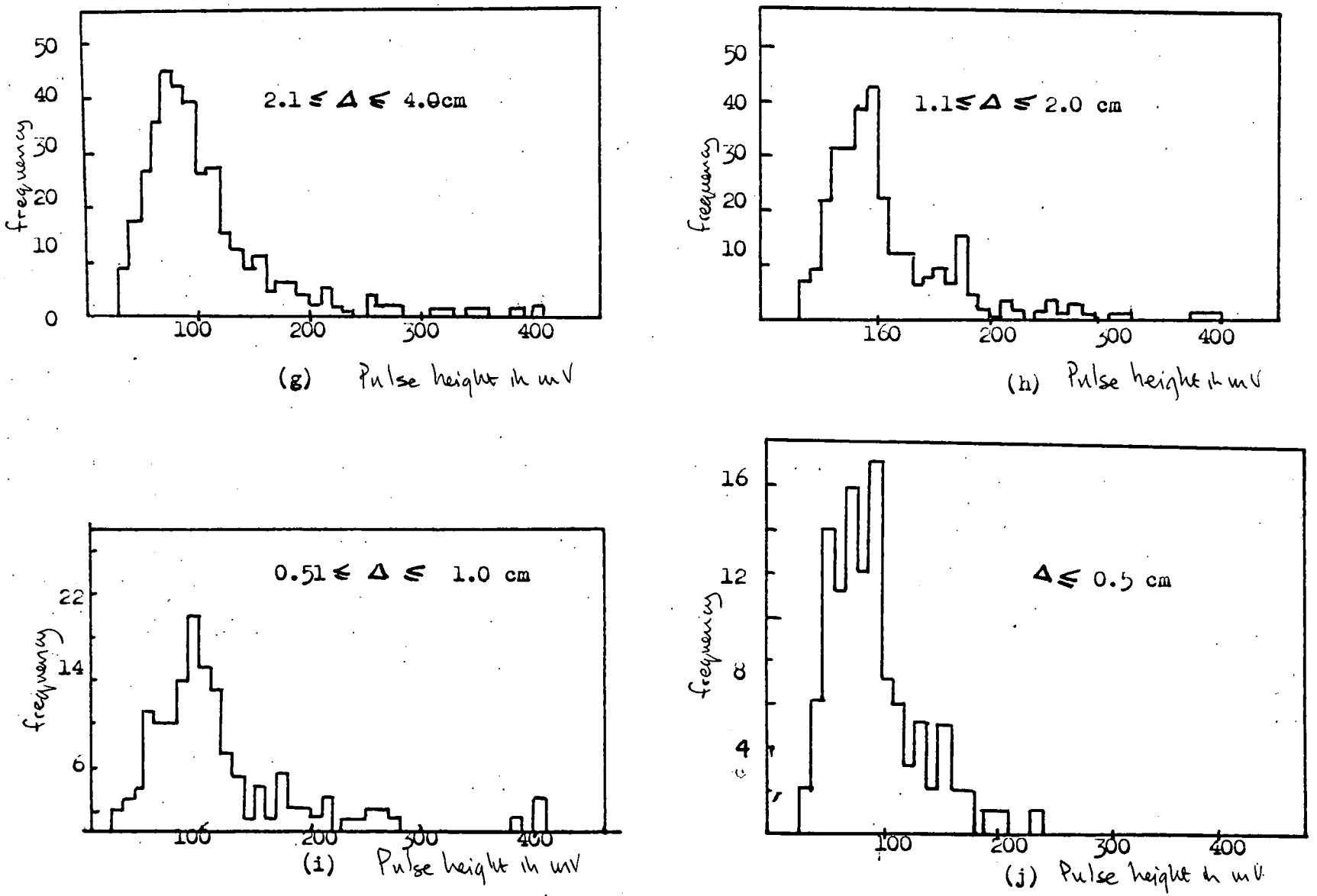

Fig. 6.7 (cont'd) Scintillation Pulse height distributions for different moment cells.

In order to compare the ionizing power of positive muons and negative muons the pulse height distributions were compiled for each. The sign of the particle of each event was determined by reference to the direction of the magnetic field and the sign of its displacement Δ. The distributions are shown in Figure 6.6.

6.5.1 The Scintillator Pulse Height as a Fuction of Momentum

The 1822 selected events were divided into ten momentum cells which were chosen so that there were sufficient events in each group to give a reliable pulse height distribution. The mean momentum of each cell in units of GeV/$_c$ together with the cell limits expressed in terms of the displacement Δ and the number of particles in each cell are given in table 6.1. Table 6.2 gives the distribution of the scintillator pulse heights within these cells. The frequency distribution of these pulse heights were drawn for each momentum cell and are shown in Figure 6.7 (a) to (j). A cut off at 200 mV was imposed to exclude high energy losses and other spurious effects in the counter. It has already been shown in section 2.4 that this will not affect the mode values of the distributions since they are insensitive to the high energy losses.

There are various methods by which the most probable pulse heights of the skewed distributions may be found and the following three methods were considered.

(i) The subjective method

Each of the skew distributions was transformed to approximately a normal curve by plotting the pulse height frequency against the logarithmn of the pulse height. This can be done because the distributions are approximately log normal. To each distribution a smooth curve was fitted and a master curve compiled from these. The peak position was marked on this master curve. The peak position of each distribution

was then found by fitting this master curve to it. This was repeated by ten different people and a mean value for each peak determined. These mean values were accepted as the most probable pulse heights for the distributions.

(ii) The Reciprocal Method

If a distribution is log normal then using arithmetic probability paper, if the cumulative relative frequency of the distribution is plotted against the reciprocal of the variable a straight line is obtained. The most probable value of the distribution is then given by the point on the straight line corresponding to the cumulative relative frequency of 50. For each cell of a distribution the cumulative relative frequency will be the number of pulses of height less than the middle value of the cell expressed as the percentage of the total number of pulses in the distribution with the cut-off at 200 mV.

This method was applied to each of the distributions and using a least squares fit to draw the best straight line in the region 10 to 90 of the cumulative relative frequency the most probable pulse heights were determined.

A similar method to this can be used by plotting the logarithm of the variable instead of its reciprocal using logarithmic probability paper. Again a straight line would be obtained providing the distribution was log normal.

(iii) The Area Method

This method has been discussed in detail by Barnaby (1961). Using the pulse height frequency distribution of all the accepted events the ordinate of the peak value was drawn in and with a cut-off at 200 mV the area under the histogram on each side of it measured with a planimeter. The ratio of these areas was 1:1.42.

TABLE 6:3

The mean, median, and the mode of the scintillator pulse height distributions

Cell in cm.	Mean in mV	Median in mV	Mode in mV by Reciprocal Method	Mode in mV by Subjective Method	Mode in mV by Area Method
$42 < \Delta \leq 80$	99.55 ± 5.5	94.2 ± 5.5	92.5 ± 3.4	80.86 ± 3.4	84.0 ± 3.4
$18 < \Delta \leq 42$	100.62 ± 4.9	94.3 ± 4.9	90.5 ± 2.5	86.0 ± 2.5	88 ± 2.5
$12 < \Delta \leq 18$	97.38 ± 4.1	97.4 ± 4.1	86.5 ± 2.5	84.88 ± 2.5	89 ± 2.5
$8 < \Delta \leq 12$	92.19 ± 3.9	90.2 ± 3.9	84.5 ± 2.2	81.88 ± 2.2	83 ± 2.2
$6 < \Delta \leq 8$	103.7 ± 4.2	97.9 ± 4.2	93.99 ± 2.1	90.33 ± 2.1	92 ± 2.1
$4 < \Delta \leq 6$	99.27 ± 3.2	92.6 ± 3.2	86.0 ± 1.8	83.35 ± 1.8	86 ± 1.8
$2 < \Delta \leq 4$	94.00 ± 2.5	87.97 ± 2.5	85.0 ± 1.3	78.22 ± 1.3	81 ± 1.3
$1 < \Delta \leq 2$	101.0 ± 5.0	90.6 ± 5.0	84.5 ± 1.6	81.22 ± 1.6	84 ± 1.6
$0.5 < \Delta \leq 1$	97.8 ± 5.04	95.3 ± 5.04	84.5 ± 2.2	83.44 ± 2.2	89 ± 2.2
$\Delta \leq 0.5$	88.4 ± 3.6	85.4 ± 3.6	81.0 ± 2.8	76.4 ± 2.8	79 ± 2.8

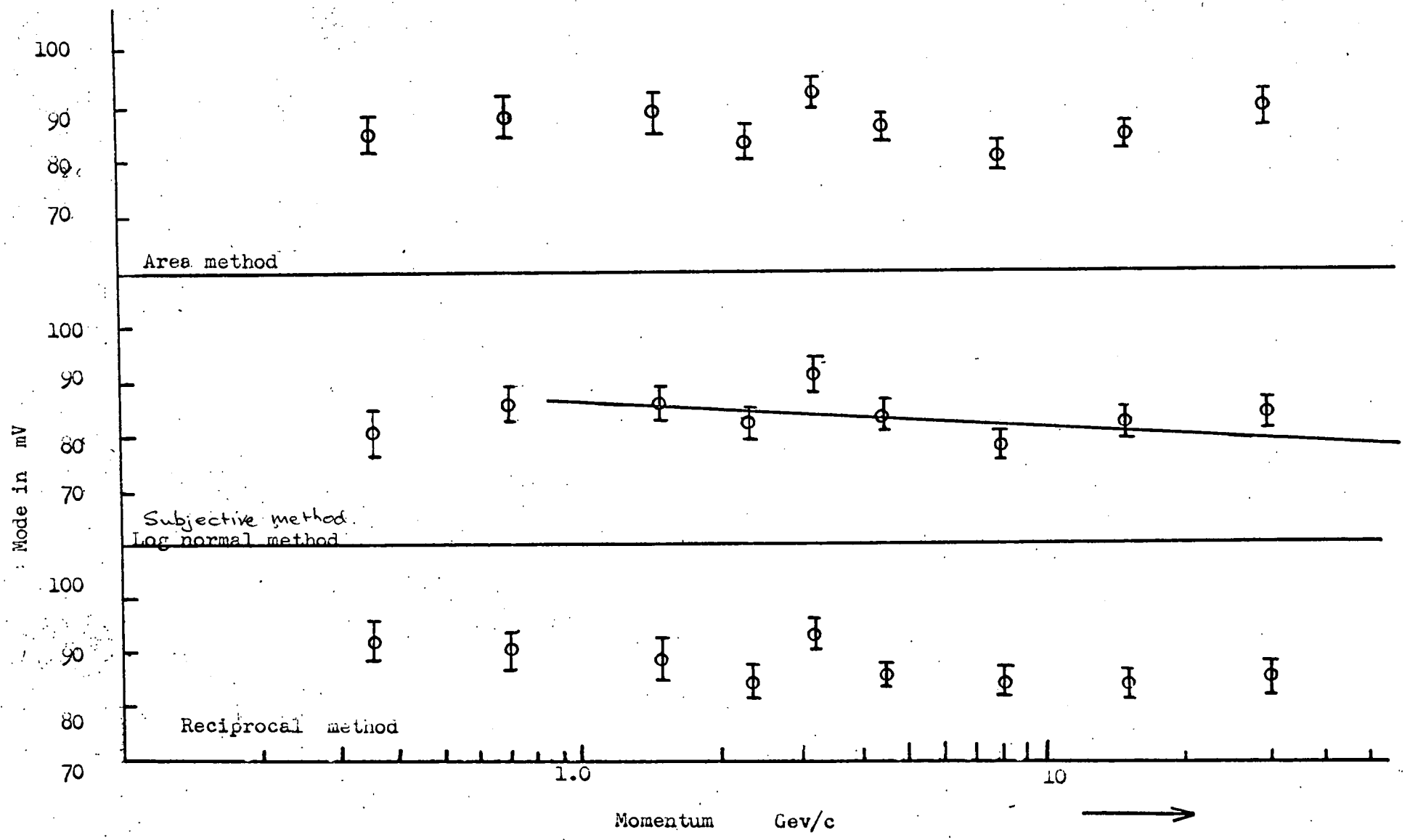

Fig. 6.8 Variation of the modes values for each method.

According to Barnaby the method is insensitive to the position of the cut-off providing the area excluded in the tail does not exceed 20% of the total area. In this case the tail of the distribution above the cut-off was 8 percent of the total area. The same cut-off was applied to each distribution and its mode value estimated by the method of successive approximation such that this ordinate divided the area in the ratio 1.1.42.

The mean and median values of each distribution were also calculated however these are dependant on the high energy tail of the distribution. Table 6.3 shows the most probable pulse heights of the distributions for each momentum cell measured using each of the three methods outlined. The mean and median values are also given. The error in estimating the most probable pulse height was taken to be the same as that for the mean value. This is given by:-

$$\text{The standard error of the mean} = \frac{\text{full width at half height}}{2.4 \cdot \sqrt{N}}$$

Where N is the number of events in the distribution up to the 200 mV cut-off.

Figure 6.8 shows the most probable pulse height plotted as a fuction of momentum for each of the three methods used. The values of the most probable pulse height obtained from each method were not the same. The subjective method is the most reliable and the results from this method have been adopted.

Since the output pulse height from the scintillation counter is directly proportional to the energy lost by ionization in the counter, the most probable energy loss due to ionization can be obtained as a fuction of muon momentum by normalising the most probable pulse height curve to the theoretical energy loss curve already calculated according to the theory of Sternheimer and given in section 2.4, figure 2.5.

TABLE 6:4

The mode and normalised mode values of the scintillator pulse height distributions

Mean Momentum GeV/c	Mode of Distribution in mV	Normalised Mode in MeV
0.36	80.9 ± 3.4	4.41 ± 0.19
0.72	86.0 ± 2.5	4.70 ± 0.14
1.50	84.9 ± 2.5	4.67 ± 0.14
2.32	81.9 ± 2.2	4.5 ± 0.12
3.18	90.3 ± 2.1	4.93 ± 0.12
4.56	83.4 ± 1.8	4.53 ± 0.10
8.04	78.2 ± 1.3	4.30 ± 0.07
15.19	81.2 ± 1.6	4.46 ± 0.09
30.48	83.4 ± 2.2	4.59 ± 0.12
98.60	76.4 ± 2.8	4.20 ± 0.15

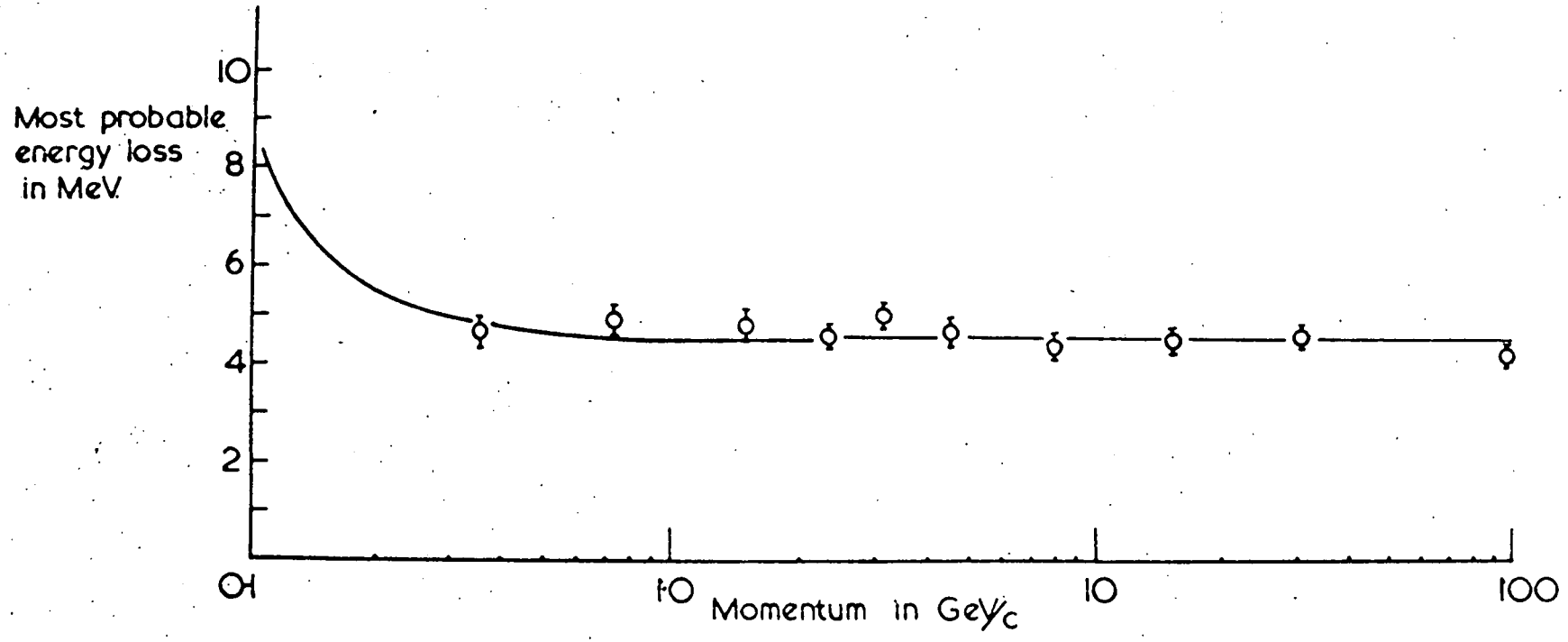

Fig. 6.9 The most probably energy loss due to ionization as a function of muon momentum

TABLE 6:5

The mode values in mV for positive and negative muons

	Reciprocal Method	Subjective Method	Area Method
μ^+	83.37 ± 2.2	83.0 ± 2.2	86 ± 2.2
μ^-	81.87 ± 2.8	81.80 ± 2.8	86 ± 2.8
$\frac{\mu^+}{\mu^-}$	1.018 ± 0.033	1.015 ± 0.033	1.00 ± 0.033

To determine the normalising factor the ~~mean~~ average value of the theoretical curve was calculated over the momentum range 1 - 100 GeV/$_c$ and compared to the ~~mean~~ average value of the experimental curve taken over the same range. The normalised values of the most probable energy loss in MeV are given in table 6.4. Figure 6.9. shows the variation of the most probable energy loss due to ionization as a fuction of muon momentum.

Finally the most probable pulse heights were determined for the pulse height distributions of positive muons and negative muons taken over the complete momentum range using the three methods already outlined. These are given in table 6.5 together with their respective ratios. The mean value of the ratio was (1.011 ± 0.035) which tends to indicate that there is no significant difference in the ionizing capacity of the two kinds of particle. It would however be difficult to detect any effect because the whole momentum range has been considered. Ideally each cell should be examined, separating the positive and negative particles, but in the present experiment the numbers were too small to do this.

6.5.2 Analysis of the Experimental Curve

There are two regions of interest on this curve the first is the form of the curve from the onset of the density effect at about 2 GeV/$_c$ and the second the form of the curve over the range 10 - 100 GeV/$_c$ where a descrease in the ionization loss is predicted by Tsytovitch. The slope for all points above 2 GeV/$_c$ has been measured by fitting a straight line using the method of weighted least squares to them. The gradient of this line-(5.0 ± 4.2)% per decade of momentum has a large error mainly because of the high mode for muons of mean momentum 3.18 GeV/$_c$. Neglecting this point the gradient is reduced to - (1.5 ± 1.1)%.

This is consistent with the Sternheimer theory which predicts a rise of about 1.5% over the range 0.2 to 10.5 GeV/$_c$ and no rise i.e. a plateau for particles of momentum greater than 10.5 GeV/$_c$

To test the Tsytovitch prediction another line was fitted to the points on the curve in the range 10 - 100 GeV/$_c$ again using the method of weighted least squares. The gradient of this line was $-(0.236 \pm 0.12)$ an overall decrease of $(2.7 \pm 1.7)\%$. This result would seem to ~~further~~ confirm the Sternheimer theory and lends little ~~no~~ support to the Tsyovitch theory which predicts a reduction of 4 - 8% below the plateau value over this range.

CHAPTER 7

Discussion

7.1 Comparison of the Present Results with Previous Work

The main aim of the present experiment was to test the Tsytovitch predictions. To improve the precision the present results have been combined with those of Crispin and Hayman (1964); this can be done because the two experiments were very similar. The experimental points have been normalised to the theoretical curve at a point corresponding to the mean momentum and mean value of the most probable energy loss of the recorded muons and are shown in Figure 7:1. A straight line has been fitted to the points above 2 GeV/$_c$ using the method of weighted least squares and has a slope of + (2.7 ± 3.3)% per decade of momentum. The mean value of the energy loss for muons having momentum greater than 10 GeV/$_c$ is (1.24 ± 0.69)% above the plateau value. These two facts clearly agree with the Sternheimer predictions and lend no support to the 4 - 8% decrease suggested by Tsytovitch.

The results of the present experiment together with those of the three experiments described in Chapter 3 are plotted in Figure 7:2. To do this the energy loss for each experiment was expressed per unit thickness of absorber; the results of Barnaby and those of Crispin and Hayman had already been combined. It is immediately evident that there is a variation in the possible values that the energy loss could take in the range of momentum 5 GeV/$_c$ to 30 GeV/$_c$. A best line has been fitted to the data over this range and this shows

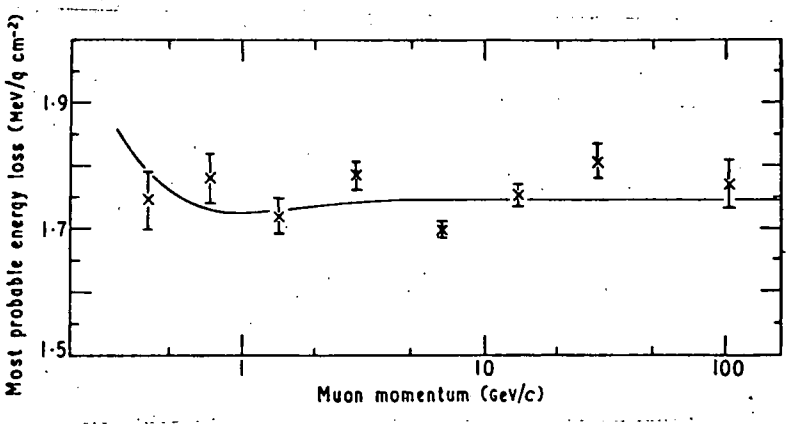

Fig 7:1 The combined results of Crispin and Hayman (1964) and the present work

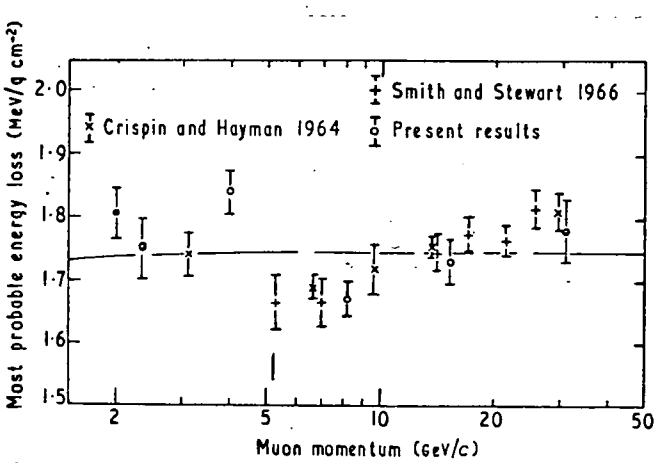

Fig 7:2 The results of Crispin and Hayman (1964), Smith and Stewart (1966) and the present work.

an increase of $(9 \pm 3)\%$ in the most probable energy loss. However because there is a lack of agreement over this range the probability that this line could lie on the plateau has been estimated to be as high as 70% so that there is little significance in the increase.

In conclusion all four experiments support the Sternheimer theory which predicts a rise of 1.5% for the momentum range 0.2 to 10.5 GeV/$_c$ and a plateau above this value and there is no evidence of a decrease of energy loss as suggested by Tsytovitch.

7.2 Discussion

To date the only results which support the Tsytovitch predictions have been from experiments on the energy loss of electrons in nuclear emulsions by Zhdanov et al (1963) and Alekseeva et al (1963). Crispin (1965) has made a very comprehensive survey of energy loss studies and shows that other workers notably Stiller and Shapiro (1953) and Jongejans (1960) who have used nuclear emulsions, give no indication of a decrease, in fact both their results support the Sternheimer theory. It should be mentioned that later experiments cast doubt on the reliability of the nuclear emulsion technique as a method of measuring the ionization loss.

Because the recent experimental work supports the Sternheimer theory, Fowler and Hall (1966) made a critical study of the various classical and semi-classical theories of energy loss of relativistic charged particles. Using perturbation theory they predict a logarithmic increase in the ionization loss similar to Sternheimer's theory and show that radiative corrections given

by Tsytovitch apply only to the case of Cerenkov radiation, where damping in the medium is negligible. If strong damping is present, as is the case for organic absorbers, any suppression effect will be smaller than that suggested by Tsytovitch. This suppression correction is also dependant on the sign of the ionizing particle so that to detect the effect charge separation would be necessary.*

More recently still Crispin and Fowler (1969) have shown that the Sternheimer results are to be understood as a representation of the ionization loss in terms of a fictitious "equivalent" Cerenkov effect. The extent to which the real Cerenkov radiation actually contributes to the ionization is expected to be small particularly in organic absorbers and hence the effect of the Tsytovitch correction will be small.

7.3 Future Work

There are two possibilities for future work:

(i) A machine experiment measuring the energy loss over a wide range of β operated under carefully controlled conditions to prevent any systematic errors. To check the validity of the results the energy loss would have to be measured at low values of β to prove the $1/\beta^2$ dependance before going on to look at the plateau expected for high values of β.

(ii) A cosmic ray experiment similar to the present one but with many more events so that the accuracy could be improved. This would however be difficult because to increase the accuracy by a factor of 10 the number of accepted events

* Fowler and Hall (1966) predicted a correction amounting to 1% with opposite sign for positive and negatively charged particles.

would have to be increased by a factor of 100 which would mean a running time for the experiment extending over a number of years.

Acknowledgements

The author is grateful to Professor G.D. Rochester for the facilities afforded him in the department and wishes to thank Dr. M.G. Thompson, his supervisor, and Professor A.W. Wolfendale for their help and encouragement at all stages of the work.

All members of the spectrograph group and the technical staff of the Physics Department are thanked for their help.

The author is grateful to the Science Research Council for the provision of a maintenance grant.

References

Alekseeva, K.I., Zhdanov, G.B. Tret'yakova, N.I., and Scharbakova, N.N., 1963, Soviet Physics, J.E.T.P., 17, 1254.

Allen, J.E., and Apostolakis, A.J., 1961, Proc. Roy. Soc. A.265, 117.

Aurela, A.N., 1965, Ph.D. Thesis, University of Durham.

Barnaby, C.F., 1961, Proc. Phys. Soc., 77, 1149.

Barton, J.C., & Crispin, A., 1962, Nuc. Instr., 16, 39.

Bethe, H.A., 1930, Ann. Phys., 5, 325.

Bethe, H.A., 1932, Z. Phys., 76, 293.

Bethe, H.A., & Ashkin, J., 1952, Experimental and Nuclear Physics, Vol. 1 (New York: Wiley), Chapter 2.

Bhabha, N.J., 1937, Proc. Roy. Soc. A, 164, 257.

Bloch, F., 1933, Ann. Phys. LPZ, 16, 285.

Bohr, A., 1948, Mat. Fys. Meddr. K. danske. Vidensk Selsk. 24, 19.

Bohr, N., 1913, Phil. Mag., 25, 10.
1915, Phil. Mag., 30, 581.

Bohr, N., 1948, Mat.- Fys. Meddr. K. danske. Vidensk. Selsk. 18, 8.

Bragg, W.H., 1912, 'Studies in Radioactivity' Macmillan and Co.

Breitenberger, E., 1956, Prog. Nucl. Phys., 4, 56

Brooke, G., 1964, Ph.D. Thesis, University of Durham.

Brooke, G., Gardener, H. Lloyd, J.L., Kisdnasamy, S., and Wolfendale, A.W., 1962, Proc. Phys. Soc., 80, 674.

Caldwell, D.O., 1955, Phys. Rev., 100, 291.

Conversi, M., & Gozzini, E., 1955, Nuo. Cim., 2, 189.

Cousins, J.E., and Nash, W.F. 1962, Adv. in Phys., 11, 349.

Coxell, H., 1961, Ph.D. Thesis, University of Durham.

Coxell, H., and Wolfendale, A.W., 1960, Proc. Phys. Soc., 75, 378.

Crispin A., 1965, Ph.D. Thesis, University of London.

Crispin, A., and Hayman, P.J., 1964, Proc. Phys. Soc., 83, 1051.

Fano, H., 1963, Ann.Rev. Nucl. Sci., 13, 1.

Fermi, E., 1940, Phys. Rev., 57, 485.

Halpern, O., and Hall, H., 1948, Phys. Rev., 73, 477.

Hayman, P.J., and Wolfendale, A.W., 1962, Proc. Phys. Soc., 80, 710.

Jones, D.G., Taylor, F.E., and Wolfendale, A.W., 1962, Proc. Phys. Soc., 80, 686.

Jongejans, B., 1960, Nuo. Cim., 16, 625.

Landau, L., 1944, J. Phys. U.S.S.R., 8, 201.

Massey, H.J., and Corben, H.C., 1939, Proc. Camb. Phil. Soc., 35, 463.

Messel, H., and Ritson, D.M., 1950, Phil. Mag., 41, 1129.

Pathak, K.M., 1967, Ph.D. Thesis, University of Durham.

Price, B.T., 1955, Rep. Prog. Phys., 18, 52.

Rossi, B., 1952, High Energy Particles. Prentice Hall : New York.

Schönberg, M., 1951, Nuo. Cim., 8, 159.
1952, Nuo. Cim., 9, 372.

Smith, A.M., and Stewart, D.T., 1966, Phys. Lett., 22, 633.

Sternheimer, R.M., 1952, Phys. Rev., 88, 851.
1953, Phys. Rev., 89, 1148.
1953, Phys. Rev., 91, 256.
1956, Phys. Rev., 103, 511.
1959, Phys. Rev., 115, 137.

Stiller, B., and Shapiro, M.M., 1953, Phys. Rev., 92, 735.

Swann, W.F.G., 1938, J. Franklin Inst., 226, 598.

Symon, K.R., 1948, Ph.D. Thesis, Harvard University (see Rossi, B., 1952, High Energy Particles.(New York : Prentice Hall)).

Tsytovitch, V.N., 1962,a Soviet Physics-Doklady, 7, 411.
1963,b Soviet Physics - JETP, 15, 320.
1963,c Soviet Physics - JETP, 16, 1260.

Wick, G.C., 1941, Ricerca Scient., 12, 858.

Williams, E.J., 1945, Rev. Mod. Phys., 17, 225.

Wolfendale, A.W., 1963, Cosmic Rays, (London : Newnes).

Zhdanov, G.B., Tretyakova, M.I., Tsytovitch, V.N., and Shcherbakova, M.N., 1963, Soviet Physics.- JETP, 16, 245.

Crispin, A., and Fowler, G.N., 1970 Rev. Mod. Phys., in the press (July issue)

Fowler, G.N., and Hall, A.G., 1966, Proc. 9th Int. Conf. on Cosmic Rays, London, 1965 (London: Institute of Physics and Physical Society), pp. 976-9.